Testing, Characterisation, And Modelling Of Nehobo Floors For Groningen Seismic Assessment

Intermediate Report: Laboratory Tests and Numerical Models

Korswagen Eguren, Paul; Meulman, Edwin; Mariani, Valentina

Publication date
2018

Document Version
Final published version

Citation (APA)
Korswagen Eguren, P., Meulman, E., & Mariani, V. (2018). *Testing, Characterisation, And Modelling Of Nehobo Floors For Groningen Seismic Assessment: Intermediate Report: Laboratory Tests and Numerical Models*. Delft University of Technology.

Project number C31B71
File reference C31B71WP0-1
Date 22 of January of 2018
Corresponding author p.a.korswageneguren@tudelft.nl

TESTING, CHARACTERISATION, AND MODELLING OF NEHOBO FLOORS FOR GRONINGEN SEISMIC ASSESSMENT

Laboratory Tests and Numerical Models

INTERMEDIATE REPORT

Authors:
Paul Korswagen, Edwin Meulman, Valentina Mariani

Cite as: Korswagen, P., Meulman, E., Mariani, V. (2017). Testing, Characterisation, and Modelling of NeHoBo Floors for Groningen Seismic Assessment. Report number C31B71WP0-1, Intermediate Report, version 3.3, January of 2018.

This research work was funded by Nederlandse Aardolie Maatschappij B.V., who is gratefully acknowledged. Any opinion, finding, and conclusion or recommendation expressed in this report are those of the authors and do not necessarily reflect the view of the funding body.

TUDelft

TU Delft Delft University of Technology Faculty of Civil Engineering and Geosciences Stevinweg 1 2628 CN Delft PO 5048 2600 GA Delft www.citg.tudelft.nl	**INTERMEDIATE REPORT** Title: Testing, Characterisation, and Modelling of NeHoBo Floors for Groningen Seismic Assessment Author(s): Paul Korswagen Edwin Meulman Valentina Mariani Date: 22nd of January 2018

Client(s): Nederlandse Aardolie Maatschappij B.V.		Version: 3.2	Status: Preliminary Report
Project number: C31B71	Project name: TUD NeHoBo Seismic Assessment Project 2017	File reference: C31B71WP0-1	

Cite as:
Korswagen, P., Meulman, E., Mariani, V. (2017). Testing, Characterisation, and Modelling of NeHoBo Floors for Groningen Seismic Assessment. Report number C31B71WP0-1, Intermediate Report, version 3.3, January of 2018.

Document checking			
	Prepared by	Checked by	Approved by
Name	Paul Korswagen Edwin Meulman Valentina Mariani	Jan G. Rots Francesco Messali	Jan G. Rots
Signature	PK, EM, VM	JR, FM	JR

Revision History

Document		Revision		
Version	Date	Date	Author	Description
1.0	21-12-2017	22-12-2017	PK, EM, VM	Draft preliminary report updated with summary and initial review comments.
2.0	22-12-2017	10-1-18	PK, EM, VM	NeHoBo Summary Preliminary Report_ comments Word document and table
3.0	10-01-2018	22-01-2018	PK, EM, VM	Final, intermediate revision.

TU Delft

Acknowledgement

This research was carried out for the benefit of seismic assessments of the Groningen building stock. A lack of knowledge was detected regarding NeHoBo floor properties and their effect on the structural response, which may induce conservatism and possibly over-designed, intrusive strengthening methods. This report describes experimental testing and computational modelling improving knowledge and understanding of NeHoBo floor properties and their role in the seismic assessments. The context was provided by CVW, NCG and NAM. The work is funded by NAM under the contract 'Testing program for structural upgrading of URM structures'. Due to a need for a quick insight into the topic by December 2017, this preliminary report is issued based upon intermediate results. The tests were carried out on NeHoBo floor samples extracted from houses at Zijlvest, Loppersum. The cooperation with Arup regarding the extraction of the samples is acknowledged.

I. Abstract

This report presents results from laboratory tests and a first modelling phase for NeHoBo hollow brick floors with a view to seismic assessment of the Groningen building stock.

The laboratory tests on specimens extracted from terraced houses in Zijlvest, Loppersum focus on the in-plane diaphragmatic action with a compressive arch and a tensile tie. In-plane bending tests deliver the flexural and direct tensile strength for the tie. In-plane shear triplet tests characterise the cohesion and friction shear-compression in the arch. Table I.1 lists the number, average values, standard deviation and 5% characteristic values for the measured properties. These properties are recommended to structural engineers in analyses of in-plane NeHoBo floor action.

Table I.1. Overview of laboratory tests performed.

Test	Number of Tests	Property	Unit	Average Value	Standard Deviation	5% Characteristic
In-Plane Bending*	4	Flexural strength	MPa	0.11	0.03	0.06
		Direct tensile strength	MPa	0.075	0.011	0.055
Shear Triplet*	6	Cohesion	MPa	0.27	0.078	0.15
		Friction coefficient	-	0.66	0.162	0.4

*The contribution of the top concrete layer was removed from these tests.

Modelling was carried out at three levels. Firstly, the floor as such was captured in an analytical strut-and-tie model, validated against FEM models. This provides ultimate in-plane floor capacity, to be compared against the demand from actual seismic forces. Secondly, the FEM models for the floor were extended to include walls stubs and pier stubs so as to study the interaction of the floor with walls and piers, including overburden and frictional capacities. Thirdly, a preliminary estimation of the earthquake forces on the floor was obtained from an analytical estimation of the predominant natural period (for the house from where the samples where extracted) and NPR-spectral demand.

The first phase of analysis suggests that NeHoBo floors possess adequate capacity to withstand the lateral loads produced by earthquakes to which they are subjected to. The measured shear-compression properties in terms of cohesion and friction are well capable of developing the compressive arch in the floors. The critical material parameter required to evaluate structures with NeHoBo floors is their direct tensile strength for developing the tension tie in the direction perpendicular to the rebar; from the preliminary experimental laboratory tests, the 5% characteristic value of the tensile strength has been observed to be 55kPa when the concrete layer is pre-damaged.
Preliminary analyses for a typical terraced house subjected to NPR-compliant hazards shows that the forces generated in the floors remain below the maximum floor capacities based upon these values and that the effect of the NeHoBo floors on the near collapse state changes only marginally with respect to concrete floors.

Additional laboratory tests are planned in order to further increase the confidence in these results. In particular, additional in-plane tests will be used to assess the influence of the potential concrete layer; shear tests at other pre-compression levels will increase the confidence in the computed friction and cohesion values; and, out-of-plane tests in both the longitudinal and transversal directions will provide additional strength and stiffness values and serve as a reference for the values obtained with the in-plane bending test. Supplementary computational modelling will benefit from additional, experimentally-determined strength and stiffness values, further model and loading variations, sensitivity studies, and more detailed interpretations.

II. Executive Summary

1800 words - 4 minutes

Problem Definition

The consultants performing seismic assessments for existing houses in Groningen show a different approach when the observed house has NeHoBo type floors (Nederlandse Holle Bouwsteen, floors from hollow clay bricks bonded by mortar). Some of the consultants consider these floor types brittle and weak, and, in the absence of knowledge, conclude quickly that the floors need to be strengthened. This leads to disturbances for the occupants as well as an increase in strengthening costs. Other consultants analyse these floors with conservative, low in-plane shear and bending properties and therefore come to similar conclusions.

To provide clarity, TU Delft has started a research program related to NeHoBo floors (Rots, 2017). This research program will provide the required parameters and material properties necessary for analysing these floor types. The parameters and material properties will be determined through testing on large and small samples received in November of 2016 from the (now demolished) terraced houses located in Zijlvest, Loppersum. In addition to this testing program for the determination of NeHoBo floor material properties, the research program also includes various analyses of structures with NeHoBo floors to provide insight into their behaviour and to conclude whether the presence of a NeHoBo floor contributes negatively to the near-collapse state when subjected to an induced earthquake (NPR, 2017) in comparison to the behaviour of a house with solid concrete floors. The comparison house was tested at the TU Delft for the 2015-2016 TUD testing campaign (Esposito, 2016a).

Experimental Determination of Material Properties of the NeHoBo Masonry Floor-System

The assessment of the in-plane capacity of the NeHoBo floor system is important for the floor to act as a proper diaphragm to transfer in-plane forces to the lateral-load-bearing structural elements. The horizontal load on the floor will result in a compression arch and tensile tie. To analyse this, material parameters are required.
In-plane bending tests with tension perpendicular to the bed joints and in-plane shear tests for the brick-mortar bed joint interface provide experimental results that give insight into the capacity of the NeHoBo floors.
For the in-plane bending test a section is cut out of the NeHoBo floor panels (1.6x1.1m) that were extracted from the Zijlvest donor houses (Loppersum) (Figure II.1).

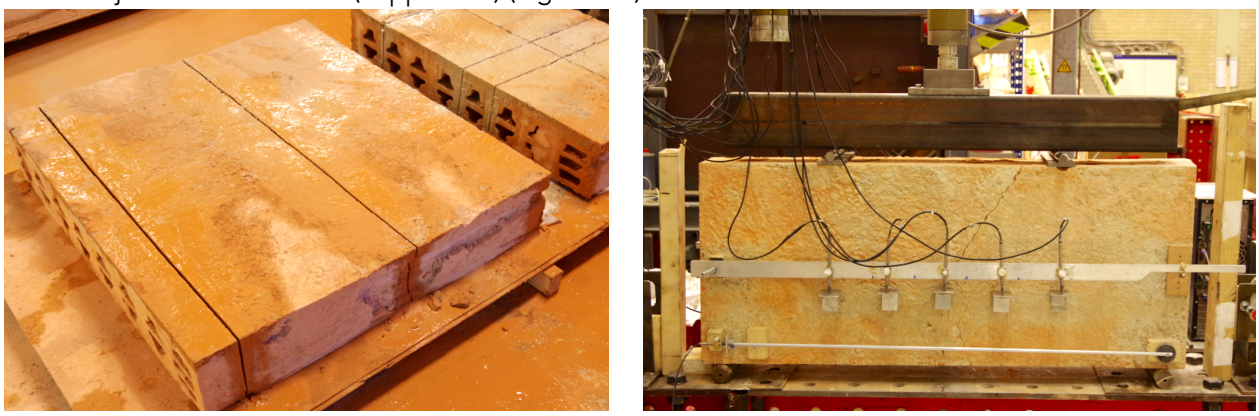

Figure II.1 (3.1&3.3). In-plane bending samples cut from NeHoBo panel (left) and four-point bending test set-up for in-plane bending of NeHoBo floor sample (right).

Almost all of the in-plane bending samples (four samples tested so far) display a severe shrinkage crack in the concrete layer before testing. This pre-damage emerged at the locations of tubes for electrical wiring in the concrete layer. Failure during the in-plane bending test occurred by cracking through the entire thickness of the sample at the location of the pre-crack in the concrete. One in-plane bending test was performed with an undamaged concrete layer (Sample TUD_NEH_4-1S). In Figure II.2 can be seen that the flexural strength capacity is significantly higher compared to the pre-damaged samples. This is expected since the concrete layer also contributes to the in-plane bending capacity opposite to when the concrete layer is already pre-cracked. Note that for the case of the undamaged concrete layer only one sample has

been tested (so far). If translated to values of strength, the four pre-cracked samples achieve an average of 110kPa in flexural strength, while the undamaged sample scored 220kPa. From the curves presented in figure II.2, the direct tensile strength can also be obtained; in this case, the tensile strength is 75kPa (and the standard deviation is 11kPa) for the four pre-damaged samples and 150kPa the average for the undamaged one. For the samples with the damaged concrete top layer, the 5% characteristic values are then 70kPa and 55kPa, for flexural and tensile strength, respectively.

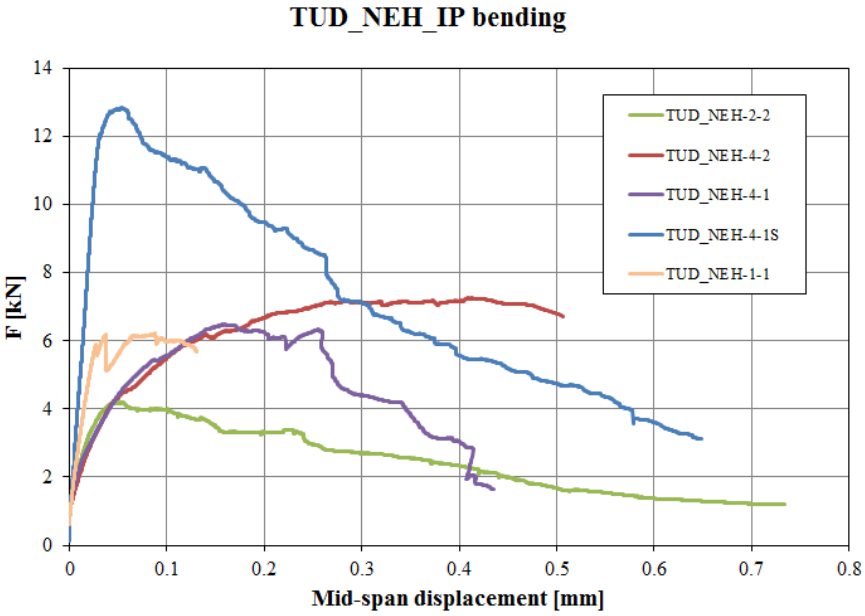

Figure II.2 (3.12): Force-displacement curve of in-plane bending test samples.

The shear samples have dimensions of about 400x300x160mm (excluding the concrete top layer) which is the size of 3 NeHoBo bricks including 2 mortar joints. A total of six NeHoBo shear samples are tested with two different pre-compression levels, respectively 0.6MPa and 0.1MPa. The shear test is performed to obtain the material properties for shear strength, cohesion and friction coefficient of the NeHoBo floor-system if only the mortar-brick interface is considered (no concrete top layer included). Eliminating the contribution of the concrete layer could be considered as the low boundary of shear capacity of the NeHoBo floor. Adding the concrete layer can only increase this capacity. Since the presence of a concrete layer and/or the damage state of concrete layer is not always certain it is reasonable to take the worst case scenario which means excluding the contribution of the concrete layer. To eliminate the contribution of this concrete top layer from the brick-mortar shear test four cuts are made in the concrete layer above the mortar joint (see Figure II.3).

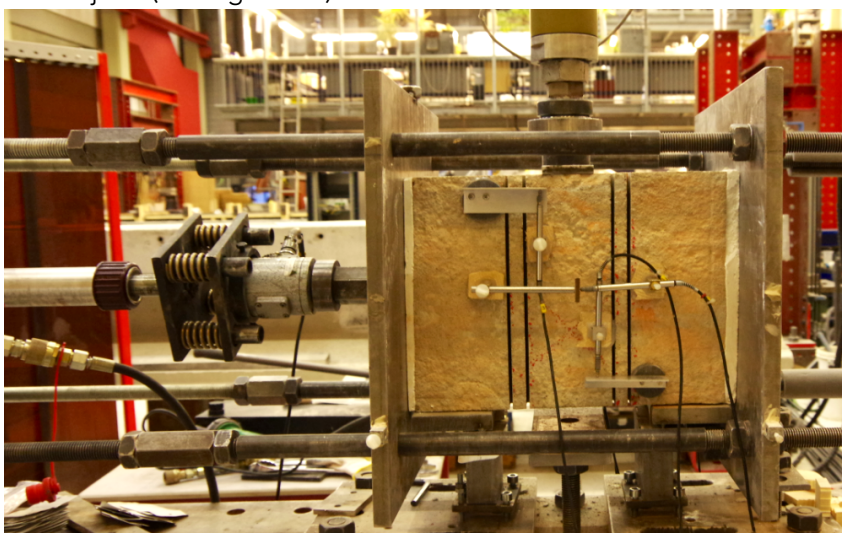

Figure II.3 (3.15) Shear test set-up with NeHoBo shear sample of which the concrete is cut at the location of the mortar joints to eliminate the contribution of the concrete layer.

Figure II.4 shows the shear test results of the NeHoBo brick-mortar interface shear samples. The displacement is presented both for the jack and the displacement sensors on the sample itself.

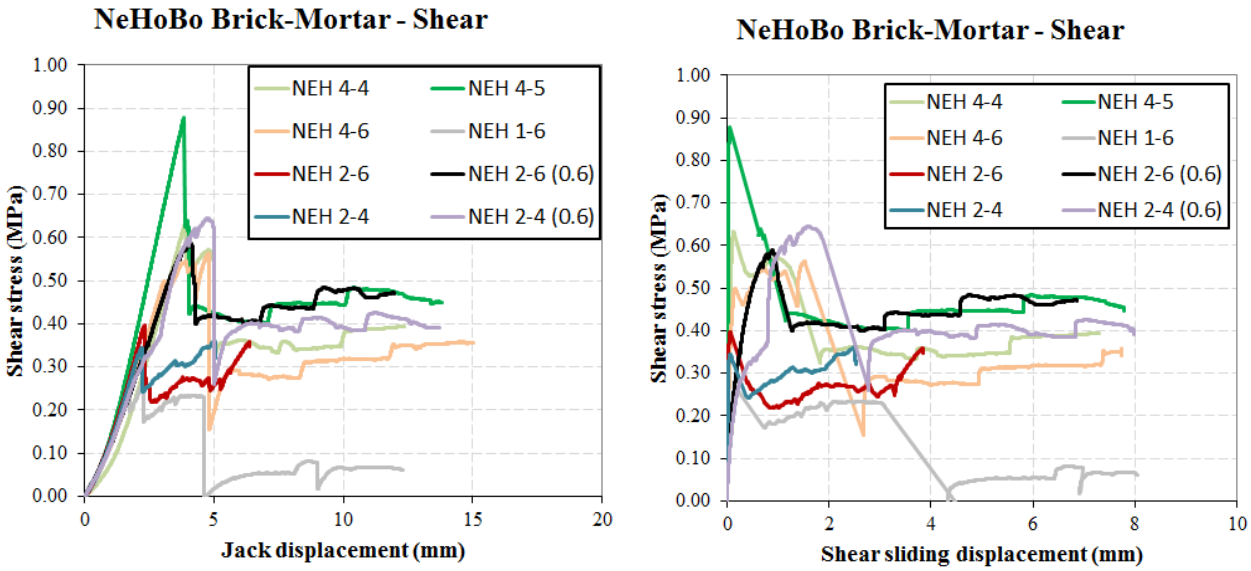

Figure II.4 (3.16). Shear stress-displacement : (Left) relative displacement of the jack; (right) relative displacement of the central brick from displacement sensor readings.

Figure II.5 shows the pre-compression stress plotted against the shear strength in which a regression line can be plotted to determine values for the cohesion and friction coefficient. The cohesion value for the tested NeHoBo floor samples is 0.27MPa and the friction coefficient is 0.66.

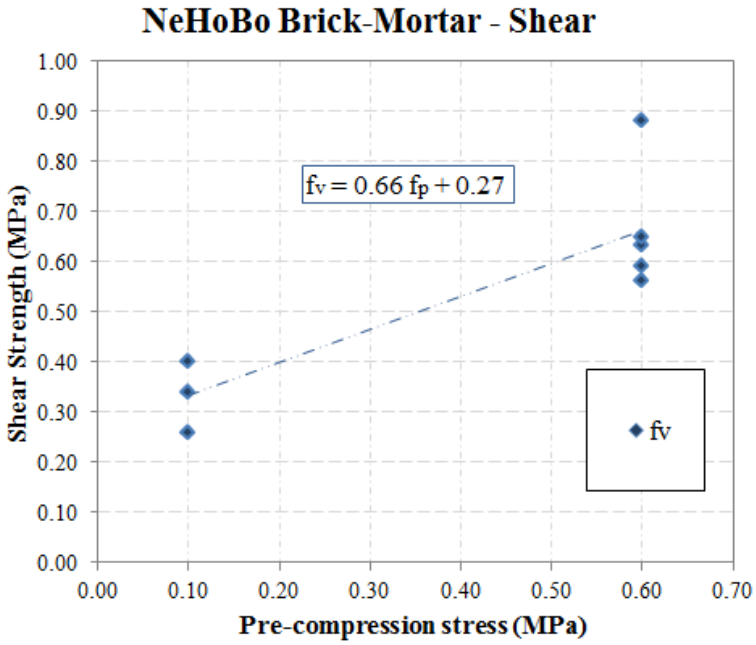

Figure II.5 (3.17). Pre-compression vs Shear strength resulting in a friction coefficient and cohesion value for the tested NeHoBo brick-mortar shear samples (fv=shear strength, fp=pre-compression stress).

The main properties obtained from the laboratory are listed in table II.1. Average values together with the standard deviation are given for the performed tests.

Table II.1. (5.1) Comparison of materials properties.

Material property		Experimental Tests			Range used in Numerical models
		Average values	Standard deviation	5% Characteristic	
Density	**kg/m³**	1666	16	N.A.	1700
Flexural strength*	**MPa**	0.11	0.03	0.0605	0 - 0.2
Direct tensile strength*	**MPa**	0.075†	0.011	0.055	0 - 0.1
Mortar-Brick Cohesion	**MPa**	0.27	0.078	0.15	0 - 0.2
Mortar-Brick Coefficient of friction	**[-]**	0.66	0.162	0.4	0.5 - 0.6

† Derived from in-plane bending test flexural strength results.
* Considering only samples with a damaged concrete layer.

Numerical and Analytical Modelling of the NeHoBo Floor-System

Numerical models were also elaborated to analyse the behaviour of NeHoBo floors. Given the potential variability in the tested material properties, these models were run for a range of parameters. The range of parameters is presented in Table II.1 where a comparison can be made between the experimental test results and the used range of parameters for the numerical models.

The computational models of the floors consist of plates supported on wall stubs. For the Zijlvest donor houses, as a case study, the floor is 5.40x7.70m². The plates are loaded in-plane on one side of the model to verify their capacity of transferring in-plane loads (see figure II.6). Many variations of these floor models were analysed, including different boundary conditions, material properties, overburdens, etc. (the reader is referred to section 4.2.2). Here it was observed that failure of the floors occurred by sliding over their supporting walls. Accordingly, the values of overburden become the most influential as they determine the capacity against sliding via friction; while the strength of the floor material is less important. For low values of overburden, corresponding to a NeHoBo floor on the upper level of a structure, considering the restraint and strength provided by the supporting wall, a capacity upwards of 20kN was obtained. For floors in the middle of a structure, restrained by walls below and on-top, with a higher value of overburden at the connection between the floor and the walls, the capacity approached 100kN.

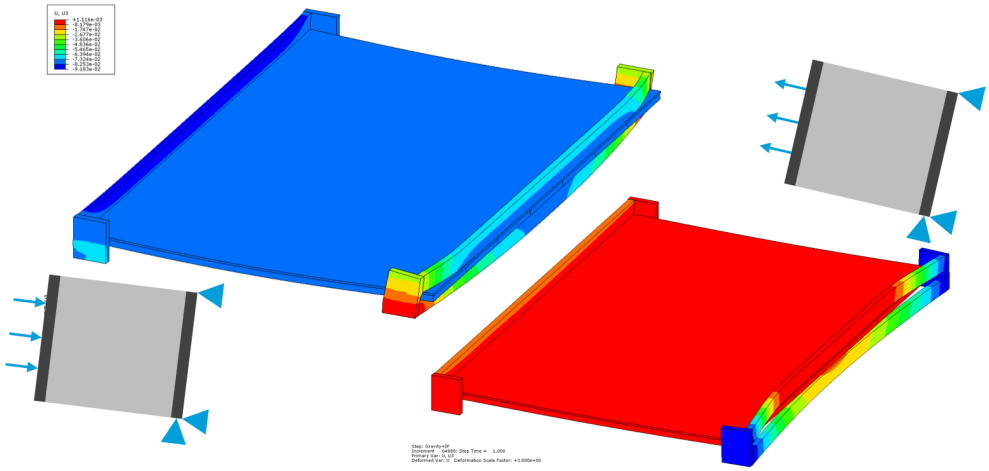

Figure II.6 (4.22). Longitudinal in-plane loading of the floor system. Slide-over of the floors at the connections with the wall stubs is observed.

An analytical calculation was performed to estimate the potential forces on the floors. The total weight of the house (including a live load, and the weight of the roof and of the outer leaves of the cavity wall) was computed to be 650kN. Considering a half section of a floor (as seen in on the left of figure II.7) and lack of lateral strength on one side of the structure, the tributary weight to be mobilised by the floor was pegged at 150kN. In the case of an induced earthquake with a PGA of 0.35g, the pseudo acceleration obtained by the NPR (2017), for the computed natural period of 2 seconds of the house, is 0.075g. This corresponds to a force of 11kN. This force is lower than the capacity of even the weaker top floor (20kN)

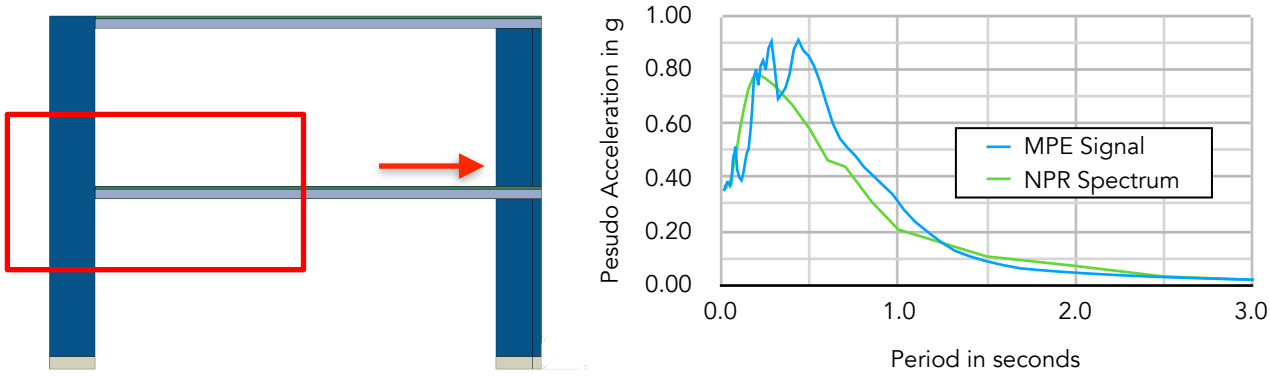

Figure II.7 (4.44 & 4.45). Sketch of the house and the tributary zone for earthquake forces running through the floor (left), and spectrum of NEN (2017) compared to a synthetic earthquake signal.

Additionally, an analytical model was used to verify the capacity of the floor acting as a deep beam (see figure II.8). Assuming an internal arm of 0.6 of the span, and 0.2 of the span as the linear tensile zone, with a tensile strength of 55kPa, the floor is capable of withstanding a distributed in-plane load adding up to 28kN; this is higher than what is required from the floor during the design earthquake.

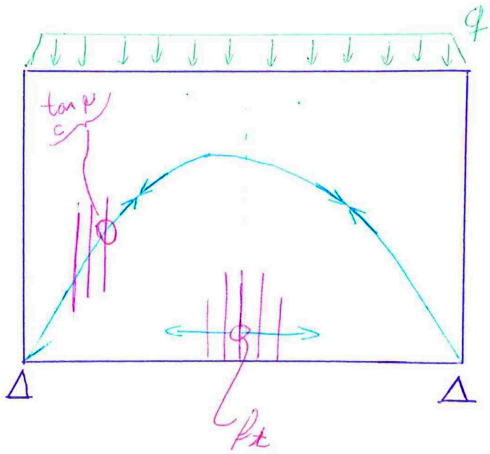

Figure II.8 (4.47). Proposed analytical model for the deep-beam behaviour of the floor.

To analyse the capacity of the floor, the use of the analytical model shown in figure II.8 is recommended. Modelling properties for the use of a continuum composite material have not yet been derived; instead, a more complex modelling approach has been taken employing estimates for the individual components of the floors (bricks, concrete, mortar) as seen in figure II.6, but this is not recommended when evaluating general buildings.

Comparison of the Near Collapse Capacity for the TU Delft Test House With a NeHoBo Floor Versus a Concrete Floor

Furthermore, the first full-scale TU Delft laboratory masonry house (Esposito, 2016) was reproduced with a computational model (see figure II.9). The house, which was assayed with a displacement-controlled cyclic pushover, was tested with solid concrete floors. The validated model with concrete floor was compared to the same model with NeHoBo floors. Both models were compared with a cyclic pushover as in the laboratory test, but also a base excitation using the signal of an induced earthquake (Tomassetti, 2017). While the NeHoBo version was more flexible than the model with concrete floors, no direct detrimental

influence towards the near-collapse state could be observed. These models, however, still require further analysis, including, for instance, parameter variations, further checks on the out-of-plane capacities of the floors, further interpretations of the horizontal restraints at the floors ends' near the loading of the arch, and mesh sensitivities.

Finally, the obtained material parameters will be used in conjunction with computational micro models to derive equivalent homogenised composite properties to be used in simpler finite element models. This has not yet been completed.

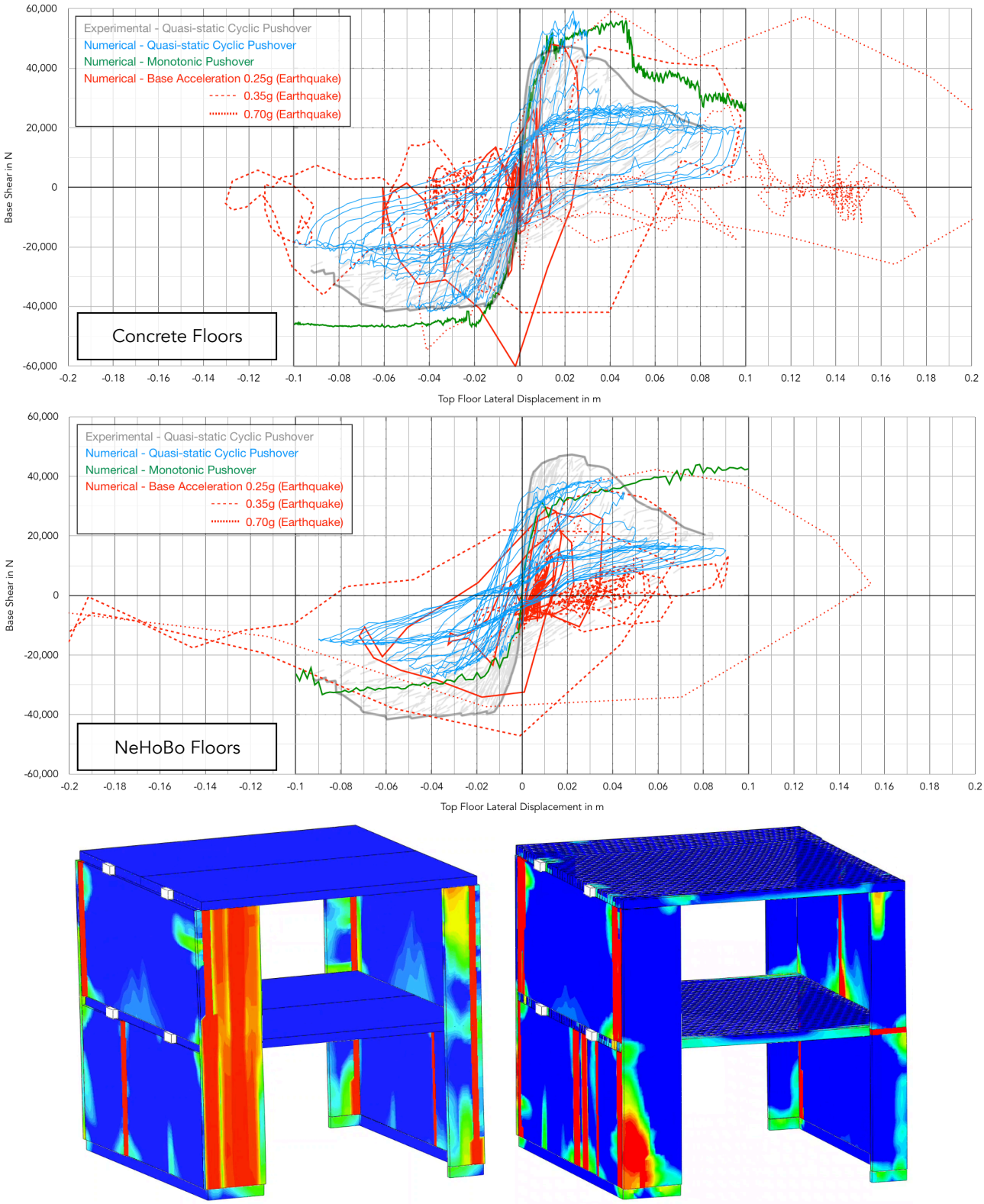

Figure II.9 (4.33 & 4.34). Force-displacement curves for the comparison of a terraced house with concrete floors or NeHoBo floors. The displacement is measured on the centroid of the floor. And bottom: model impressions showing crack areas (in red) for the concrete floor case (left) and the NeHoBo floor case (right) for the cyclic pushover to 100mm.

The first phase of analysis suggests that NeHoBo floors possess adequate capacity to withstand the lateral loads produced by earthquakes to which they are subjected to. The measured shear-compression properties in terms of cohesion and friction are well capable of developing the compressive arch in the floors. The critical material parameter required to evaluate structures with NeHoBo floors is their direct tensile strength for developing the tension tie in the direction perpendicular to the rebar; from the preliminary experimental laboratory tests, the 5% characteristic value of the tensile strength has been observed to be 55kPa when the concrete layer is pre-damaged.

Preliminary analyses for a typical terraced house subjected to NPR-compliant hazards shows that the forces generated in the floors remain below the maximum floor capacities based upon these values and that the effect of the NeHoBo floors on the near collapse state changes only marginally with respect to concrete floors.

For consultants it is recommended to employ a cohesion of 0.27MPa as average value (0.15MPa as the 5% characteristic), a friction coefficient of 0.66 (0.4) and a direct tensile strength of 0.075MPa (0.055MPa) in analyses for in-plane NeHoBo floor action.

Additional laboratory tests are planned in order to further increase the confidence in these results. In particular, additional in-plane tests will be used to assess the influence of the potential concrete layer; shear tests at other pre-compression levels will increase the confidence in the computed friction and cohesion values; and, out-of-plane tests in both the longitudinal and transversal directions will provide additional strength and stiffness values and serve as a reference for the values obtained with the in-plane bending test. Supplementary computational modelling will benefit from additional, experimentally-determined strength and stiffness values, further model and loading variations, sensitivity studies, and more detailed interpretations.

III. Table of Contents

Chapter 1

Introduction

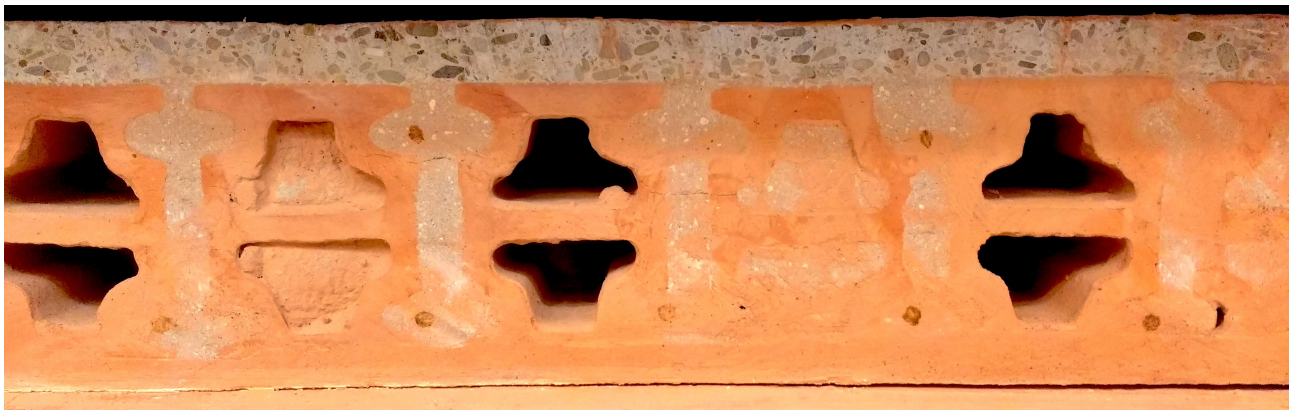

TU Delft

1. Introduction

1.1. Definition of the Problem

The consultants performing seismic assessments for houses in Groningen take different approaches in case the house has NeHoBo type floors. Some consider these floor types brittle and weak and, without a proper analysis, conclude quickly that the floors need to be strengthened or, even worse, should be replaced by a (pre-cast) concrete floor. This leads to disturbances for the occupants as well as an unnecessary increase of strengthening costs. Other consultants analyse these floors with conservative, low in-plane shear and bending properties and therefore come also to similar conclusions.
To provide clarity, TU Delft has started a research program related to NeHoBo floors (Rots, 2017). This research program will provide the required parameters and material properties for analysing these floor types. The parameters and material properties will be determined through testing on large and small samples received in November of 2016 from the (now demolished) terraced houses located in Zijlvest, Loppersum. In addition to this testing campaign, the research program also includes various analyses of NeHoBo floors to provide insight into the behaviour and to conclude whether the presence of a NeHoBo floor negatively contributes to the near-collapse state due to an induced earthquake (NPR, 2017) in comparison to the behaviour of a house with solid concrete floors. The comparison house was tested at the TU Delft for the 2015-2016 TUD testing campaign (Esposito. 2016a).

1.2. Scope of Research

Next to concrete and timber floors, pre-fabricated NeHoBo floor systems are widely used in houses in the Netherlands built between 1950 and 1980. Several types of NeHoBo floor systems exist, this report will focus on masonry floor systems.
Masonry NeHoBo floors consist of prefabricated plates that resemble a piece of masonry wall. They are masoned off-site as a wall of approximately one meter in height and a length corresponding to the desired span. Steel reinforcement (rebar) is laid in the bed joints (longitudinal joints). The plates are hoisted, turned 90-degrees, and placed on-site. Concrete is poured between the plates, and often, a simple concrete layer is also poured on top. See figure 1.1 and figure 1.2.
Later, the plates were also prefabricated in a factory.

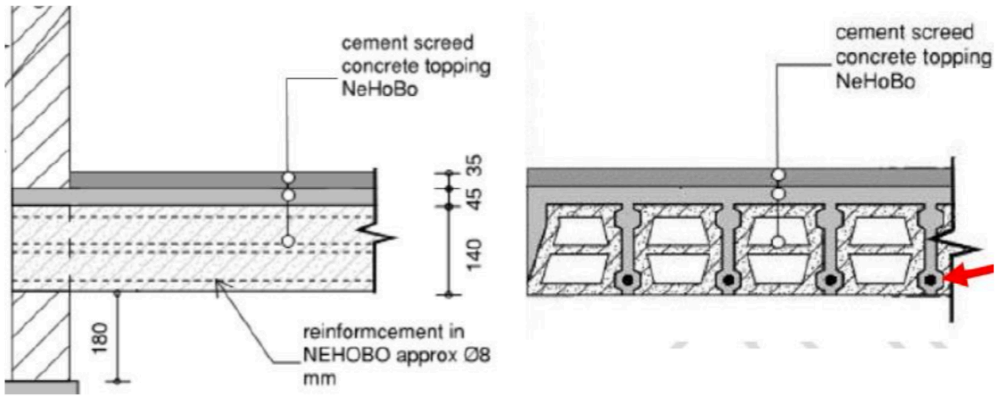

Figure 1.1. By ARUP. Masonry NeHoBo floor-system.

As part of the structural research of the vulnerability against earthquakes in the area of Groningen being performed by the TU Delft, it is necessary to understand and characterise these floor systems. Hence, in November of 2017, a characterisation project has been started.
Floor samples (figure 1.2 and figure 1.3) have been extracted from existing (now demolished) houses in Zijlvest, Loppersum (see figure 1.4) and assayed in the laboratory. To select and perform the most relevant laboratory tests, preliminary computational models were run based on initial estimates of the material properties.

This report provides a summary of these initial estimates, details the models being performed and their preliminary results, presents the results of a few laboratory tests run, and draws a first set of observations gathered from these tests and models.

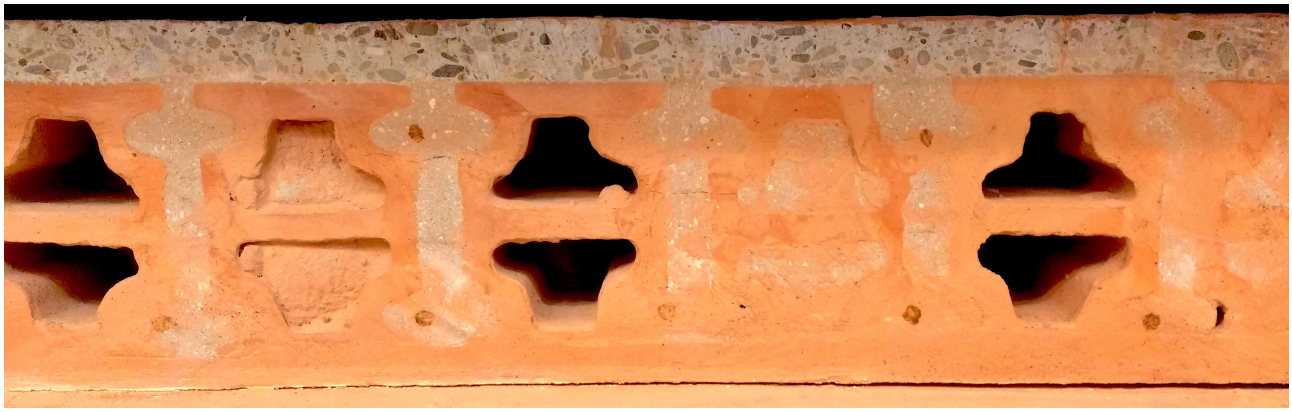

Figure 1.2. Section of NeHoBo floor sample.

Figure 1.3. Full-view of extracted sample of 1.10x1.60m.

The assessment of the floor-system will focus on determining their stiffness and strength for in-plane actions in various directions to verify their competence as a diaphragm. As such, it should be capable of transmitting the in-plane forces to the lateral-load-bearing structural elements.

1.3. Plan of Approach

To characterise the NeHoBo floors, adapted versions of standard laboratory tests are used. These tests are used to output the most relevant properties necessary for the evaluation and modelling of NeHoBo floor systems.
In combination with finite element computational micro models, additional material properties necessary for simpler computational models are determined.

Further, computational models are used to evaluate the behaviour of NeHoBo floors and their influence on the full-structure behaviour.

The report starts with a theoretical introduction in chapter two about the requirements and behaviour of floors. Next, in chapter 3, the laboratory tests conducted to investigate the material properties of NeHoBo floor systems are presented. This is followed, in chapter 4, by a description of several computational models of the floors run at various modelling scales. Finally, in chapter 5, the main conclusions are listed.

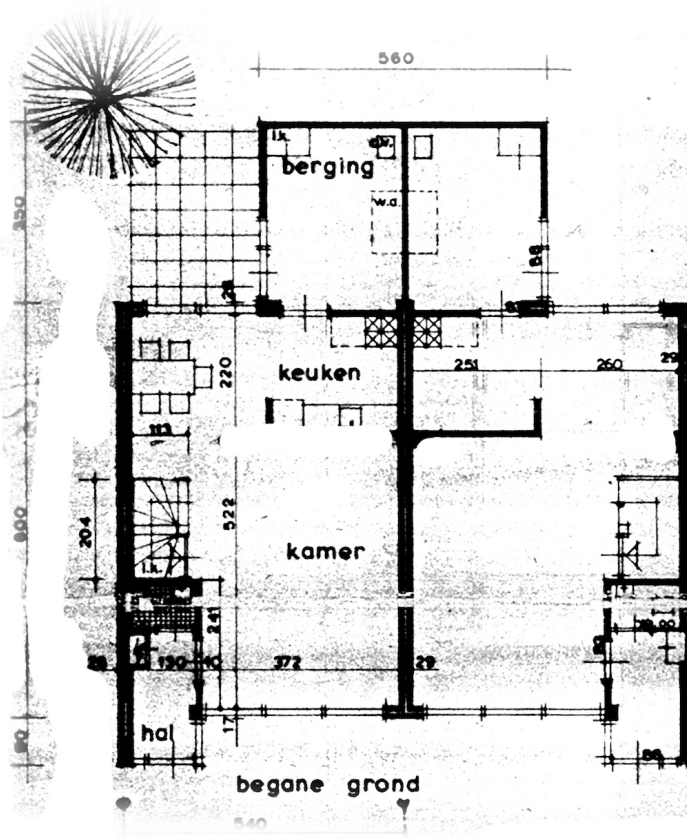

Figure 1.4. Architectural blueprint of the ground floor of one of the Zijlvest donor houses.

Chapter 2

Background: Diaphragm Action and Failure Mechanisms for Floor-systems

TU Delft

2. Background: Diaphragm Action and Failure Mechanisms of Floor-systems

(Theoretical part and literature study, in progress)

A study performed by de Roo (1991) on the in-plane shear properties of a prefabricated concrete floor focused on the sliding between the prefabricated beamlets when these had been joined with mortar. Here, both the stiffness and strength of the entire floor were of interest. Similar loading and failure mechanisms are expected for the NeHoBo floor system, though a higher complexity is also anticipated.
Tena-Colunga (2015) studied various types of floor-systems and determined that a mortar-brick-concrete layer system (the closest to the NeHoBo system) was comparatively rigid if the concrete layer had sufficient bond with the bricks. This effect will be studied.

2.1. Diaphragm Action of Floors During Lateral Loading

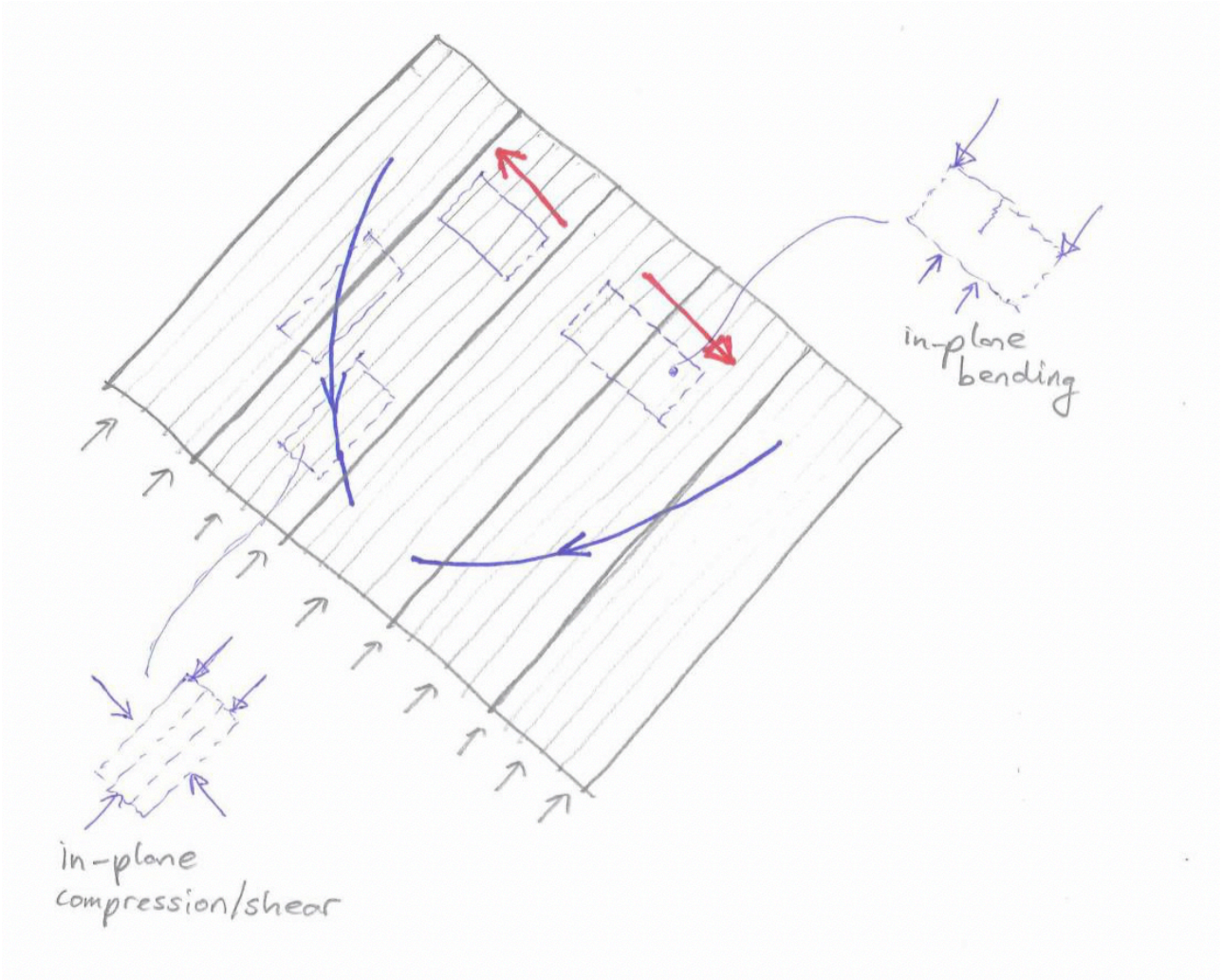

Figure 2.1. Illustration of in-plane stresses on the floor when subjected to lateral loading.

Chapter 3

Experimental Testing and Characterisation of NeHoBo Floor Samples

TU Delft

3. Experimental Testing and Characterisation of NeHoBo Floor Samples

As described in chapter 1 and the project proposal (Rots, 2017) the assessment of the in-plane capacity of the NeHoBo floor system is important to assure that the floor to acts as a proper diaphragm by transfering in-plane forces to the lateral-load-bearing structural elements. The horizontal load on the floor will result in a compression arch and tensile tie.
In-plane bending tests in the direction of the bed joints and shear tests for the brick-mortar interface provide experimental results that give insight in the capacity of NeHoBo floors. The experimental results are used to validate and calibrate numerical models that are described in chapter 4.

3.1. In-Plane Bending Test

In this section the in-plane bending test of the NeHoBo floor is described. The experimental test provides the in-plane flexural strength of the NeHoBo floors in the direction of the bed joints. The same in-plane bending test set-up, sensor configuration and displacement control system is used as in the TUD 2016 test campaign (Jafari. 2017). In section 3.1.1 the samples and a brief description about the test procedure is given. The material test report of the TUD 2016 test campaign (Jafari. 2017) describes the details about the test procedure. Section 3.1.2 describes the experimental test results.

3.1.1 Sample Description & Testing Procedure

For the in-plane bending test a section is cut out of the NeHoBo floor panels (1.6x1.1m) that were extracted from the Zijlvest houses (Loppersum) (Figure 3.1). The samples are about 1100x450x200mm. This means the in-plane bending sample has 8 bricks in length and 1,5 bricks in height (Figure 3.3 right).

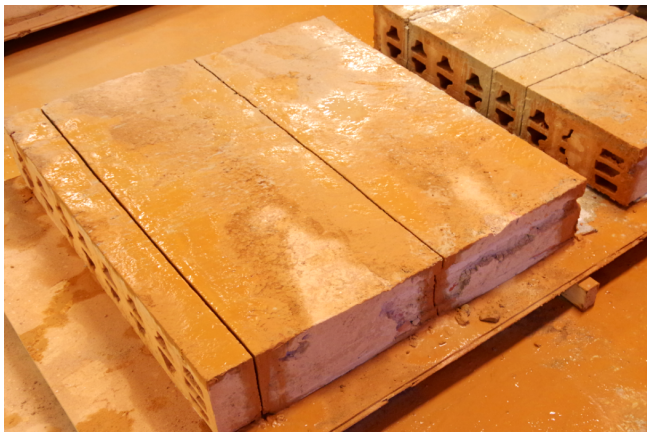

Figure 3.1. In-plane bending samples cut from NeHoBo panel.

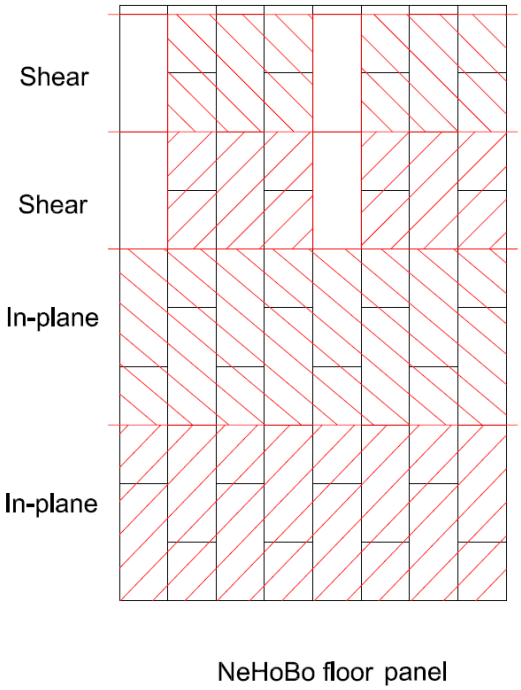

Figure 3.2. Samples cut from NeHoBo floor panel

Figure 3.2 shows how the samples are cut from the NeHoBo floor panels. The red lines are the cut lines and the marked area indicates the In-plane and shear samples. The shear test will be discussed in more detail in section 3.2.

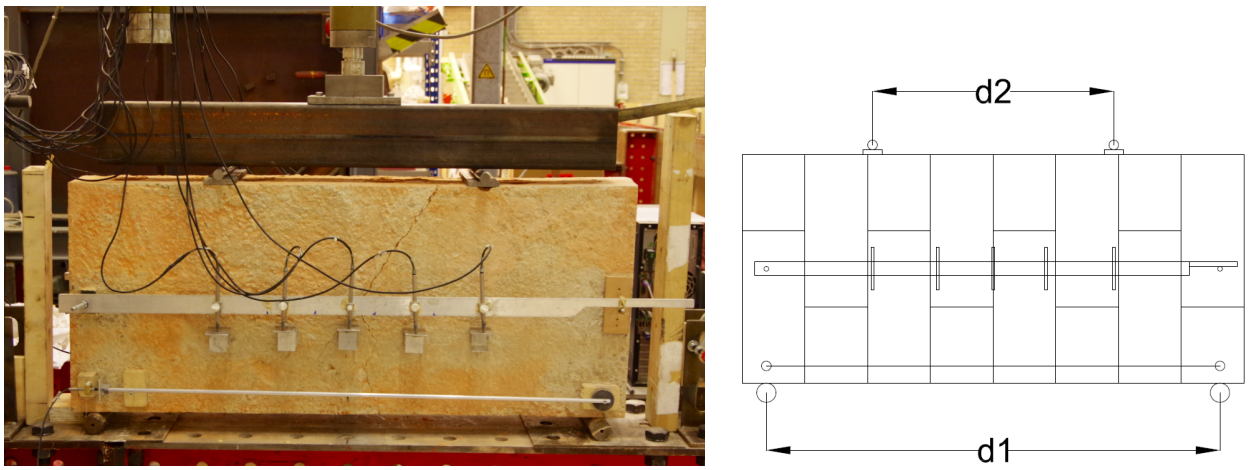

Figure 3.3. (left): four-point bending test set-up for in-plane bending of NeHoBo floor sample. (right): In-plane bending sample configuration.

Figure 3.3 (left) shows the four-point bending test set-up that is used for the in-plane bending test of the NeHoBo floor sample. In Figure 3.3 (right), for simplicity, the joints are merged together with the bricks and are now represented as thin lines. Five vertical displacement sensors are attached to a beam and positioned at the middle of the sample. These sensors measure the displacement of the sample due to bending. At the bottom part of the sample a horizontal displacement sensors is placed. This is the jack displacement control sensor. In other words, the displacement of the sample is controlled according to the value that is measured at this sensor. With this control system, the post-peak behaviour of the sample can also be tested. The same sensor configuration is applied to the other side of the sample.

3.1.2 Experimental Results

The first in-plane bending sample tested is a section from the NeHoBo panel shown in Figure 3.4. As can be seen, there is a significant crack in the top concrete layer. In Figure 3.5 of sample TUD_NEH-2-2 it can be seen that there is a tube for electrical wiring at the location of the crack. The same sample is shown in the test set-up in Figure 3.3. This figure is from before the test was performed, the diagonal crack where the tube is located is clearly visible. Figure 3.5 (right) and Figure 3.6 show the crack at final failure of the sample in bending from the concrete layer side and the plaster side.

Figure 3.4. NeHoBo floor panel number 2 showing a severe crack in the top concrete layer.

Figure 3.5. Sample TUD_NEH-2-2 (left): crack in concrete layer at location of tube for electrical wiring in the top concrete layer. (right): Cracking of the concrete layer along the initial crack in the concrete layer.

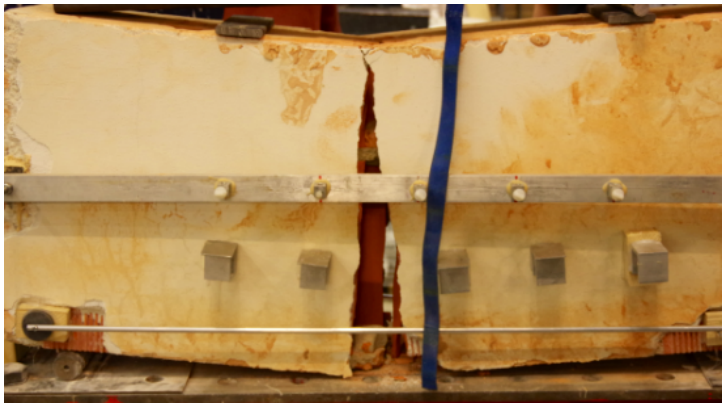

Figure 3.6. Sample TUD_NEH-2-2 back side view of crack at final failure of sample in bending

Sample TUD_NEH-4-1 has also a crack in the concrete layer (see Figure 3.7). Although there is no tube for electric wiring located at the crack.

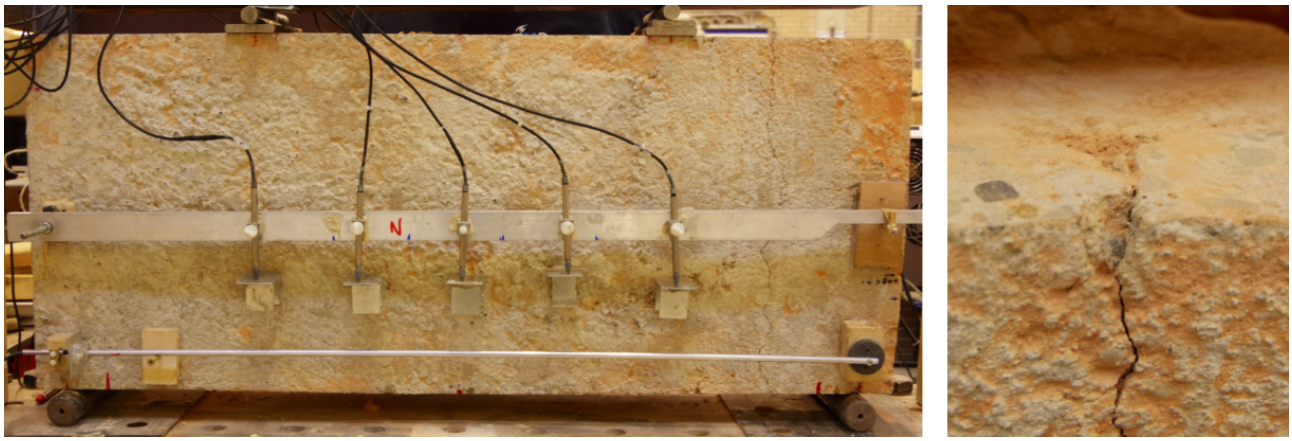

Figure 3.7. Sample 4-1 (left): Crack in concrete layer visible on right side of the sample running from top to bottom. (right): Crack zoomed in on the top part of the sample, no tube for electrical wiring is visible.

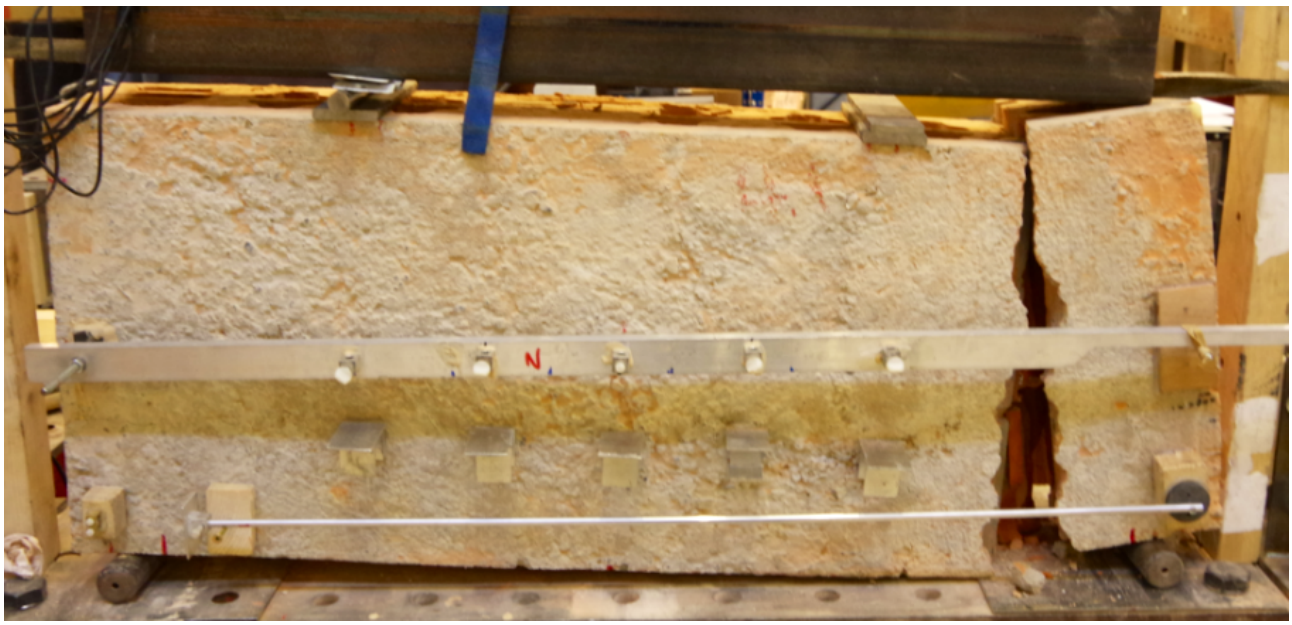

Figure 3.8. Sample TUD_NEH-4-1 failure due to in-plane bending.

Sample 4-1 shows failure due to bending at the location of the pre-test crack in the concrete layer. It appears that a crack in the concrete layer can more easily be increased or extended instead of forming another crack somewhere else in the concrete layer. The stress in the sample is focussed at the cross section where the crack is located. The crack went through the mortar interface and separated one brick row from the sample. The left part of the broken sample is re-tested (named Sample 4-1S) since it did not show any significant damage due to the test and does not have a severe crack in the concrete top layer like the previous samples (Figure 3.9). The sample is in this case 1/8 shorter than the other samples. Based on in-plane bending tests performed on masonry, with different height-length ratios, in the 2015 TUD test campaign (Esposito. 2016b.) it will not significantly change the flexural strength results that come out of this test.

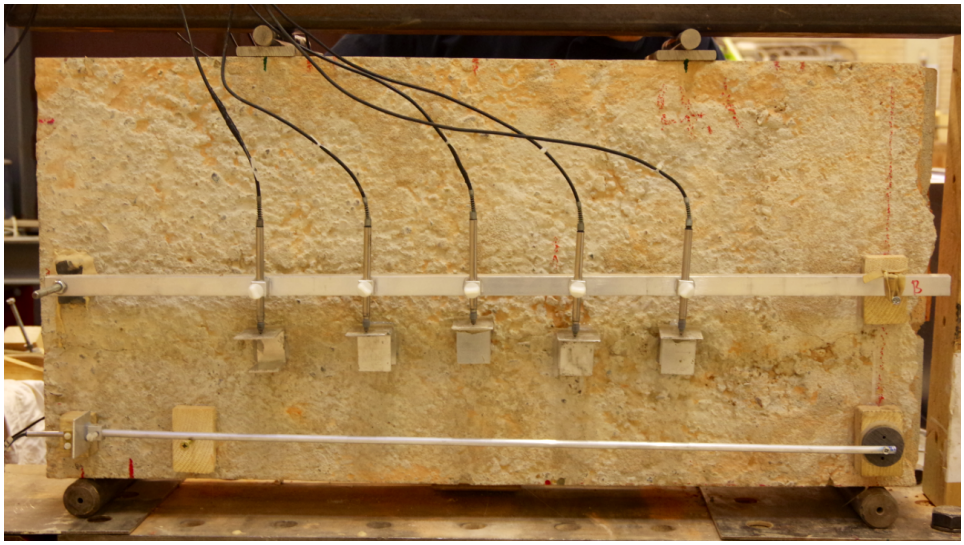

Figure 3.9. Sample TUD_NEH-4-1S

Figure 3.10 and Figure 3.11 show that the crack propagated partly through the bricks and partly through the brick-mortar interface. It is likely that the concrete layer cracks first due to its higher stiffness and then forces the crack through the thickness of the samples, where the crack propagates through the bricks or follows the brick-mortar interface.

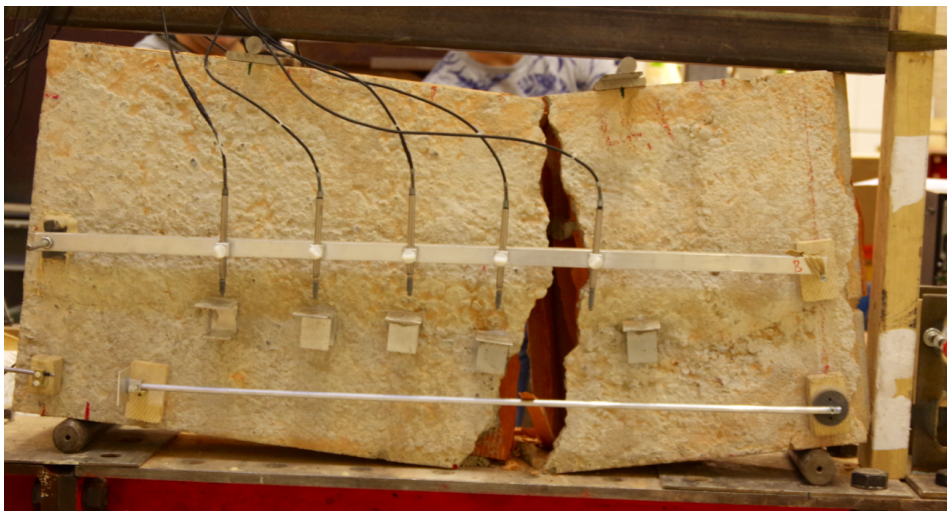

Figure 3.10. Sample TUD_NEH-4-1S

Figure 3.11. Sample TUD_NEH-4-1S

Figure 3.12 shows the force-displacement curves of the five in-plane bending test samples. It can be seen that sample TUD_NEH-4-1S has a significantly higher peak load compared to the other samples. This sample had no severe crack in the concrete layer, the other four samples did. Sample TUD_NEH-2-2 and TUD_NEH-4-2 showed similar cracking on the right side of the sample following a vertical crack in the concrete. In both cases the crack was outside the two loading points meaning that at the location of the crack the maximum bending moment is not present. The flexural strength for these two samples is determined at the location of the crack, based on the bending moment at that location. For the other samples the maximum bending moment is used to calculate the flexural strength described in the material test report of the TUD 2016 test campaign (Jafari. 2017).

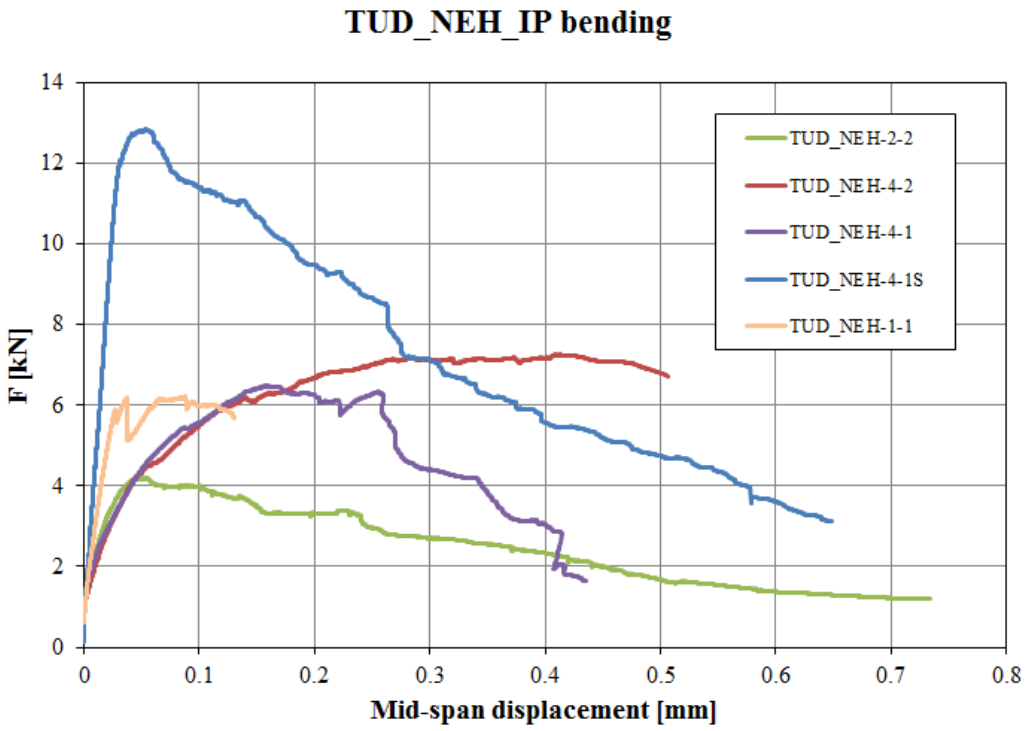

Figure 3.12. (Left): Force-displacement curve of in-plane bending test samples.

Table 3.1 shows the flexural strength values form the tested NeHoBo in-plane bending sample. The average flexural strength found for all five tested samples is 0.13MPa. Only considering the pre-cracked concrete layer samples give an average of 0.11MPa. Sample TUD_NEH_4-1S, which has an undamaged (no severe crack) concrete layer, has a significantly higher flexural strength, 0.22MPa (Table 3.1). This makes sense since in that case the concrete layer also contributes to the in-plane bending capacity opposite to when the concrete layer is already pre-cracked. Note that for the case of the undamaged concrete layer only one sample has been tested so far.

Table 3.1. Test results from in-plane bending test of NeHoBo floor.

Sample	Flexural strength [MPa]	Direct tensile strength [MPa]†
TUD_NEH_2-2	0.11*	0.08
TUD_NEH_4-2	0.10*	0.07
TUD_NEH_4-1	0.08	0.06
TUD_NEH_4-1S**	0.22	0.15
TUD_NEH_1-1	0.16	0.09
Average pre-cracked samples	0.11	0.075
Average all samples	0.13	0.09

* Flexural strength calculated with bending moment at crack location outside the two loading points.
** No pre-crack in the concrete layer and the sample is 1/8 shorter compared to the other samples
† Derived from in-plane bending test flexural strength results.

The direct tensile strength is derived by using the force-displacement curve on a logarithmic scale. The point of deflection in the graph indicates the transition from elastic to plastic deformation. Meaning cracks are forming in the sample and the related strength at that moment can be considered as the direct tensile strength. The average direct tensile strength of all five tested samples is 0.09MPa. The ratio of the direct tensile strength and the flexural strength is about 0.69.

3.2. Shear Test Brick-Mortar Interface

In this section the shear test for the brick-mortar interface is described. The test is similar to the triplet shear test on masonry that were performed in 2015-2016 at the TU Delft (Jafari. 2017). In section 3.2.1 a description of the samples and testing procedure is given. Most detailed information can be found in the material tests report of the 2016 TUD test campaign (Jafari. 2017). Slight deviations from this procedure due to the NeHoBo shear sample will be discussed. Section 3.2.2 describes the experimental test results.

3.2.1 Sample Description & Testing Procedure

This shear test provides the shear strength, cohesion and friction coefficient for the NeHoBo floor-system if only the mortar-brick interface is considered (no concrete top layer included). The NeHoBo floor panels from the Zijlvest houses have a concrete top layer. To eliminate the contribution of the concrete top layer from the brick-mortar shear test four cuts are made in the concrete layer above the mortar joint (see Figure 3.13). In this way, the material properties of only the brick-mortar interface are obtained and not an combination of brick-mortar and concrete. In the numerical models described in chapter 4 also interface elements are used. The obtained material properties from this shear test can then be applied to a specific interface, in this case the brick-mortar interface. Eliminating the contribution of the concrete layer could be considered as the low boundary of shear capacity of the NeHoBo floor. Adding the concrete layer can only increase this capacity. Since the presence of a concrete layer and/or the damage state of concrete layer is not always certain it is reasonable to take in this case the worst case scenario which means excluding the contribution of the concrete layer.

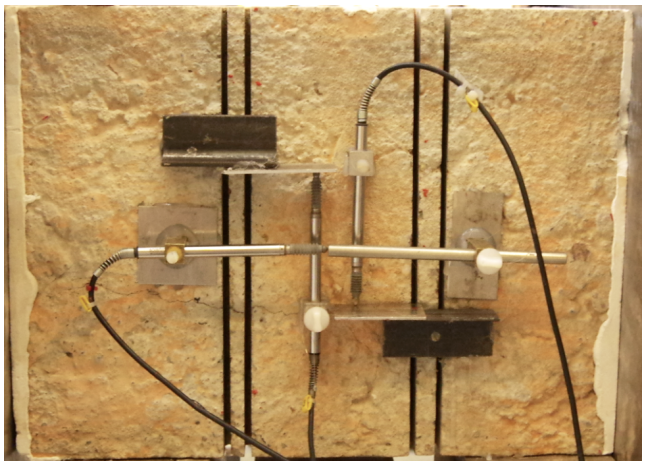

Figure 3.13. NeHoBo brick-mortar shear sample top concrete layer cut above mortar joints to eliminate the contribution of the concrete layer.

The shear samples have dimensions of about 400x300x160mm (excluding the concrete top layer) which is the size of 3 NeHoBo bricks including 2 mortar joints. The shear samples are cut out of NeHoBo floor panels (figure 3.14 & Figure 3.2).

Figure 3.14. Shear samples cut from NeHoBo floor panel.

For the shear tests the same test set-up is used as in the 2016 TUD test campaign (Jafari. 2017) (Figure 3.15). By means of a horizontal, manually-controlled jack the pre-compression is applied to the shear sample. A computer-controlled vertical jack applies a displacement to the centre brick of the NeHoBo shear sample.

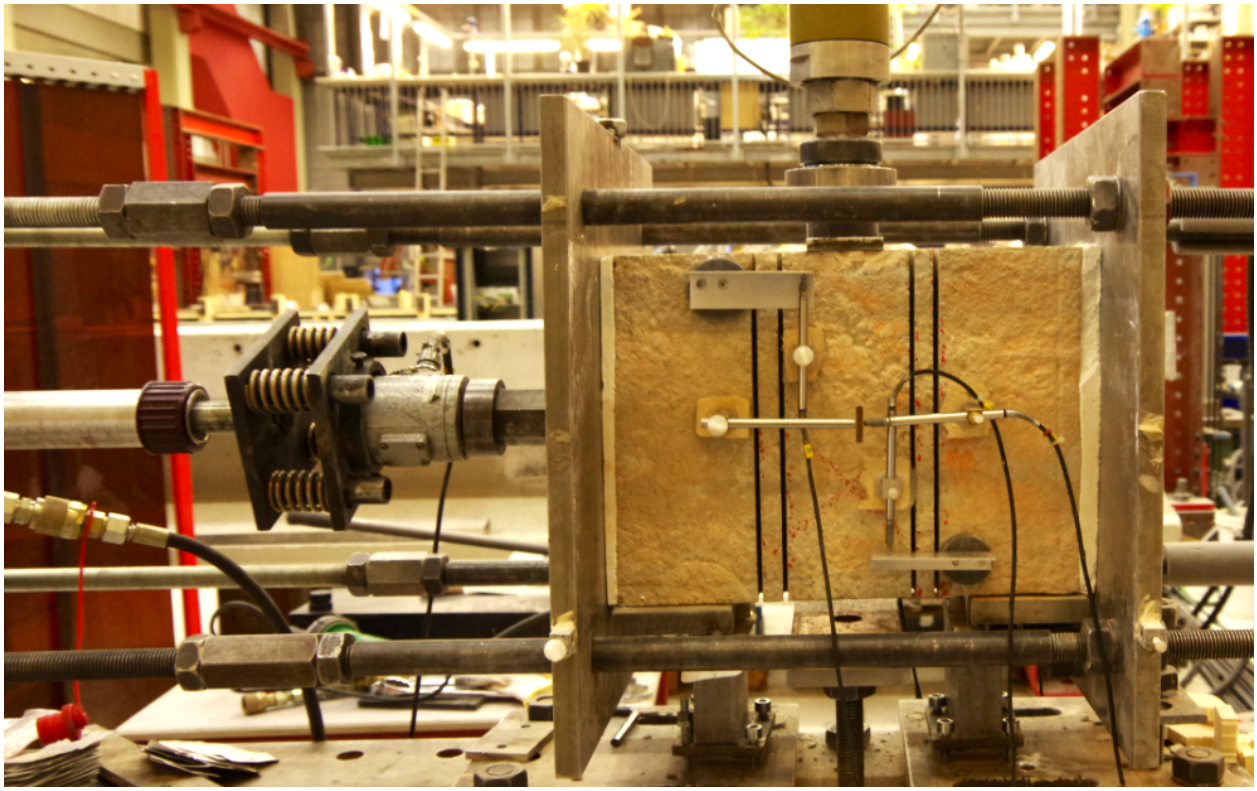

Figure 3.15. Shear test set-up with a horizontal jack (left side) and vertical jack (top side middle section) applying a load on the sample.

3.2.2 Experimental Results

A total of six NeHoBo shear samples are tested with two different pre-compression levels of 0.6MPa and 0.1MPa, respectively. These values are lower compared to the pre-compression used in the 2016 TUD test campaign (Jafari. 2017). The reason is that the NeHoBo shear samples are larger compared to the triplet brick test of 'waalfromaat'. Load capacity limitations of the test setup required to use lower pre-compression levels. The 0.1MPa and 0.6MPa are selected to have sufficient spread in pre-compression levels so later a regression line can be drawn between test results of both pre-compression levels. This regression line indicates the shear strength at zero pre-compression or also known as cohesion. The gradient of the regression line provides the friction coefficient. Two samples tested at 0.1MPa pre-compression showed some issues with keeping the sample stable in the test set-up. The sample started rotating after initial shear strength was reached. The pre-compression had to be increased to 0.6MPa to have a stable situation after the initial shear strength was reached, indicated with (0.6) behind the sample name.

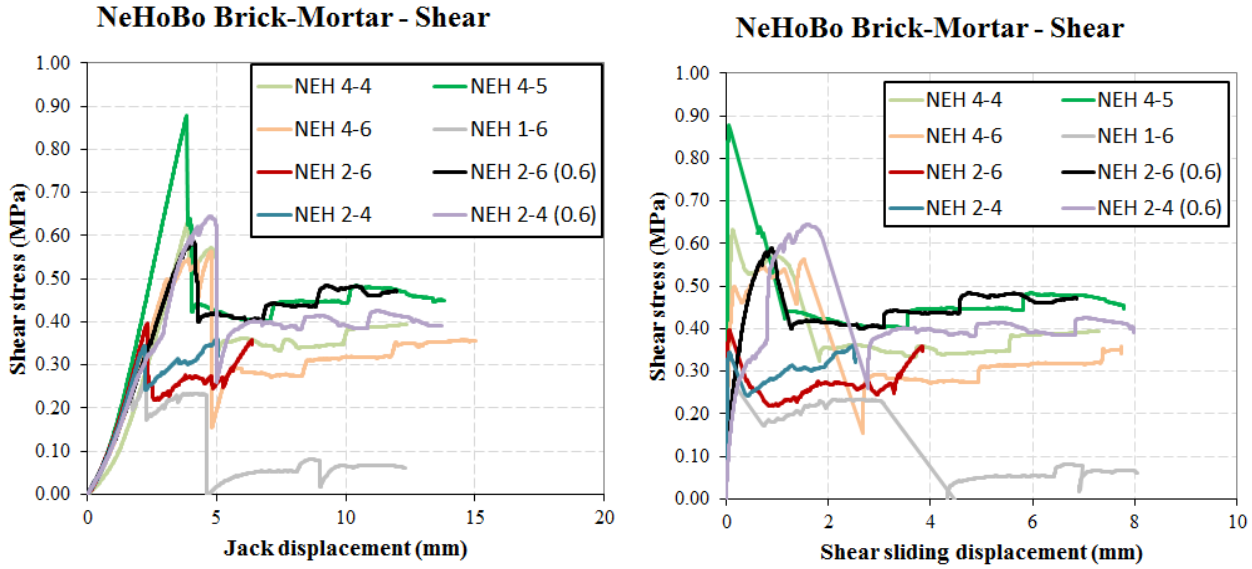

Figure 3.16. Shear stress-displacement : (Left) relative displacement of the jack; (right) relative displacement of the central brick from displacement sensor readings.

Figure 3.16 shows the shear test results of the NeHoBo brick-mortar interface shear samples. The displacement is presented both for the jack and the displacement sensors on the sample itself. Table 3.2 shows more clearly the shear strength of each sample in combination with the applied pre-compression.
Figure 3.17 is a plot of Table 3.2 in which a regression line is plotted to determine values for the cohesion and friction coefficient. The cohesion value for the tested NeHoBo floor samples is 0.27MPa and the friction coefficient is 0.66.

Table 3.2. Shear test brick-mortar shear strength results of NeHoBo floor-system.

Sample	Pre-compression [MPa]	Shear strength [MPa]
TUD_NEH_4-4	0.60	0.63
TUD_NEH_4-5	0.60	0.88
TUD_NEH_4-6	0.60	0.56
TUD_NEH_1-6	0.10	0.26
TUD_NEH_2-6	0.10	0.40
TUD_NEH_2-6 (0.6)	0.60	0.59
TUD_NEH_2-4	0.10	0.34
TUD_NEH_2-4 (0.6)	0.60	0.65

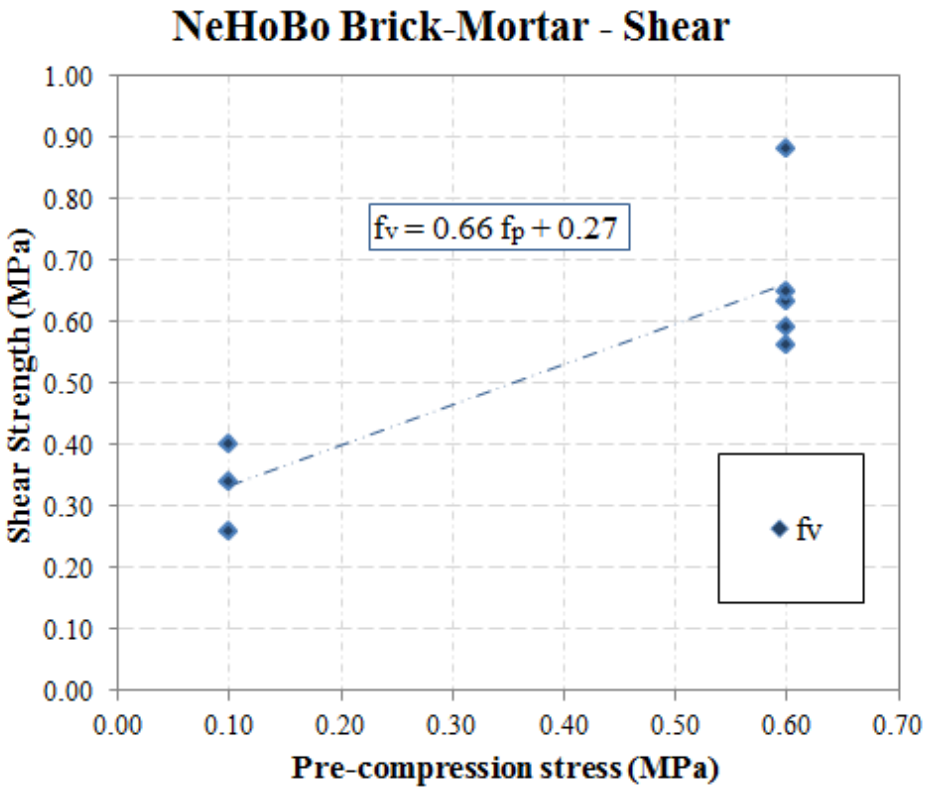

Figure 3.17. Pre-compression vs Shear strength resulting in a friction coefficient and cohesion value for the tested NeHoBo brick-mortar shear samples (fv=shear strength, fp=pre-compression stress).

All six tested samples showed the same failure mechanism. The bond between mortar and brick shears off showing details of the brick (ribs) clearly in the mortar (figure 3.2 right) indicating a clean debonding at the interface of the mortar and brick. In Figure 3.18 some damage to the brick is visible caused by local stress due to the application of the vertical load to the middle brick.

Figure 3.18. Sample 4-5

Figure 3.19 shows cracks on the plaster on the non-concrete side of the NeHoBo floor. It was noticed during the preparation of both in-plane bending and shear samples in the test set-up, that the plaster is very poorly bonded to the NeHoBo floor; it could usually be removed by hand. Therefore, it can be assumed that the plaster layer has no significant contribution to the load bearing capacity of the NeHoBo floor.

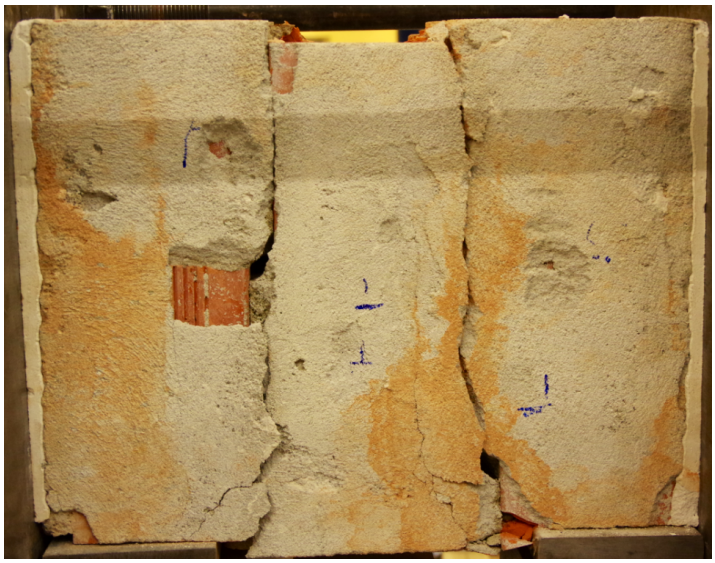

Figure 3.19. Sample 4-6

3.3. Density Measurement of NeHoBo Floor-System

Single bricks are cut from the NeHoBo floor panels as can be seen in Figure 3.20. The single cut-out brick could be considered as a unit cell having half a bed joint on both side, head joint on one side and including the top concrete layer. Four of these single NeHoBo floor bricks are used to measure the density of the NeHoBo floor. Table 3.3 shows the mass and dimensions of the four single bricks resulting in the corresponding density of the NeHoBo floor.

Figure 3.20. Single brick cut from NeHoBo floor panel.

Table 3.3. Density measurement of NeHoBo floor-system.

Sample	Mass [kg]	Length [mm]	Width [mm]	Tickness [mm]	Density [kg/m3]
1	10.67	294	117	188	1650
2	10.94	298	118	188	1655
3	12.33	304	128	188	1685
4	12.09	295	129	190	1672
				Average:	1666

3.4. Discussion of Experimental Results

The most critical parameter in the characterisation of NeHoBo floors is their tensile strength in the direction perpendicular to their span (perpendicular to the rebar direction). As in masonry, where cracks can easily propagate horizontally through the bed joints, in the NeHoBo floor, cracks propagate longitudinally between the mortar and brick. It would seem that the bond between the mortar and the bricks is weak, leading to a low resistance to tension. Poor masonry is characterised also by weak values of brick-mortar bond (see table A.1 in the appendix).

During the in-plane bending test, flexural strength values of around 130 kPa were found. Direct tensile strength values have been derived from the force-displacement curve by determining the point were the elastic behaviour finished (approximately two-thirds of the flexural value). Considering only the four samples where the concrete top layer was noticeably damaged, an average of 75kPa as direct tensile strength is obtained, with a standard deviation of 11kPa. The conservative 5% characteristic from these four samples results in 55kPa.

Nevertheless, this does not take into account the potential contribution of the concrete top layer as it is highly unlikely that this is cracked longitudinally over every joint. Moreover, it is important to realise that the samples have been extracted from a donor house, a procedure which may have produced stresses in the sample, and that the samples have been transported and further cut into the tested specimens. All of these factors could reduce the capacity of the samples. In this light, the characteristic value of 55kPa is conservative.

Chapter 4

Computational Models for NeHoBo Floor-systems

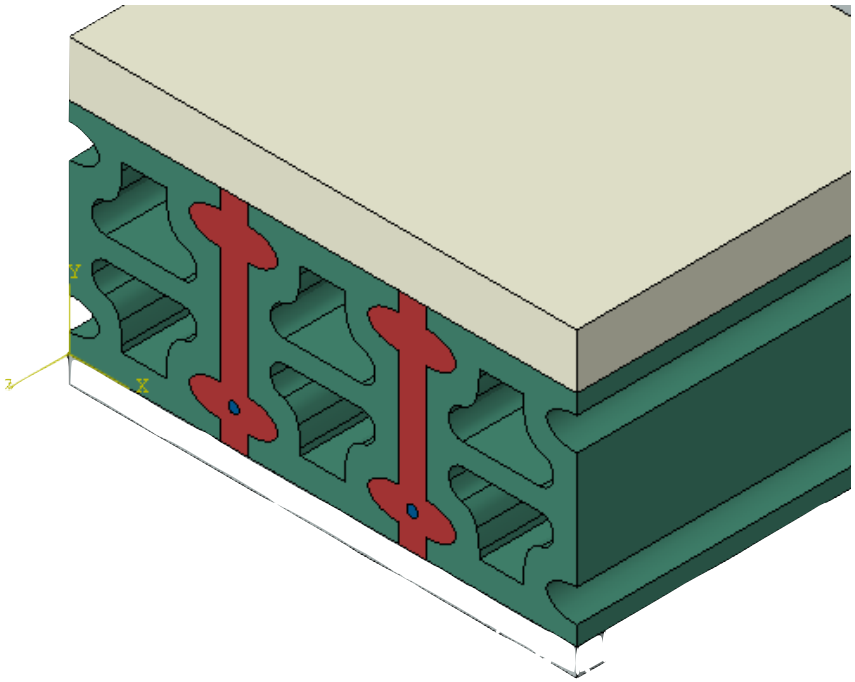

TU Delft

4. Computational Models for NeHoBo Floor-systems

Along with testing in the laboratory, the floor system and its components were analysed with numerical and analytical models. Computational models were run to gain insight into the laboratory tests and determine whether they would output the required material properties for the models, allowing to focus on obtaining the most influential properties. The models were also used to improve the understanding of the floor system and assess its failure mechanisms. Finally, in this preliminary report, the models were continuously adapted to better reflect the observations made in the laboratory.

The models were elaborated at various levels depending on the scale and complexity of the model. Similar model scales as for masonry are used: micro models, detailing individual bricks and mortar joints; meso models, detailing the connections between bigger components but using a composite material without distinguishing individual bricks; and macro models, incorporating entire structures.
This study will utilise primarily meso-level models for the floor system and entire structures. Insight into the behaviour of tests and relationships between the properties of the components and the composite will be studied with micro models. Table 4.1 provides an overview of the models.

First, the micro models are presented, illustrating the relationships of the components and the local failure mechanisms that govern the strength of the floor as a composite.
Secondly, models of the floor are described. These models incorporate the floor as an equivalent material (that is, without differencing the individual components such as bricks and mortar) and its interaction with the boundaries provided by the supporting walls. Here, four types of floor models are studied: a first with individual masonry plates including the top concrete later; a second with the concrete layer as a separate component to the plates; a third, where the concrete layer is neglected and each line of bricks is modelled as a strip where the connection between bricks is achieved via interfaces; finally, a fourth model with plane-stress elements in DIANA FEA is used to cross-validate the results.
Thirdly, two variants of a house model are studied. First, a model of the houses in Zijlvest is used to estimate the forces to which the floor and its connections are subjected to during earthquake motions. Next, a model of the first TU Delft laboratory house (Esposito, 2016a) is used to assess the influence of NeHoBo floors on the response of the original structure that employed stiff concrete floors.

Finally, analytical models (hand calculations) are performed to better understand and verify the outcomes of the numerical models.

Table 4.1. Overview of computational models.

Micro Models	Floor Models (Meso level)	House Models (Macro level)
In-plane bending test	Composite plates (1)	Zijlvest House
Shear test	Independent concrete layer (2)	First TU Delft laboratory house with NeHoBo floors
Out-of-plane bending test	NeHoBo strips (3)	
	2.5D Plane Stress (4)	

4.1. Material Properties

The floor system and its elements need to be characterised for the models. The macro material (composite), its components and their interaction, and the interaction with other building elements need to be known.

4.1.1. Materials

The NeHoBo floors are composed of bricks, mortar, concrete, and rebar. Because of their assembly into a single component, the NeHoBo floors are anisotropic. The material can be characterised for each individual component and for the composite, see table 2.1.

The bricks were measured to be 160mm tall and 110mm in width. The concrete layer on top is 30mm thick for a total slab thickness of 190mm. The longitudinal joints are 20mm in width. For a more precise characterisation, see chapter 3.

The rebar has been measured to be 8mm in diameter occurring at every longitudinal mortar joint in the bottom of the slab, and at alternating joints at the top (see figure 1.2). The rebar is ribbed, though the height of the ribs is yet to be determined.

Table 4.2. Estimates for material properties.

Material	Type	Young's Modulus	Poisson ratio	Density	Tensile Strength	Fracture Energy in Tension (Mode I)	Softening	Compressive Strength
Brick	Quasi-brittle	8 GPa	0.15	2000 kg/m^3	3 MPa	500 N/m	Linear	30 MPa
Mortar	Quasi-brittle	5 GPa	0.15	2100 kg/m^3	1.4 MPa	10 N/m	Linear	10 MPa
Concrete	Quasi-brittle	10 GPa	0.15	2300 kg/m^3	1.4 MPa	10 N/m	Linear	15 MPa
Rebar	Elasto-Plastic	200 GPa	0.3	7800 kg/m^3	350 MPa	N.A.	N.A.	N.A.
NeHoBo* (longitudinally)	Quasi-brittle	2 GPa	0.15	1700 kg/m^3	0.2 MPa	50 N/m	Linear	15 MPa
NeHoBo* (transversally)	Quasi-brittle	2 GPa	0.15	1700 kg/m^3	0.2 MPa	20 N/m	Linear	15 MPa
Wall**	Quasi-brittle	2 GPa	0.15	2000 kg/m3	0.2 MPa	100 N/m	Linear	N.A.

Shaded cells indicate estimates pending laboratory tests at the time of modelling.
* Without the steel reinforcement. **Considering masonry values for the failure mechanism of vertical cracks.

Original brochures from the manufacturer detail some of these properties, for instance, the steel quality for the rebar and the compressive strength of the brick material (not the hollow bricks themselves). The remaining properties are estimated based on recent tests on masonry properties such as brick and mortar tensile strength (see attached table A.1), and some preliminary results of the laboratory tests.

4.1.2. Interfaces

The composite is held together by the bond between bricks, mortar and concrete. This bond can be characterised by its tensile strength, cohesion, and friction (Mohr-Coulomb failure surface). Depending on the level of mesh refinement of the contact surface, the shape of the bricks and ribbed surface (see figure 1.2) can be included in these values: a flat surface will use higher values to account for the actual, greater contact area.
The connection between pre-fabricated panels (plates) is also relevant when modelling the floor.

Moreover, the behaviour of the floor depends on its connection to neighbouring structural elements, in particular, the walls that support them. As such, the interface between the floor plates and the supporting walls becomes important.

Initial estimates for these interfaces are provided next (see table 2.2) based on recent masonry tests (see annexed table), in particular bond wrench tests and shear tests.

Table 4.3. Interface characteristics for connections between components.

Material 1	Material 2	Bond Strength	Cohesion	Friction Coefficient	Fracture Energy in Tension (Mode I)	Softening	Normal Stiffness	Tangential Stiffness
Brick	**Mortar Concrete**	0.2 MPa	0.4 MPa	0.7	20 N/m	Exponential	100 GPa/m	60 GPa/m
Plate	**Plate**	0.1 MPa	0.15 MPa	0.6	10 N/m	Exponential	100 GPa/m	60 GPa/m
Plate	**Wall**	0.1 MPa	0.15 MPa	0.6	10 N/m	Exponential	100 GPa/m	60 GPa/m
Plate*	**Plate***	0 MPa	0 MPa	0.5	N.A.	N.A.	100 GPa/m	60 GPa/m

*Assuming no cohesion.

The values assumed are conservative when considering that the bricks have ribbed surfaces which could significantly increase the bond values measured in recent masonry tests.

4.2 Computational Models With Abaqus (Explicit)

Highly non-linear behaviour is expected when modelling the failure mechanisms of the NeHoBo floor system. Because of this, explicit solving of non-linear models is preferred, this is done with "Abaqus". Models solved implicitly are conducted in DIANA FEA.

4.2.1. Micro Models

To gain additional insight into the local failure mechanisms of the floor system and better design and understand laboratory tests, micro models are being explored. The micro models discretise the individual components of the floor-system and the bond between them (see figure 4.1).
The main goal of the micro models is to understand failure mechanisms and select the relevant properties for the composite material models.

A few micro models have been produced so far: a short model loaded out-of-plane as a proof of concept, a model resembling the four-point in-plane bending test to be performed in the laboratory, and a model of the in-plane bending test. The shear test was no reproduced because its behaviour was deemed straight-forward.

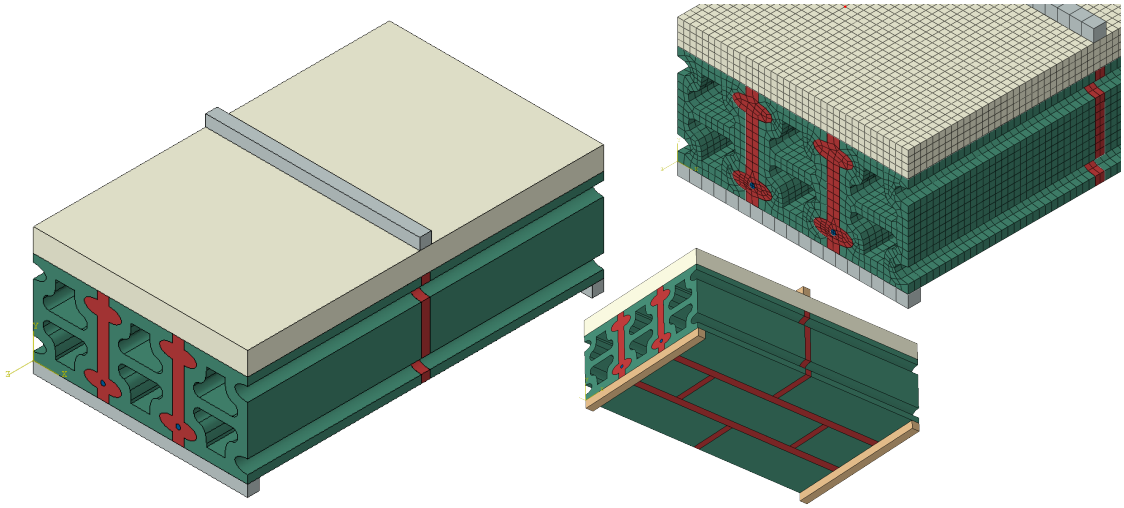

Figure 4.1. Detail available in the micro model; top right, model mesh.

Proof of Concept

The model shown in figure 4.1 was deformed by supporting it at the two extremes and pushing it down in the top middle. This lead to cracking at the middle head joints, debonding the mortar from the bricks. The crack continued upwards and broke the concrete top layer (figure 4.2a). Next, a new crack formed at the inner head joints, but did not proceed to the concrete layer (figure 4.2b); instead, the middle brick failed in bending (4.2b). The longitudinal mortar also cracked following the previously mentioned cracks (figure 4.2c). The rebar did not reach its yield strength because its embedded length in the mortar was not sufficient to develop a high force (due to the model being too short). Nonetheless, the model proved the feasibility of the approach, requiring only 3 hours of computation time.

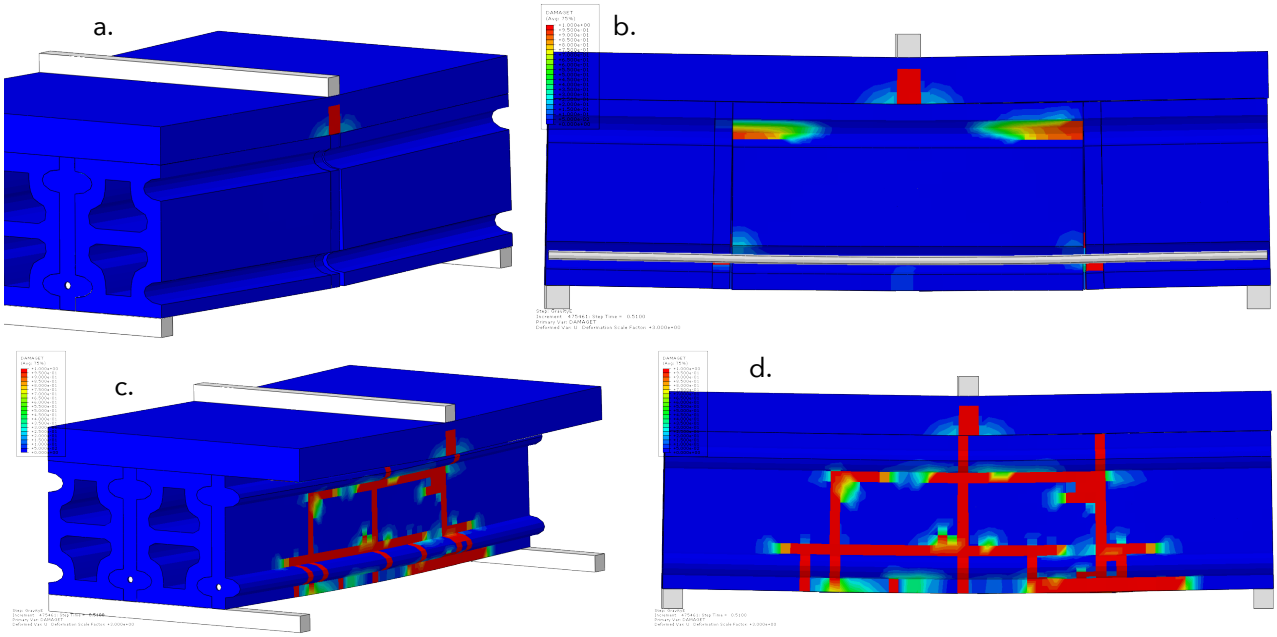

Figure 4.2. Failure mechanism of the out-of-plane, proof-of-concept model.

In-Plane Four-Point Bending Test

One of the upcoming laboratory tests has been implemented with the micro model approach (figure 4.3). Since the rebar is not expected to influence the results much, it was modelled as an embedded element (instead of a solid) so that the model mesh was improved.

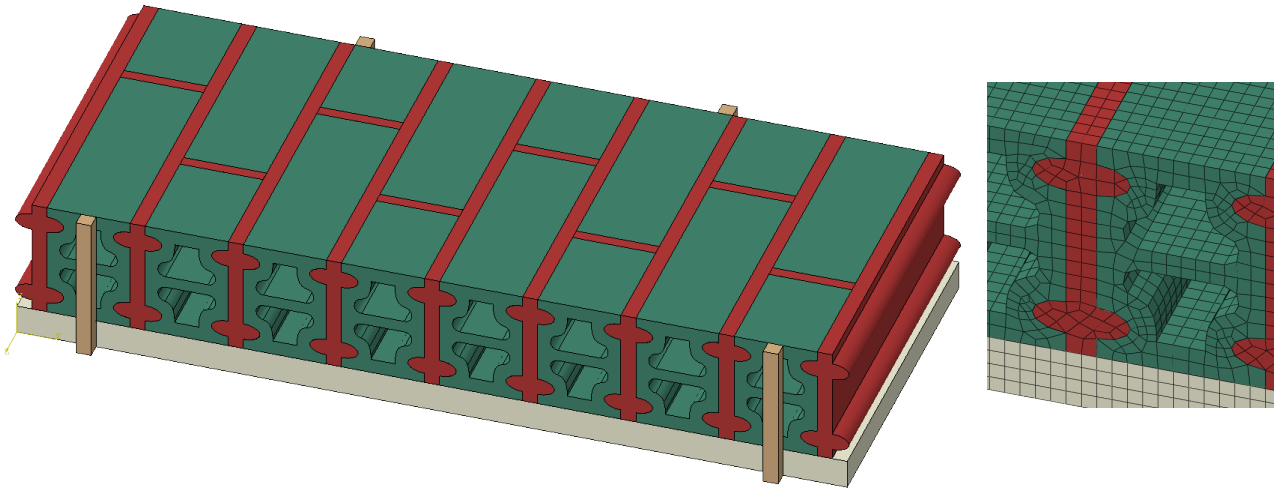

Figure 4.3. Micro model of in-plane bending test. Bottom view.

Failure of the sample occurred at the longitudinal joints in-between the bricks. The top concrete layer, being stiffer, was the first to crack. Then, the crack followed different paths depending on a combination of the mortar stiffness, strength, and bond strength.
If the mortar-brick bond was weak (see table 2.2), failure occurred by debonding of the interface (figure 4.5a). If the interface was stronger (1MPa compared to 0.15MPa), failure occurred by cracking of the mortar (figure 4.5b), but, depending on the stiffness of the mortar, failure would occur at the inlets (figure 4.5c) or through the joint (figure 4.5b). Failures "a" and "c" are expected to be the most prominent.
Whether the crack appears at the middle joint or one joint to the side will depend on the stiffness configuration of the sample; here, modifying the mortar stiffness, lead to a different joint being activated.

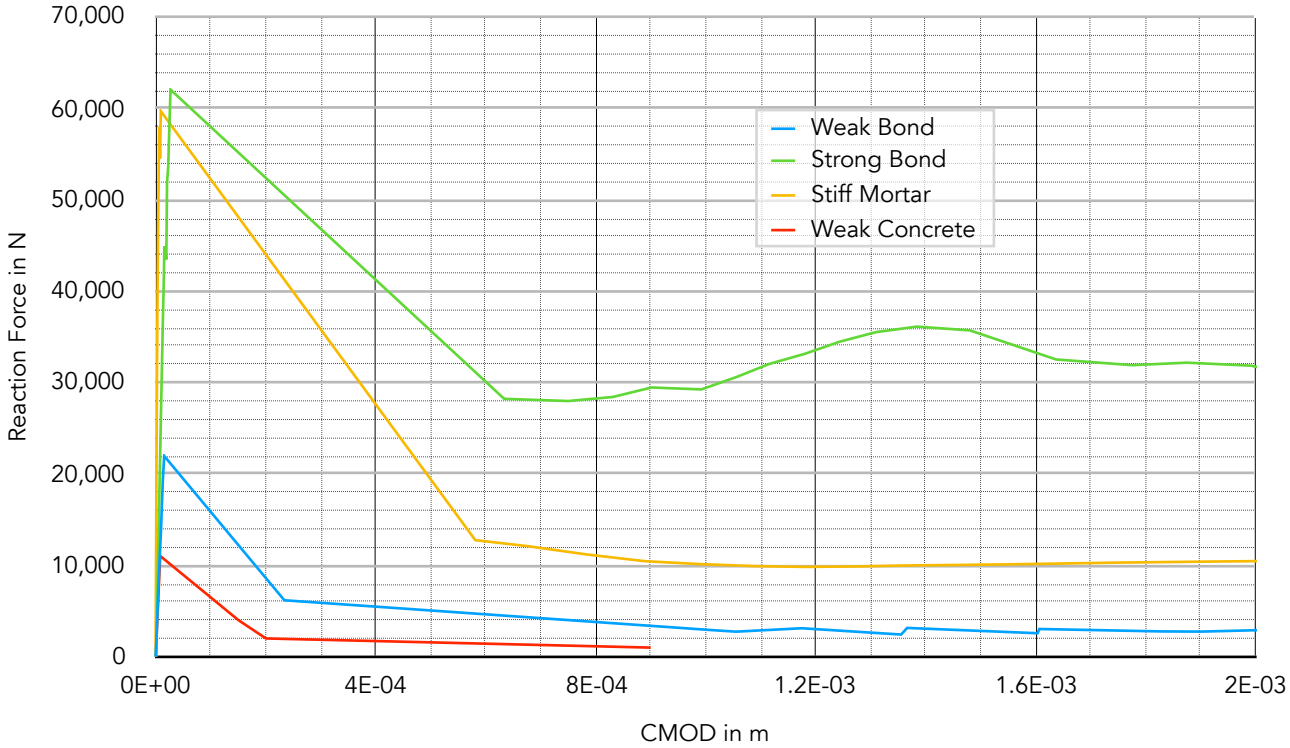

Figure 4.4. Force against crack mouth opening displacement for some variations of the in-plane micro model.

From the preliminary results of some laboratory tests, the bond between mortar and brick seems to be weak. Moreover, the concrete layer is often damaged or, in other NeHoBo configurations, is not present; for this reason, the capacity is expected to be lower, close to the lowest curve in figure 4.4.
One additional model, with a crack on the concrete above a brick, will be conducted.

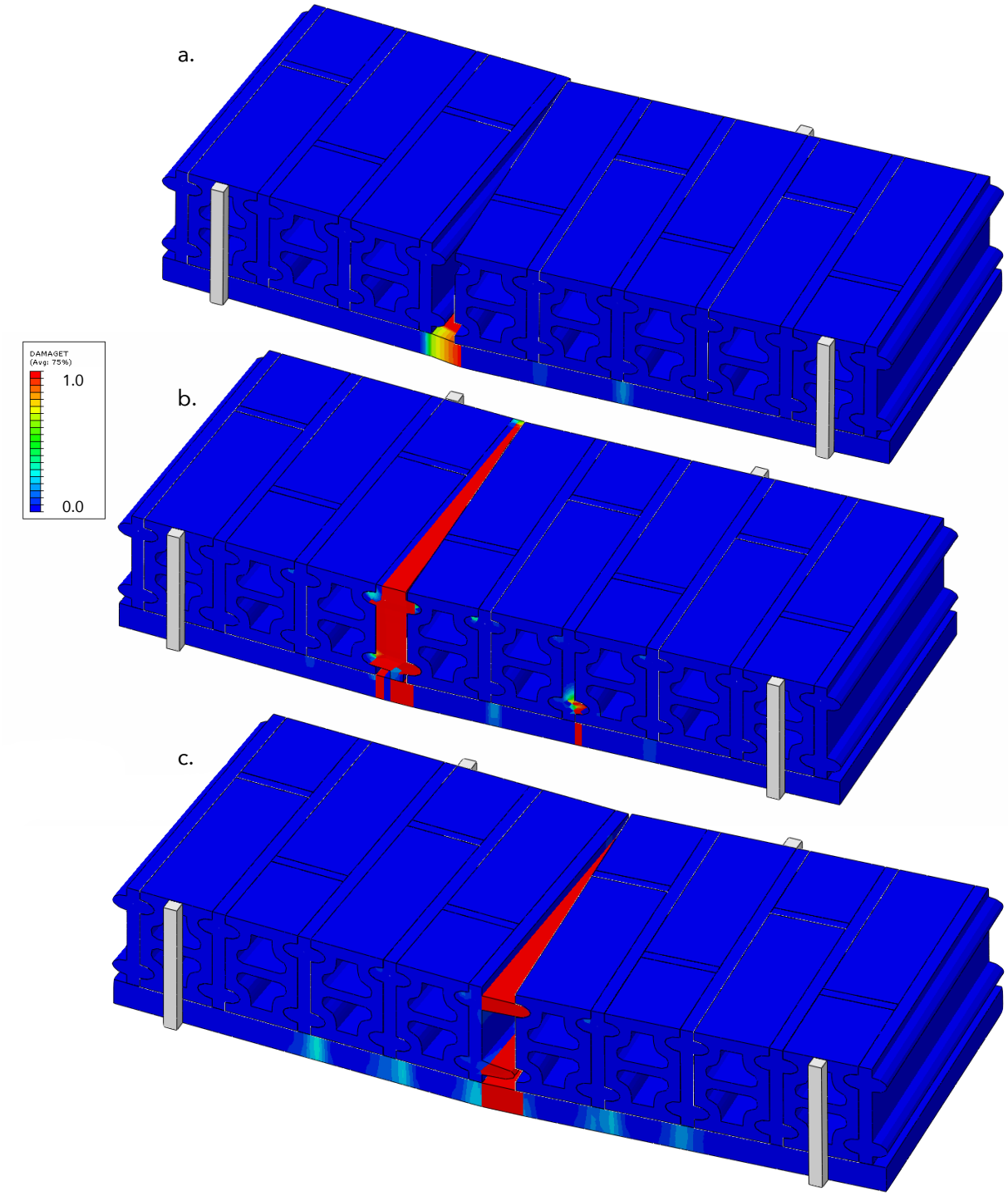

Figure 4.5. Similar failure mechanisms depending on various configurations of bond and mortar strength and stiffness.

It was not possible to foster a crack through the brick without recurring to unrealistic combinations of material properties for the components. It is likely that the concrete layer adhered to the stiffer brick over a longer surface also prevents the brick from cracking. If, however, the mortar was assumed to be twice as strong as the brick material (for masonry, the mortar has usually a fifth of the strength of the brick), then fracture of the bricks was observed (see figure 4.6). This occurred through the weaker centre of the brick (figure 4.6a) and in the zone where shear stresses were also present in the sample. Debonding of the broken part of the brick and then shearing along the longitudinal mortar joint completed the failure (figure 4.6b).

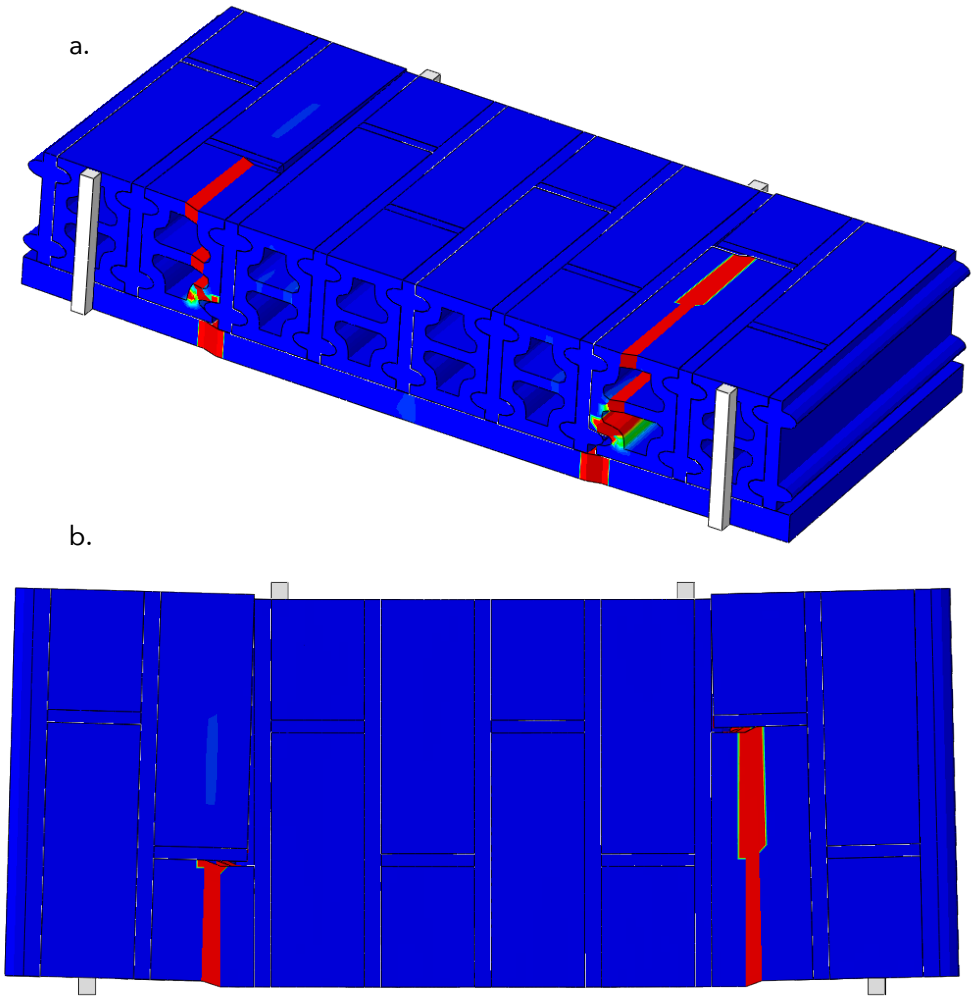

Figure 4.6. Fracture of the bricks when the brick material is weaker than the mortar material.

Out-of-Plane Bending Test

The floors were designed to withstand gravity loads out of plane. They include rebar in the mortar joints to achieve greater bending capacity. The samples fulfilled this function for several decades before they were extracted. Accordingly, a high bending capacity and higher toughness is expected in this test. Figure 4.7 shows the damage and deformation of the sample at peak load.
A simple calculation to compute the bending moment results in a similar capacity as observed in the force-displacement curve shown in figure 4.8. With an arm of 0.15m and a rebar yield force of 17kN per mortar joint, the peak bending moment is around 11kNm for the four mortar joints depicted in figure 4.7. The spacing between the supports, and between the application points of the load, are approximately 1.2m and 0.6m, respectively. This means that to obtain a bending moment of 11kNm, the total reaction force must be 75kN. This is comparable to figure 4.8.

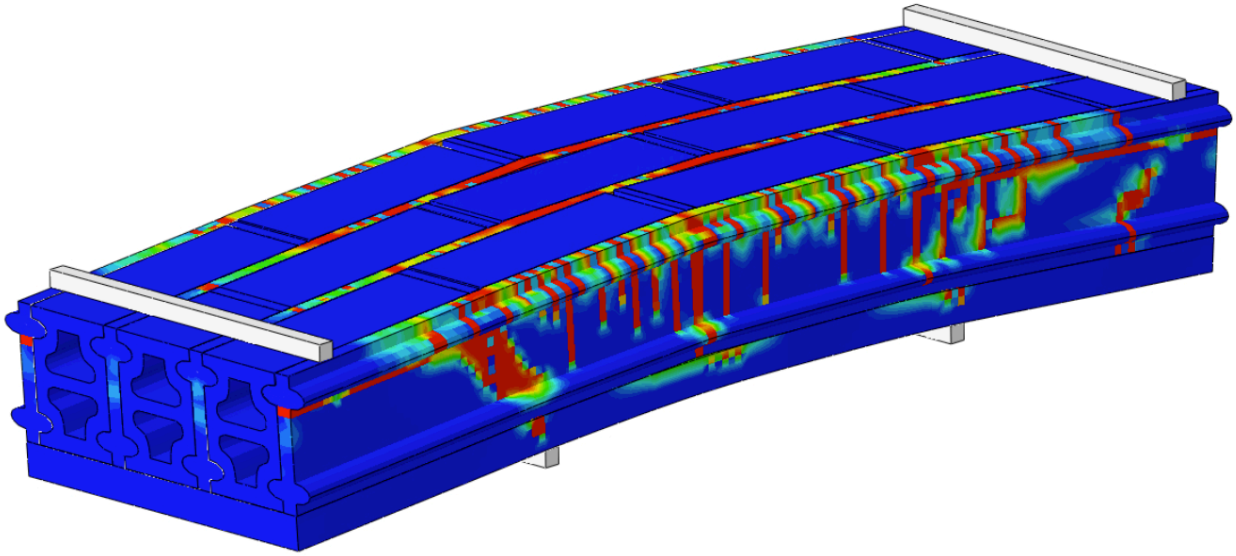

Figure 4.7. OOP bending test at peak load deformation. RC beam-like behaviour is observed.

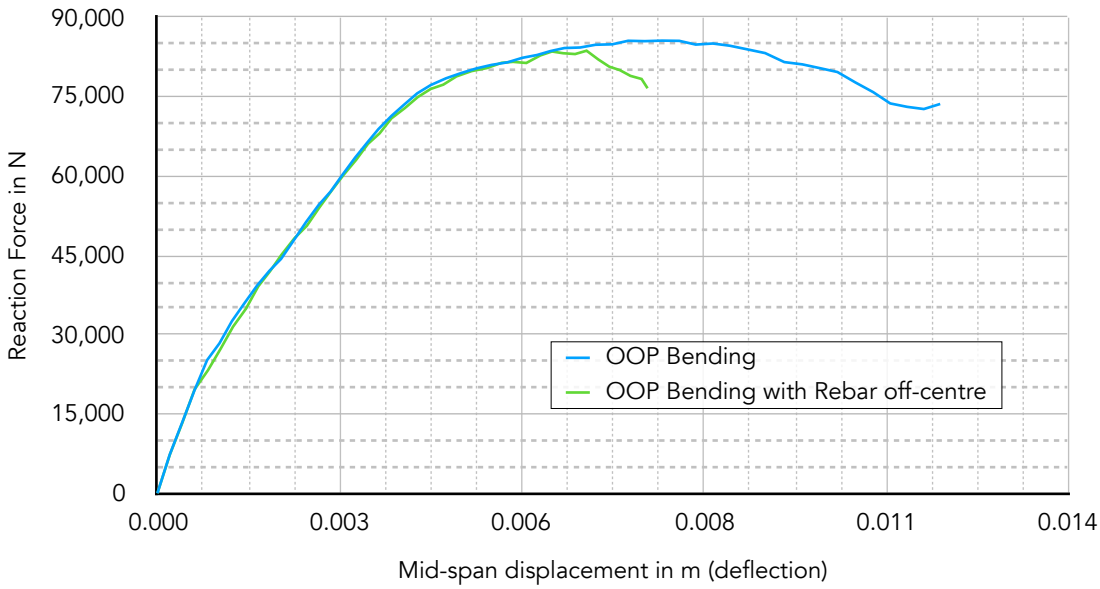

Figure 4.8. Force-displacement curve for the OOP bending test.

Samples in the laboratory were observed to have defects in the placing of the reinforcement. A variation of the model was run with the samples 20mm off-centre; here, the models showed a similar capacity, but reduced toughness.

4.2.2. Meso Models

The behaviour of the floor system as a diaphragm is being studied with a model that incorporates individual plates with composite material properties, and wall stubs to provide realistic boundary conditions to the floor (see figure 4.9).
Non-linear composite material properties are used for the plates and for the wall stubs (see table 2.1). The interface between each plate and between the plates and the walls is also non-linear (see table 2.2).

Model 1 - Composite Plates

Each plate is 1.10m wide and 4.40m long. The entire floor is then 4.4x6.6m^2. This results in a ratio identical to the Zijlvest donor houses, but with a smaller area which allows for faster calculation times. The wall stubs are 100mm in width and 400mm tall.
These models are used to get insight into the expected failure mechanisms and are the first step for producing a more refined model (see next subsection).

To simulate realistic boundary conditions, an overburden of 0.15 MPa is applied at the top wall stubs (simulating the weight of one level of walls, another floor and a roof) and a load of 2 kN/m^2 is present on the floor plates additional to the self-weight. This guarantees a normal stress between the plates and their supports. Further, to adequately withstand the gravity loads and considering the low tensile strength of the NeHoBo composite material (see table 2.1), the plates are embedded with rebar in their longitudinal direction.

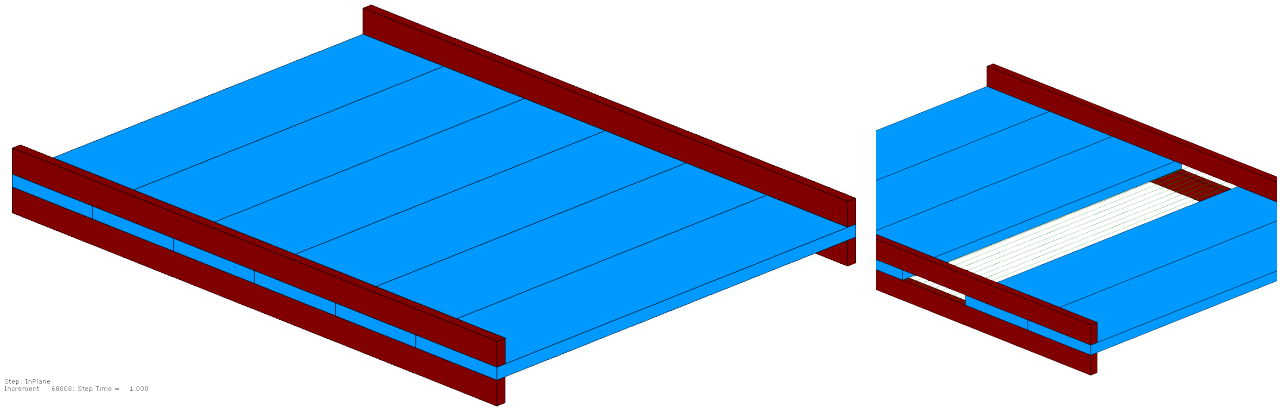

Figure 4.9. Meso model of the floor system with six plates (blue) and four wall stubs (brown). Right, one plate is hidden to show the direction of the embedded reinforcement.

The floor system is then subjected to gravity loads in combination with in-plane loads to simulate stresses and failure from diaphragm action. The models require 15 minutes of computation time.

A brief, graphical overview is presented next.

Gravity Loads (Out-of-Plane)

The self-weight and load on the plates causes vertical deflexions typical of simply-supported slabs. For the assumed loads, the computed deflexion is 11mm (see figure 4.10). For the span of 4.4m, this corresponds roughly to a ratio of 1/400 which is in agreement with deflexion ratios recommended by building codes. Note that if the plates are used for longer spans, the deflexion will increase.

For slabs containing rebar, it is typical for tensile cracks to occur, transferring the tensile loads on the bottom of the plates to the reinforcement. Such cracking appears to be present in the modelled slab and should be acceptable for its normal behaviour (see figure 4.11).

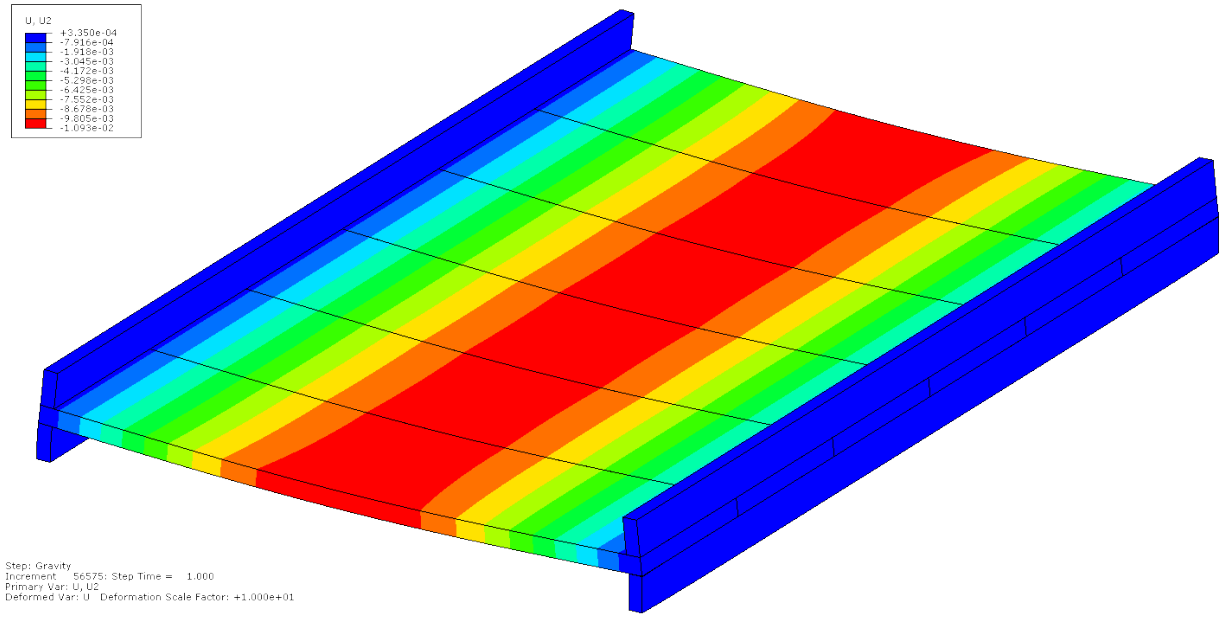

Figure 4.10. Deformation due to gravity loads. The maximum deflection is 11mm (red, center). Deformed shape is magnified by 10.

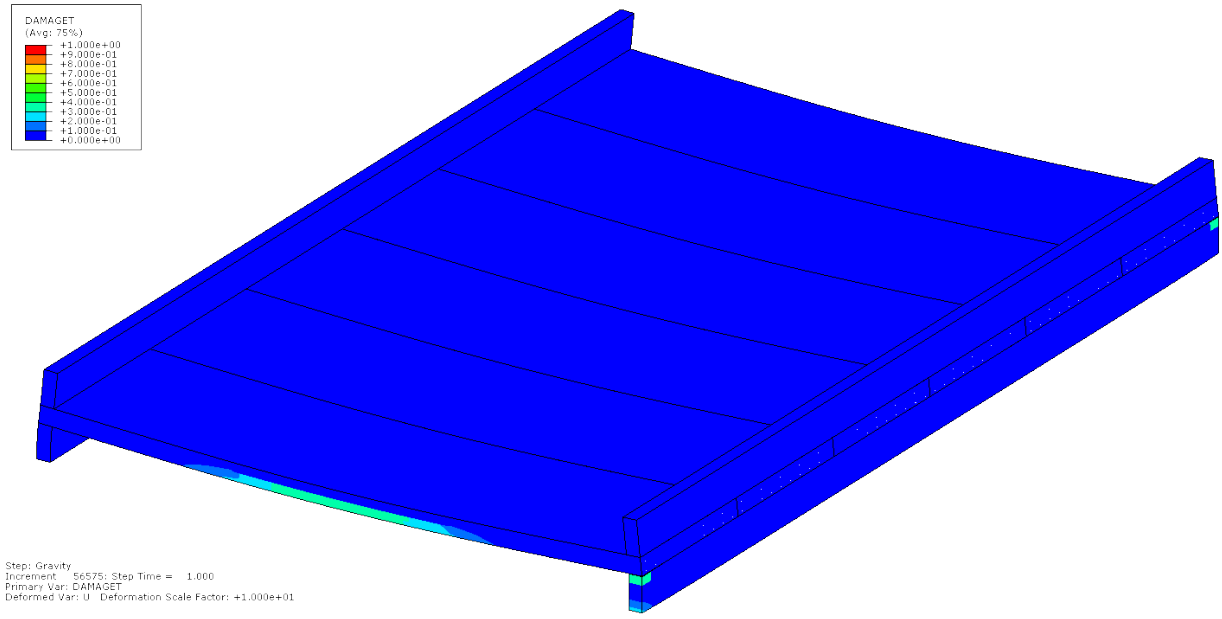

Figure 4.11. Zones with tensile cracks. Minor cracking is visible on the bottom side of the plates at the mid-span.

The load on the plates was increased steadily until their collapse. The collapse load was found to be around 20 kN/m^2 in total, corresponding to a safety factor of 3.7. This high value is probably due to the fact that the slabs' design was set for a free span of 5.30m.

Nonetheless, the out-of-plane behaviour of the model is as expected.

In-Plane Loads

The floor was then subjected to varying in-plane loads and varying boundary conditions.

First, the wall stubs on one side underneath the floor were restrained longitudinally, as if connected to a rigid longitudinal wall, and the floor plates were pushed in-plane at the other side. See the sketch in figure 4.12.

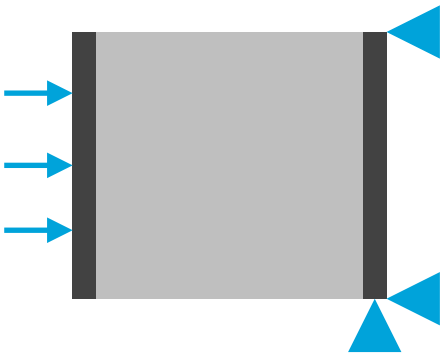

Figure 4.12. Sketch of in-plane loading.

The load was increased until failure. The capacity was measured to be around 10 kN/m. Failure occurred by sliding of the floors above the restrained wall. See figure 4.13. No opening or sliding between the plates was measured.

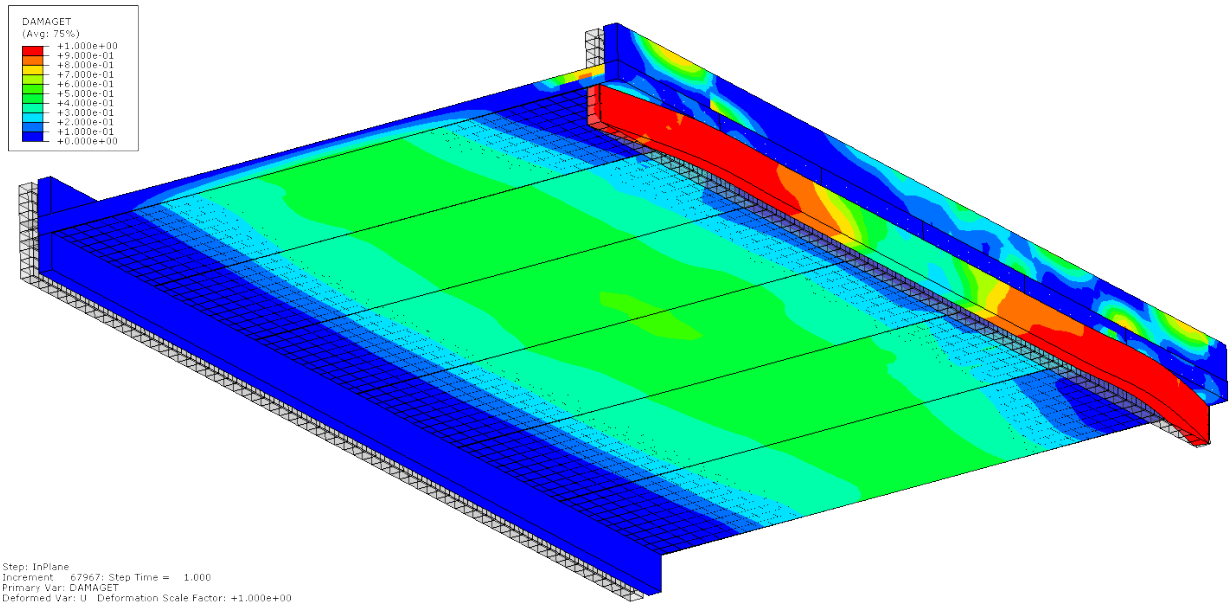

Figure 4.13. Bottom view. Sliding of the plates over the supporting wall, with out-of-plane movement of the wall.

The analysis was redone for the case of no cohesion between floor plates, but results were similar. The overburden on the top wall stubs was also removed in a subsequent analysis, but no opening or sliding apart of the plates was seen.
It would seem that if the friction and cohesion between plates and walls is broken, the plates move together and slide over their supporting wall.

An additional variation was run where the floor plates themselves were restrained (model boundaries were applied to the floor elements). This is **not** a realistic assumption as in reality the floors are resting over the walls, and if there is some longitudinal restrain, this is provided by the lateral walls which are not connected to the floors. In fact, in some building practices (and it seems this was the case for the Zijlvest houses), the non-load bearing walls (the lateral walls) are continuous and run outside the floor plates.
Nonetheless, if the floors are restrained, opening of the plates can be observed. The capacity is approximately three times greater than the slide-over mechanism. This is observed in figure 4.14.

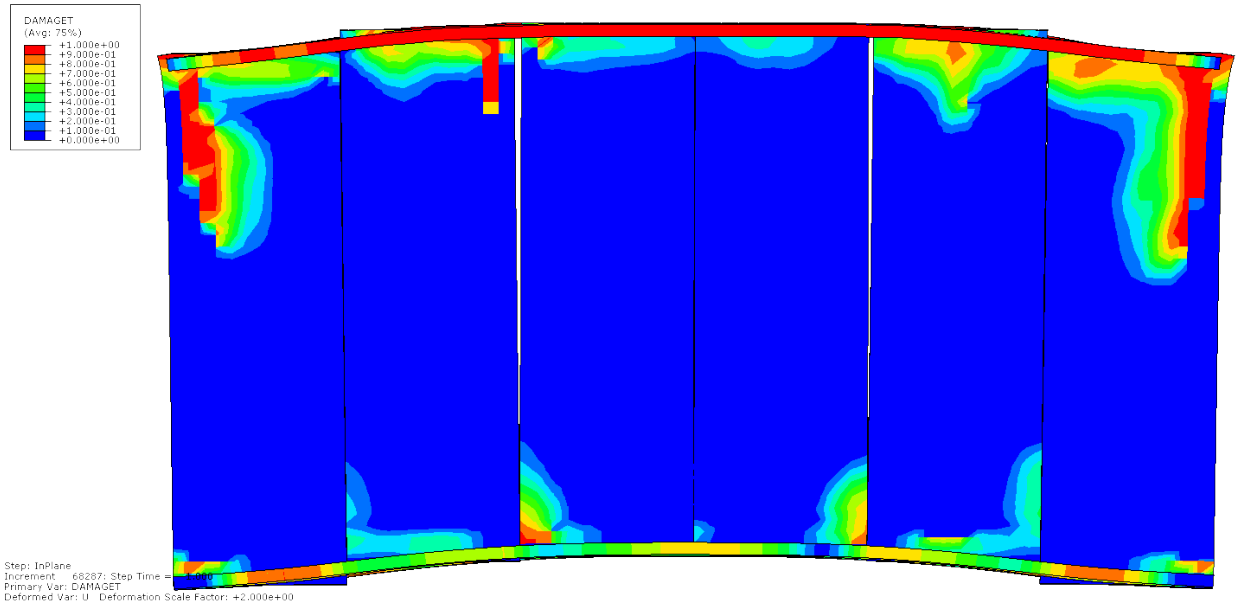

Figure 4.14. Top view of non-realistic restraint on the floors causing plate separation. Deformed shape magnified by two. Red shows zone with tensile cracks.

Other variations such as: pushing with an in-plane load following a parabolic distribution with a high point in the centre of the span, a uniform load pushing only on the first three plates, and making permutations of these with and without cohesion between the plates; all yielded sliding over the supports without opening up of the floor.

Additionally, the floors were loaded in in-plane shear, that is, transversally to the direction of the plates. See figure 4.15. This situation is unlikely to occur in the house, because the load-bearing walls are stiff. Nonetheless, the capacity and failure mechanism were observed.

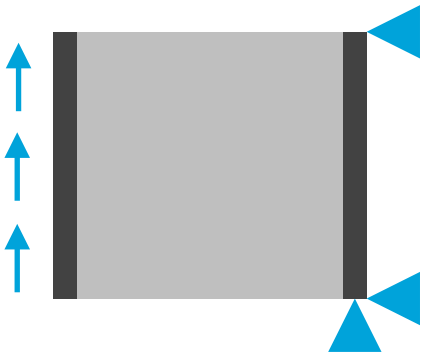

Figure 4.15. Sketch of in-plane, transversal loads.

In this case, again sliding over the supporting walls was observed; however, if the cohesion between the plates was neglected, the failure followed a combination of sliding over the walls and in-between the plates. See figure 4.16.

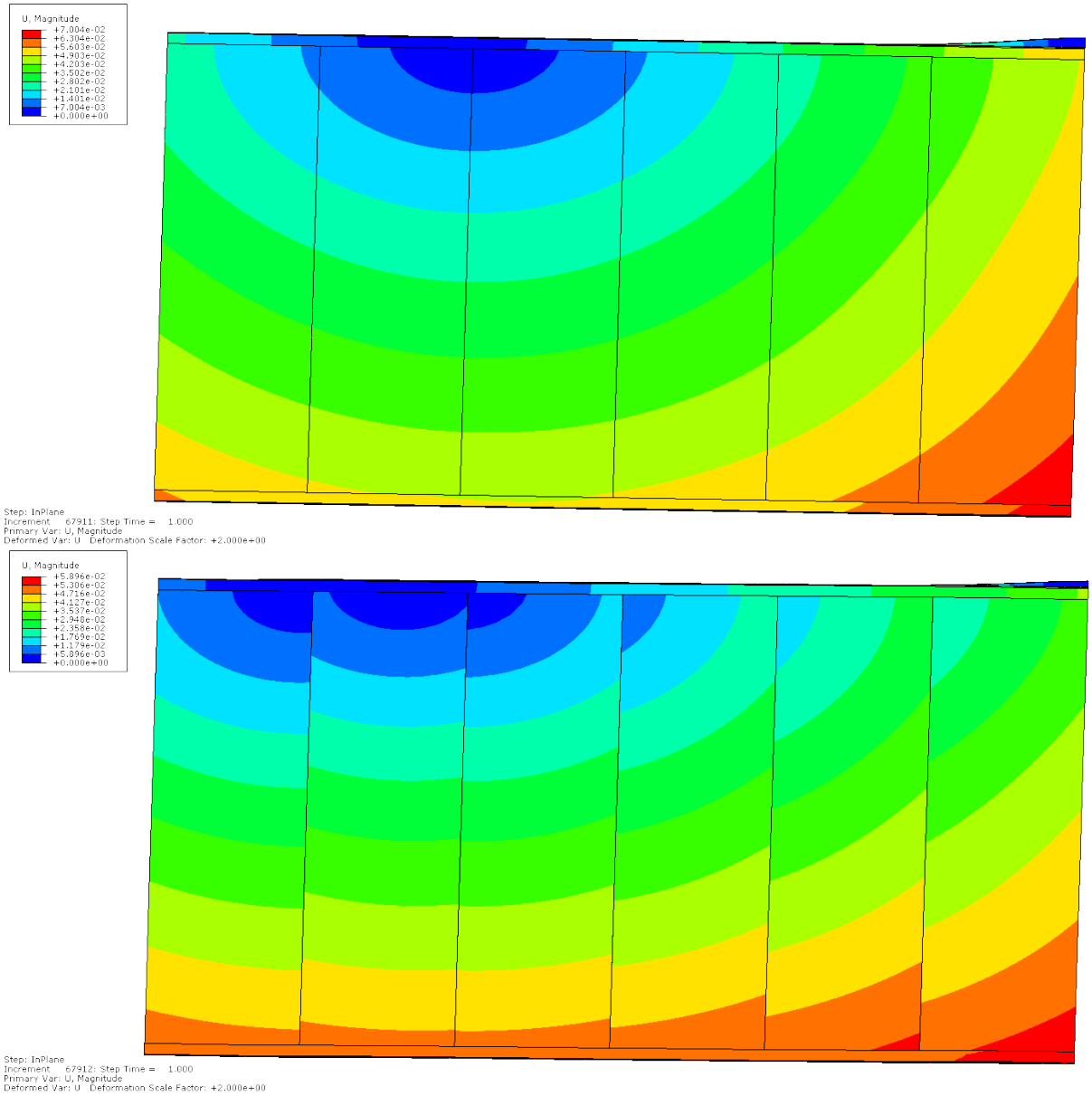

Figure 4.16. Deformation from shear load in-plane. Top, with cohesion between plates; bottom, without cohesion.

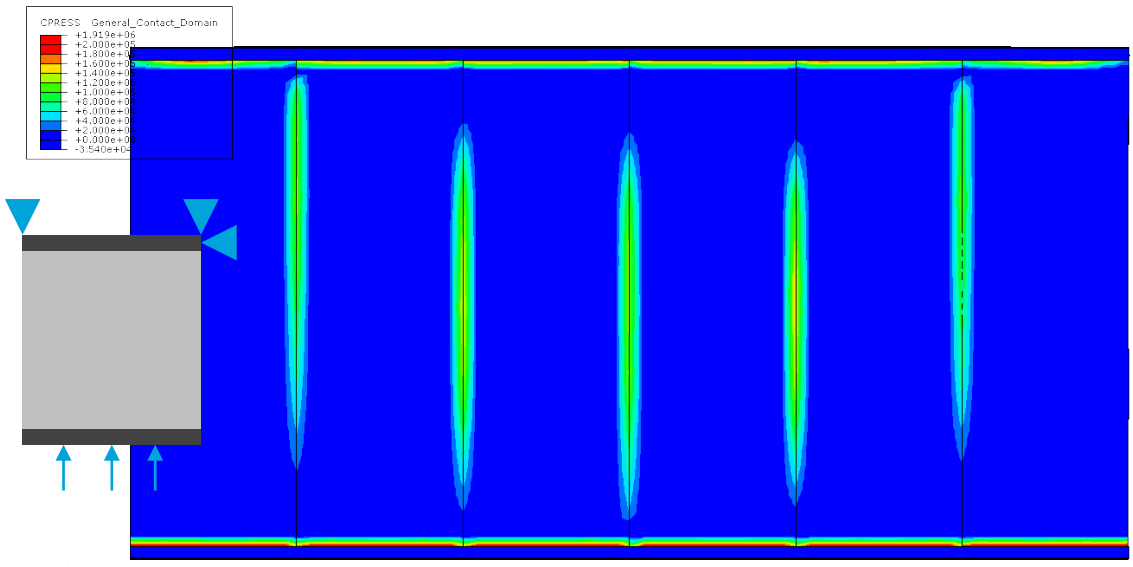

Figure 4.17. Contact stresses in between the plates reveal the expected compression arch.

Finally, to simulate additional (realistic) restraints at the corner of the floors, perhaps due to ties to the lateral walls, longitudinal stubs were incorporated in the model (see figure 4.18). Nevertheless, the predominant failure was still slide-over of the floors, though in the case without cohesion between the plates, some sliding between the plates at the sides was also visible (figure 4.18).

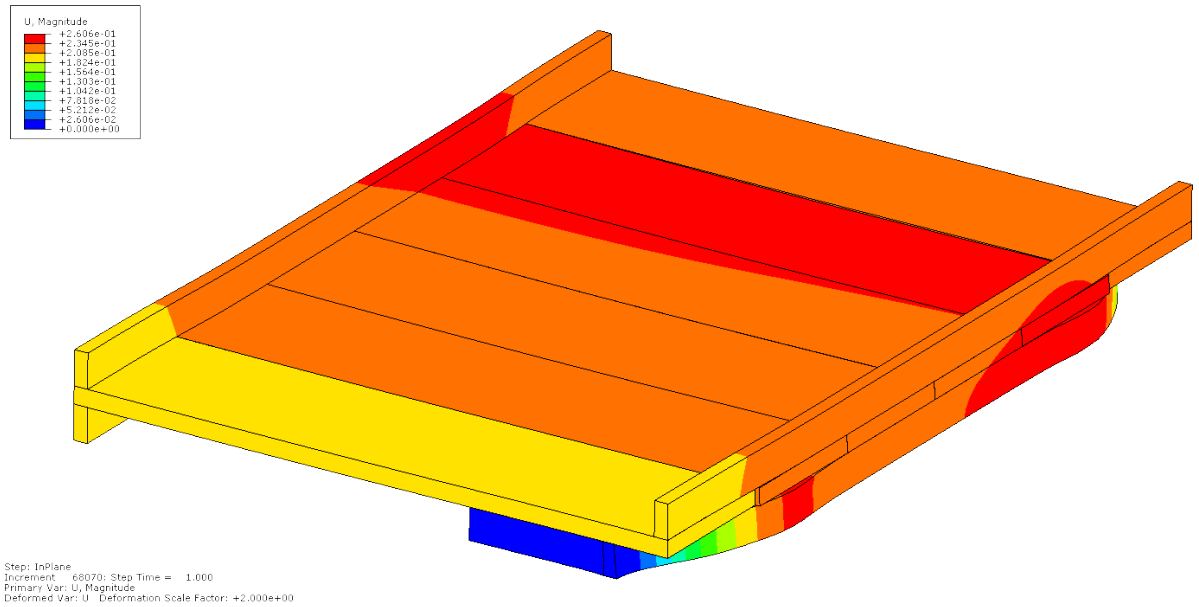

Figure 4.18. Deformation from in-plane push with lateral wall stubs. In this case, the plates at the extremes remain slightly behind, sliding against the other plates.

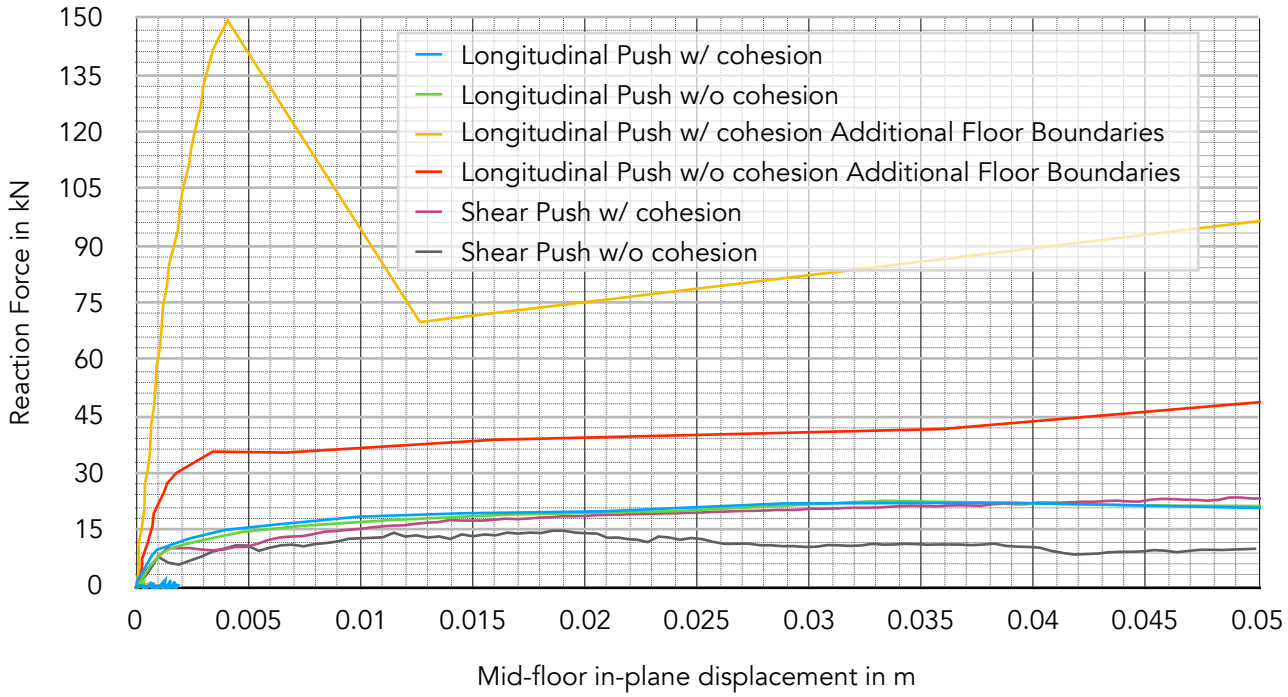

Figure 4.19. Reaction force against mid-floor (longitudinal) or floor-edge (transversal) displacement.

Table 4.4. Summary of results from some of the analysed cases.

Case	Initial Stiffness kN/mm	Capacity kN
Longitudinal Push w/ cohesion	19	25
Longitudinal Push w/o cohesion	10	22
Longitudinal Push w/ cohesion - Additional Bdrs.	62	104
Longitudinal Push w/o cohesion - Additional Bdrs.	25	62
Shear Push w/ cohesion	9	22
Shear Push w/o cohesion	5	18

In sum, these exploratory models reveal that the failure mechanism for the transmission of forces through the floors are governed by the connections. In particular, the stresses at the connections and the influence of the wall stubs seem to be important. This will be explored with a more complex model.

Model 2 - Floors With Independent Concrete Layer and Side Piers

To produce a more realistic picture of the floors and their surroundings, the floor model was improved by:

- Increasing the dimension of the spans to better reflect the donor houses, to 5.40x7.7m^2
- Separating the concrete layer from the masonry plates and defining an interface between them,
- Incorporating stubs of walls on the side and placing the restraints on the bottom face of these.

An impression of the model is observed in figure 4.20.

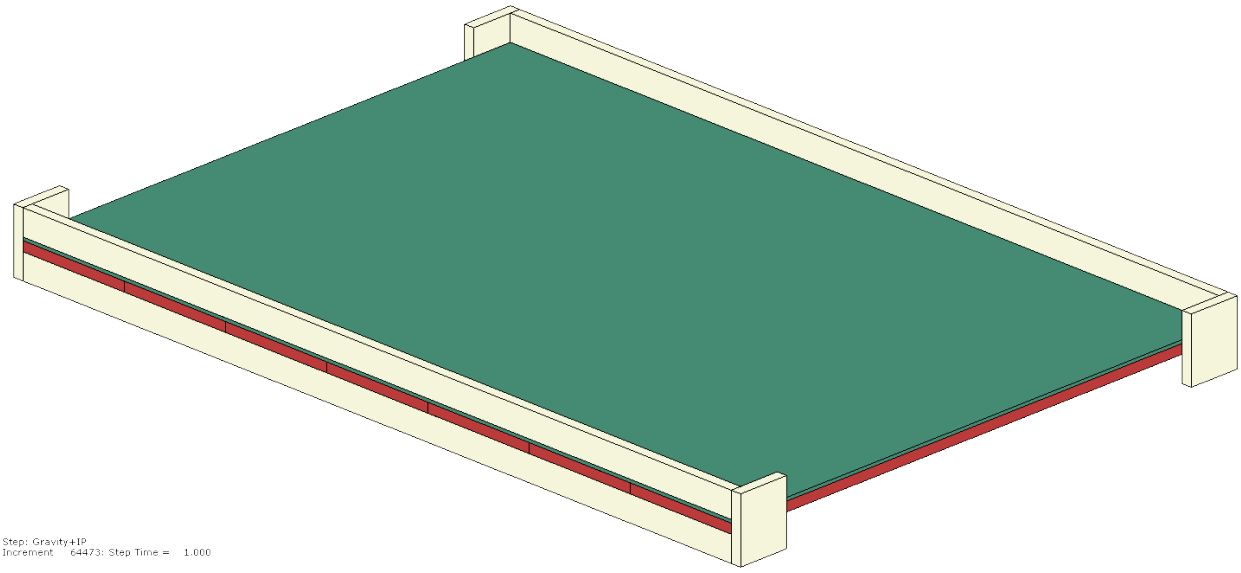

Figure 4.20. Model impression for the series of floor models 2.

Additional properties of the model that need to be noted are:

- An overburden of 0.15 MPa was applied on the top face of the upper wall stubs, simulating the presence of one additional floor level and a roof,
- The self-weight of the floors (around 3 kN/m^2) and a live load of 2kN/m^2 are acting on the floor,
- The bottom face of the stubs of the load-bearing walls were restrained in the gravity direction,
- The bottom face of the stubs of the side piers were restrained in the longitudinal directions,
- The loads in in-plane directions of the floors were applied on the side faces of the floors.

To better illustrate how in-plane loads travel through the floors in this model, a single point load was contrasted with a distributed load while observing the principal stresses on the floor. This is depicted in figure 4.21. The arch effect of the single point load is not recognisable when the load is distributed, however, the tensile stresses on the other side of the floor, perpendicular to the direction of the load, are clearly observed. These stresses could be problematic for the NeHoBo floor.

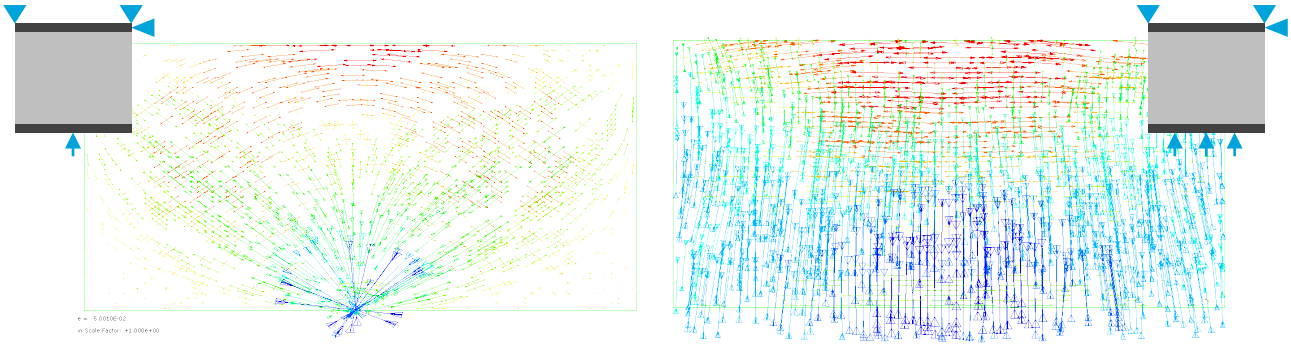

Figure 4.21. Travel direction of stresses through the floor.

The failure mechanism observed for the case of longitudinal in-plane loading was similar to the one seen with the first models (floor model 1): the floor plates slide over the supporting walls (see figure 4.22 and figure 4.23). In this case, because the restraints are placed on the side piers, a higher deformation of the wall stubs is possible.

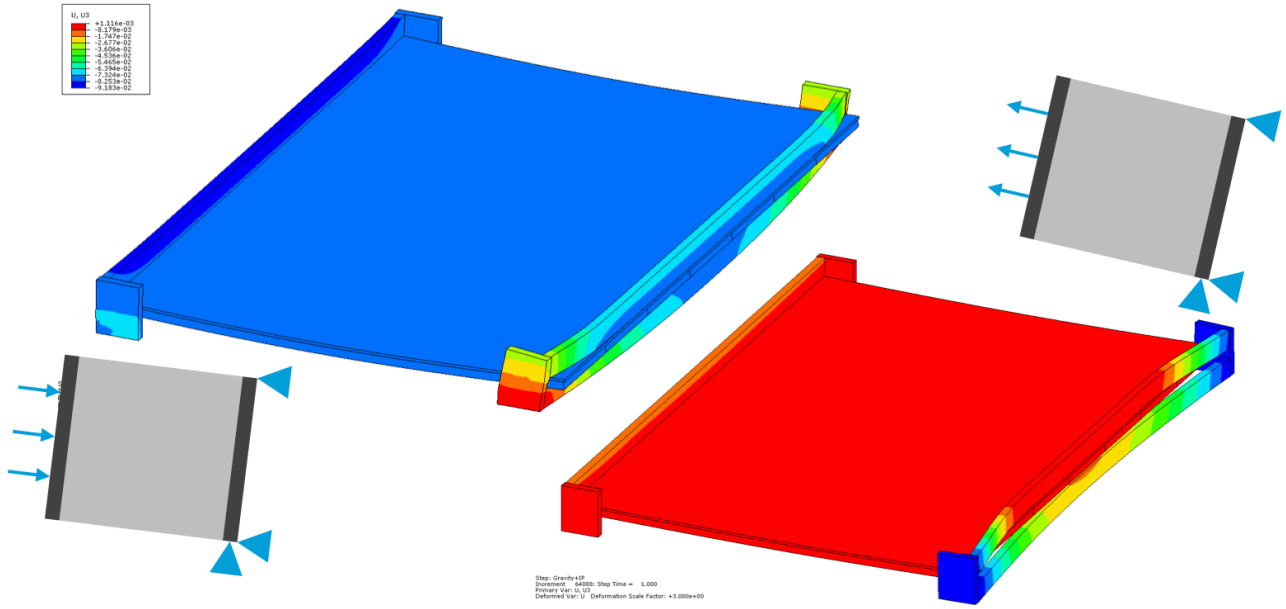

Figure 4.22. Longitudinal in-plane loading of the floor system. Slide-over of the floors at the connections with the wall stubs is observed.

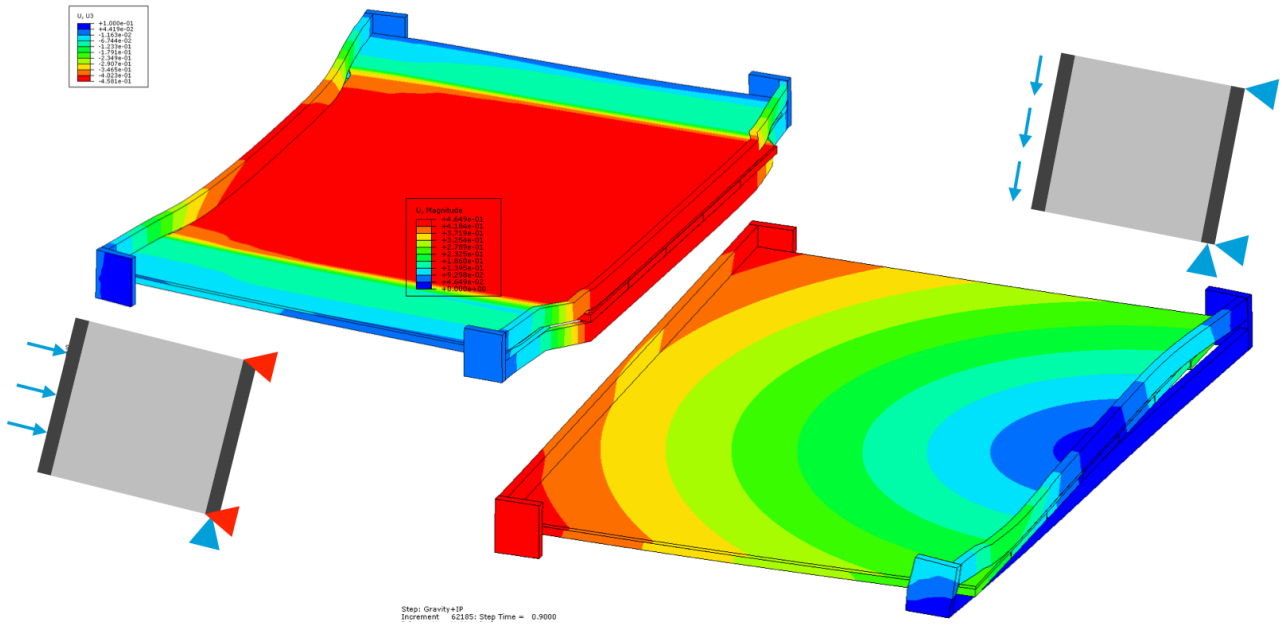

Figure 4.23. Over-constrained case and in-plane shear case for floor models 2.

The models were run in two stages:
First, a gravity stage were the stresses and deformations produced by the gravity loads were computed. In this stage, the upper wall stubs were not connected to the side piers. In was assumed that the interlocking of the side piers with the bearing walls was achieved after most of the deformation of the floors had taken place, since they were built afterwards.
Then, a second stage were the floors were pushed (or pulled) against one of the restrained sides. In this case, the upper wall stubs became interlocked (tied) to the side piers, in the assumption that they were built with brick interlocking.

While the failure mechanisms were similar, because there is a greater overburden on the floor-wall interface due to the increased span of the floor in comparison to the first floor models (Model 1), and the upper wall stubs also provide a restraint via their connection to the side piers, a greater force capacity was expected for these models. This can be confirmed in figure 4.24. The capacity of the various modes relative to each other is the same as for model 1: the over-constrained case has a significantly higher capacity, followed by the longitudinal in-plane case, lastly, the shear in-plane case. Also, in this case, both longitudinal push and pull output similar curves.

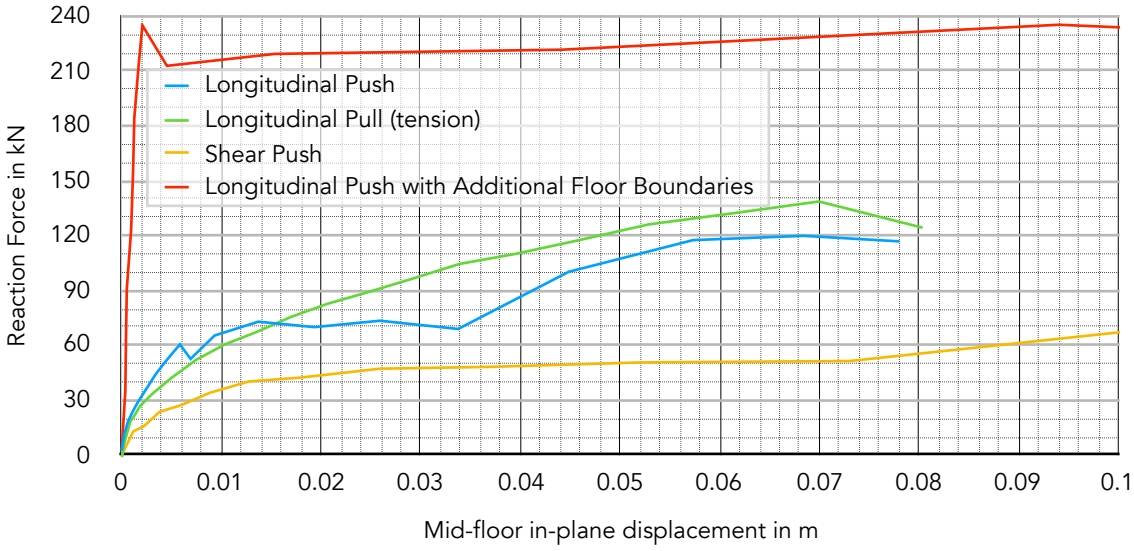

Figure 4.24. Force-displacement curve for floor models 2.

While the base material properties of these models are as described in table 4.2 and table 4.3, they were later varied to observe which parameters were most affecting to the final capacity of the floors (sensitivity). This was done by generating plausible combinations of parameters and permutating these with scenarios. The dependancy of each category was regressed from two or three scenarios that only varied that category. This is summarised in table 4.4 and in figure 4.25.
The sensitivity is computed for a variation of, for instance, 50% of the first parameter listed for each scenario.

Table 4.4. Variation of parameters per category for the sensitivity analysis of floor models 2.

Scenarios	A Overburden	B Intraplate Interface	C Inter-wall Interface	D Strength of Concrete	E Strength of Plates	F Stiffness of Plates	G Strength of Walls
1 Base	5kN/m² + 0.15MPa (28.5kN/m)	f_t=0.1MPa c=0.15MPa μ=0.6	f_t=0.1MPa c=0.15MPa μ=0.6	f_t=1.4MPa Gf=40N/m	f_t=0.2MPa Gf=50N/m	2GPa	f_t=0.2MPa Gf=50N/m
2	4kN/m² + 0.05MPa (15.8kN/m)	f_t=0MPa c=0MPa μ=0.5	f_t=0MPa c=0MPa μ=0.5	f_t=5MPa Gf=100N/m	f_t=0.1MPa Gf=20N/m	4GPa	Linear Elastic
3	6kN/m² + 0.3MPa (46.2kN/m)	f_t=0.3MPa c=0.5MPa μ=0.7	f_t=0.3MPa c=0.5MPa μ=0.7	f_t=1MPa Gf=20N/m	Concrete: f_t=1.4MPa Gf=40N/m E=10GPa		f_t=0.4MPa Gf=75N/m
Computed sensitivity	13.4% per 10%	2.5% per 50%	3.5% per 50%	<1% per 50%	1% per 50%	-13% per 50%	2.5% per 50%

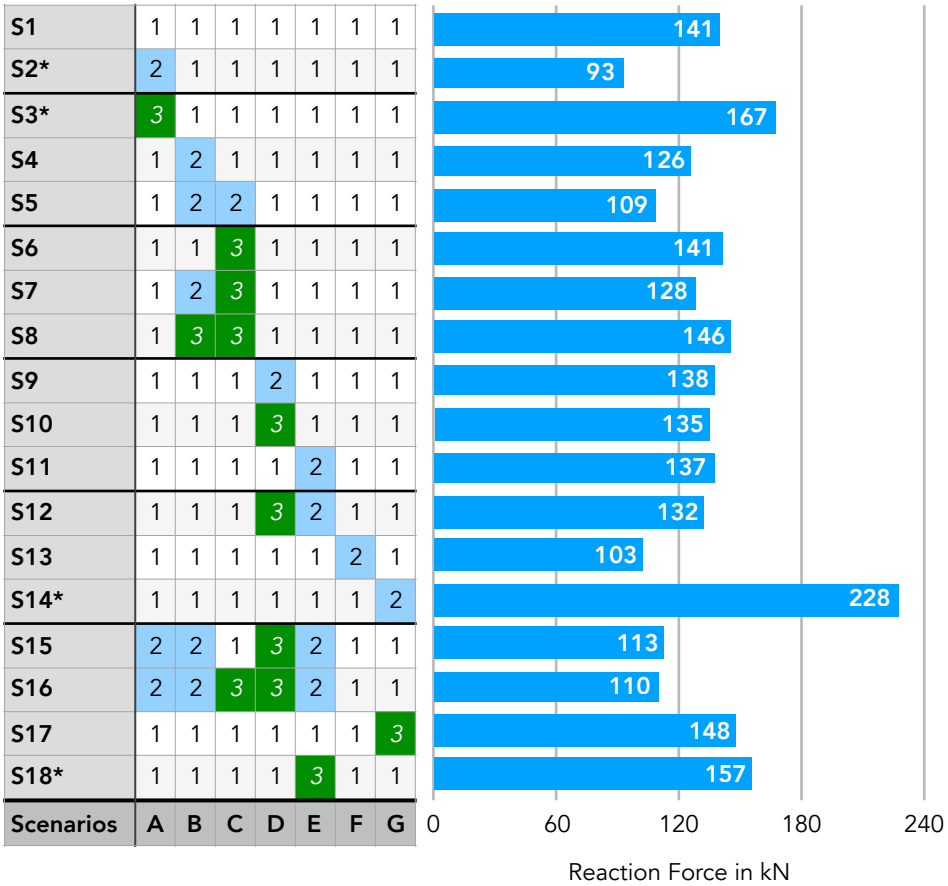

Figure 4.25. Results from the sensitivity analyses for longitudinal push in-plane.

The capacity of each scenario was read from the maximum of a log-parabolic fit to the force displacement-curve obtained from each model.
An example of this is presented for the scenario S2 in figure 4.26.

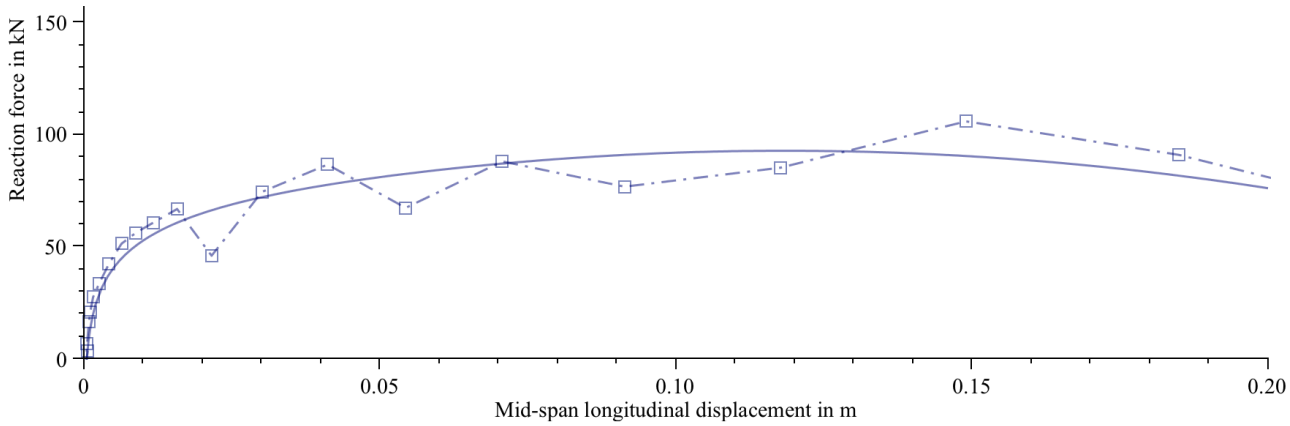

Figure 4.26 Example of log-parabolic fit to the force-displacement curves of the models.

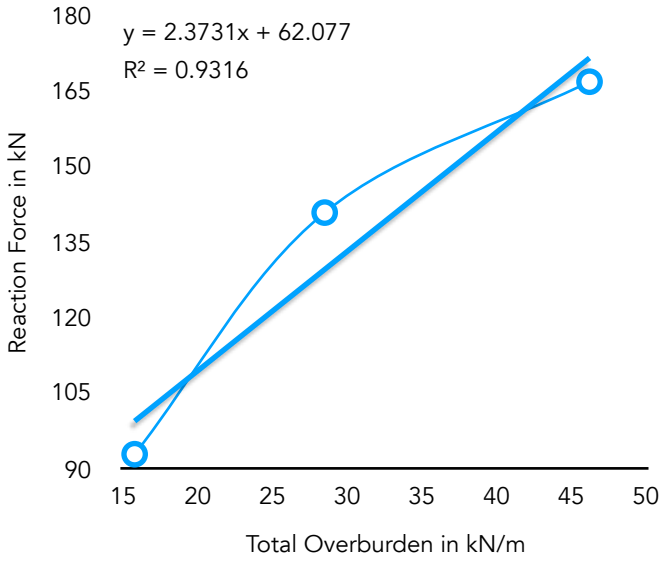

Figure 4.27. Example of regression for computed sensitivity values. Category A for overburden changes.

From the results, the following can be observed:

- The values have an average of 130kN and, neglecting cases than cannot be mixed (marked with *), a standard deviation of approximately 15kN. If the range of the parameters is within the estimated values, a capacity for longitudinal push of 100kN can be confidently expected;
- The capacity is highly influenced by the normal force at the connection, which is defined by the overburden in the model;
- The stiffness of the connection governed by the stiffness of the plates and of the walls, also influences the capacity importantly. Stiffer plates focus sliding on a lower area, reducing the capacity; while, stiffer walls, expand the area where sliding occurs, increasing the capacity;
- The strength of the plates and of the interface between the places have a low influence on the capacity.

Model 3 - Floors as Strips Without Concrete

Based on the results from model 2 and some preliminary laboratory results, it was considered that removing the concrete layer and modelling each row of NeHoBo bricks (strip) with a low adherence between the strips may lead to a reduced capacity. Consequently, the models were modified by:

- Removing the concrete layer;
- Modelling each row as a strip with friction and cohesion between each strip;
- Displacing one set of wall stubs against the other, instead of pushing the side of the strips. This allows for both floor-wall connections to be activated;
- Reducing of the self-weight of the floor according to laboratory measurements (also because there is no concrete).

These modifications can be seen in figure 4.28.

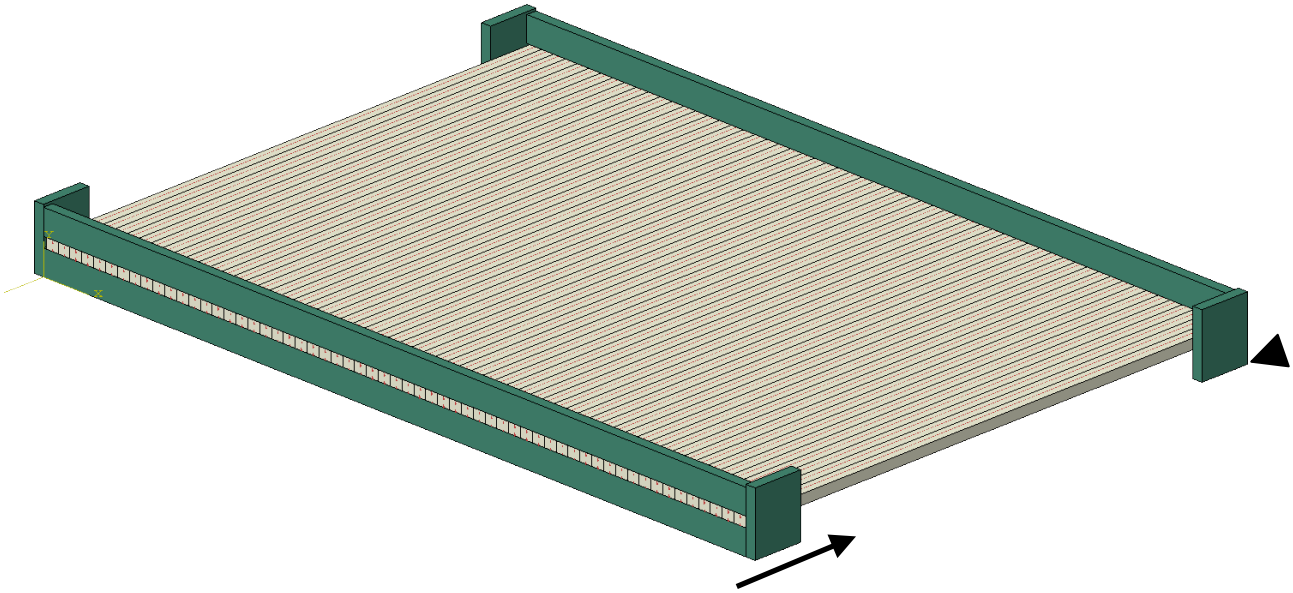

Figure 4.28. Impression of floor model 3 (strips).

Again, the failure mechanism observed was similar to that of previous models: slide-over of the floors was seen. The cohesion between the strips was not broken (figure 4.29).

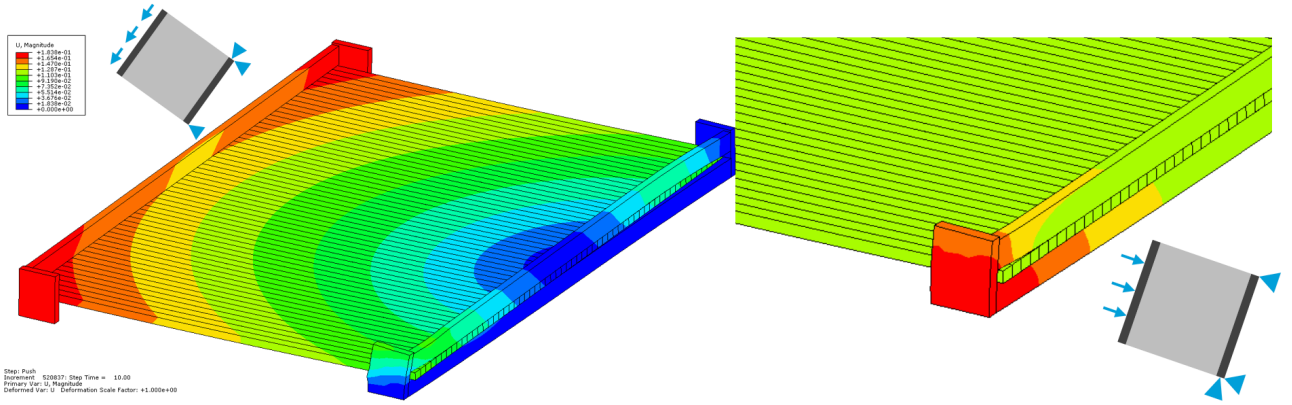

Figure 4.29. Failure mechanisms for the two principal in-plane loads for model 3.

Since the explicit model is run on a time-domain, noise can appear in the results. In the case of the NeHoBo strips, progressive damage of the great number of contact surfaces in between the strips and with the wall stubs leads to vibrations in the model that appear as oscillations of the reaction force. This can be seen in figure 4.30. Nevertheless, it is possible to trace a line through the average of the vibrations. In figure 4.30, a log-parabolic curve has been fit to the data.

As expected, the capacity of the floor is lower (95kN longitudinally and 45kN) in comparison to models 2. Since models 3 do not include the concrete, the overburden stress at the floor-wall interface is 9% lower.

For this difference, a reduction of 13% of the capacity is expected (see table 4.4, column A), which corresponds to a capacity of 110kN. The remaining 15kN are likely due to the other variations in the model. The capacity in in-plane shear is also reduced, but less intensively than for the longitudinal case; the reduction is likely due to the reduced overburden.

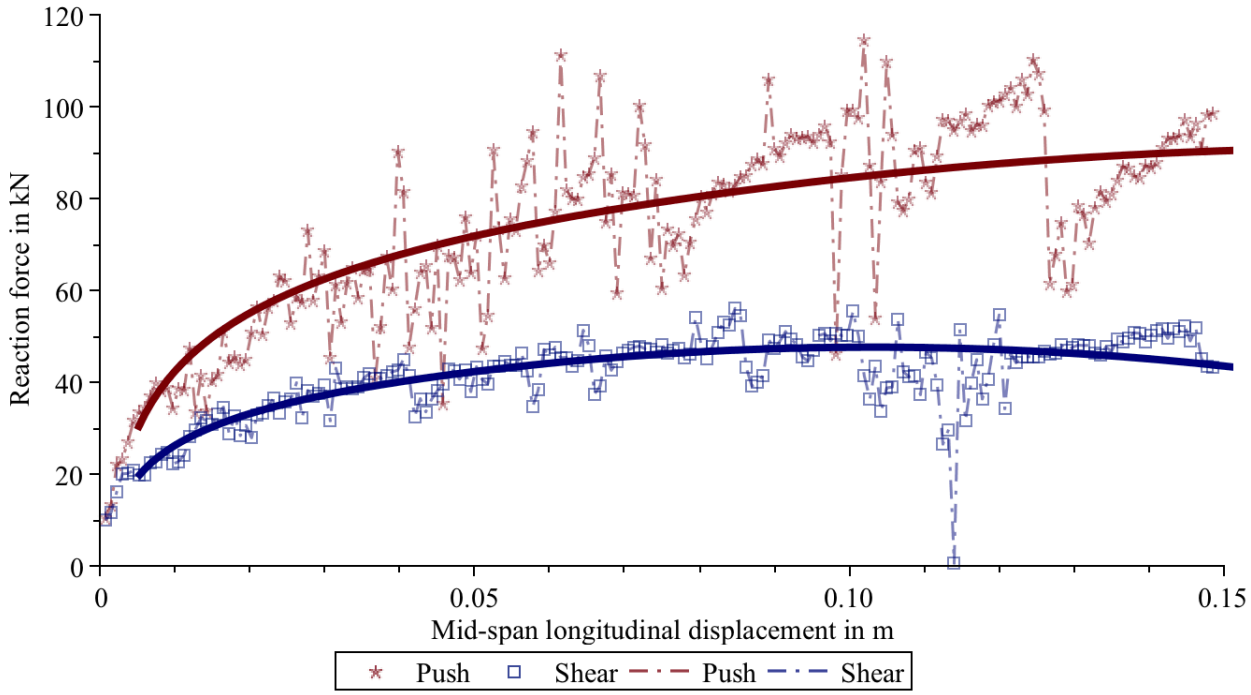

Figure 4.30. Log-parabolic fit to noisy data from floor models 3 (strips).

In sum, the floor models reveal that the critical part of the floor is its connection to the rest of the structure. The failure mechanism of the floor is influenced by that of the rest of the structure. Stronger and stiffer walls will lead, in combination with the floors, to a stronger structure. Conversely, a stronger floor may help weak walls in providing lateral strength to the structure.
However, to assess the influence of the floor on the behaviour and capacity of the structure, a more extensive model is needed. This is studied in the next subsection.

4.2.3. Full-Structure Models

Two models of a full structure have been elaborated: an approximate model of the Zijlvest house to estimate the forces on the floor, and a validated model of the first TU Delft laboratory house {BUILD_01} (Esposito, 2016a) to assess the influence of NeHoBo floors; from here on denoted simply as "laboratory house". See figure 4.31.

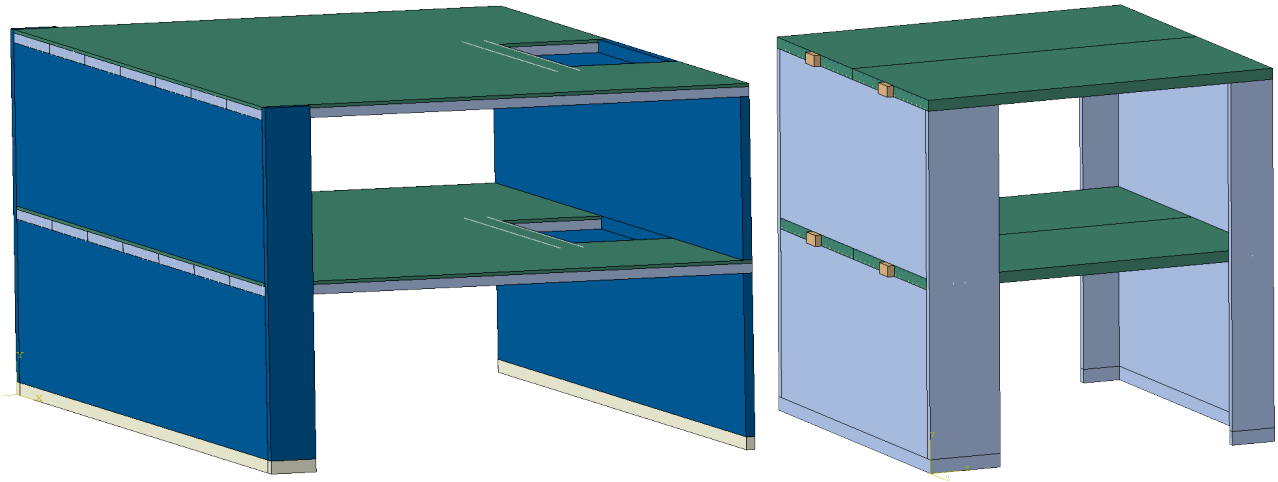

Figure 4.31. Left, approximate model of the Zijlvest donor house with two NeHoBo floors; right, model of the validated TU Deft laboratory house with solid concrete floors.

Zijlvest House Model

The Zijlvest donor house was reproduced insofar possible using available structural and architectural blueprints; nonetheless, important simplifications were implemented by:

- Neglecting the structural participation of the roof, of outer leaves of cavity walls (non-structural), and of the inner walls (non-bearing);
- Reduction of the terraced configuration to only one house and considering only one side of the party wall (the party-wall has two structural leaves);
- Ignoring the participation of the outer attachments (such as garages);
- Consolidating the longitudinal piers distributed for the terraced houses into one pier for the single house.

These have been deemed to be conservative simplifications, reinforced by the following inclusions:

- Attachment of the mass of outer cavity leaves, roofs, and other non-structural elements to the elements in the model;
- Inclusion of the opening for the stairs in a critical section of the floor;
- Variation of the position and number of longitudinal piers.
- Variation of the top floor between timber and NeHoBo plates.

The material model for the masonry walls of the house was validated using the model of the laboratory house which was built specifically resembling the house typology of the Zijlvest donor house.

The Zijlvest house model was subjected to varying intensities of an earthquake accelerogram applied at the base in both horizontal and vertical degrees of freedom. The earthquake signal employed was designed by Tomassetti (2017) for predicted high-intensity earthquakes in Groningen. To consult more information regarding the applicability of the signal, the reader is referred to the referenced literature.
The accelerogram was scaled to 0.25g or 0.35g for each horizontal direction and the forces on a section cut through the floor were recorded.
Roughly, normal forces of up to 4kN were observed throughout the models for the highest acceleration, coupled with in-plane shear forces of up to 3kN.

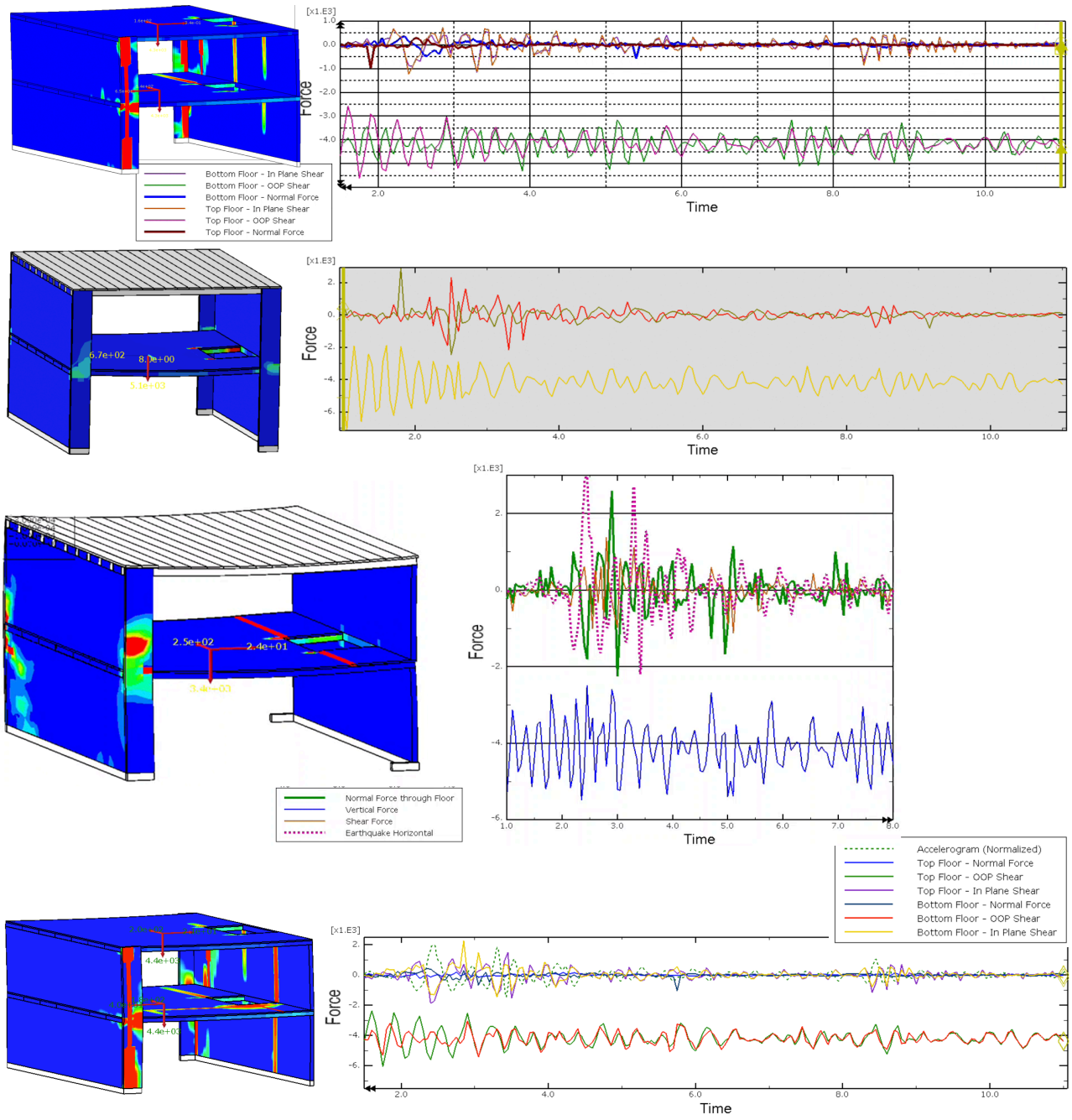

Figure 4.32. Examples of models for the Zijlvest donor house used to gain insight into the forces that need to be transmitted by the floor. From top to bottom: 2 NeHoBo floors at 0.25g, top timber floor at 0.35g with four piers, top timber floor at 0.35g with two piers, 2 NeHoBo floors at 0.35g with antisymmetric piers.

The highest forces were observed for the model with only two piers on the opposite side of the opening for the stairs with two NeHoBo floors. In this model, only the wall at the side of the stairs carries the additional mass of the outer cavity leaf, as the inner party wall double-structural.

This was a logical observation, since it is for this model that more accelerated mass needs to travel to the resisting lateral elements.

Due to the vertical component of the earthquake, the vertical stress at the connection is likely reduced. From the vertical vibrations of the floor, it would seem that a reduction of around 30% takes place; this is probably associated with a reduction of capacity in the order of 40%.

If the values from floor model 3 are considered, it would mean that the connection between the floor and walls can withstand approximately 55kN of normal force. This is one order of magnitude higher than the solicitations to the floor. Whether this expected force is realistic is discussed in section 4.4.

Nevertheless, it is possible that the reduced in-plane stiffness and strength of the NeHoBo floors detrimentally contributes to the overall strength of the structure. This will be assessed next.

Validated Model of the Laboratory House

To assess the potential effect of NeHoBo floors on a structure, a validated model will be used. Employing the previous, unvalidated model of the Zijlvest house for a comparison between floor systems would result in highly uncertain results because the correctness of the model is unknown. In this case, the contribution of the NeHoBo floors as beneficial or detrimental to the structure would become inconclusive.

To date, the TU Delft has performed two cyclic pushover tests on masonry assemblages (full structures). In particular, the first house was designed to be representative of houses like the Zijlvest donor house by being built from calcium-silicate bricks, having continuous façade piers (side piers), and including interlocking between the piers and the bearing walls.
In this light, it is reasonable to assess the influence of the NeHoBo floor by comparing a model of the original house (which had rigid concrete floors) to one with NeHoBo floor strips (see floor models 3).
The model of the original house with concrete floors has been calibrated (and as such, validated) to match the laboratory results with a sufficient degree of accuracy. The floors in this model are then replaced and compared.
For additional details about the masonry assemblage, the reader is referred to the report by Esposito (2016a). Here, a brief summary of the chosen properties for the model are listed:

- There is interlocking between the side piers and the bearing wall;
- There are anchors between the side piers and the floors consisting of 6mm rebar. Five and three anchors for the wide and narrow piers, respectively. In the case of the NeHoBo floors, the anchors are embedded into the the two strips next to the piers;
- The two concrete plates are connected with reinforcement and wet joints;
- Four jacks apply in-plane forces on the side of the floors. The displacement is controlled at the top floor and the forces of the middle-floor jacks are set to match the forces of the jacks at the top. From the laboratory results, the displacement at the middle floor is observed to be roughly 50% of the displacement at the top floor. The model is run displacement-controlled in this configuration.
- 20 full cycles with linearly incrementing displacement are run up to a maximum displacement of 100mm at the top for both directions, this is a slight adaptation from the experiment;
- The walls are modelled with a concrete damage plasticity model;
- A non-linear interface with tensile strength, cohesion, friction, damage, and plastic compression hardening is included at the contact of wall and concrete; also at the contact of the first row of bricks and the rest of the walls. Hardening in compression is used to mimic toe-crushing at a stress of 5MPa.

Table 4.5. Material properties for the laboratory house model.

Material	Type	Young's Modulus	Poisson ratio	Density	Tensile Strength	Fracture Energy in Tension (Mode I)	Softening	Compressive Strength
Concrete	Quasi-brittle	35 GPa	0.15	2300 kg/m^3	5.6 MPa	40 N/m	Linear	65 MPa
Rebar	Elasto-Plastic	200 GPa	0.3	7800 kg/m^3	500 MPa	N.A.	N.A.	N.A.
Masonry	Quasi-brittle	3.5 GPa	0.15	2000 kg/m3	0.2 MPa	80 N/m	Linear	5 MPa
NeHoBo (Strips)	Quasi-brittle	2 GPa	0.15	1700 kg/m3	0.2 MPa	20 N/m	Linear	15 MPa

Table 4.6. Interface properties for the laboratory house model.

Material 1	Material 2	Bond Strength	Cohesion	Friction Coefficient	Tension			Tangential Stiffness	Compression	
					Fracture Energy (Mode I)	Softening	Normal Stiffness		Normal Stiffness	Plastic Stress
Brick	**Concrete NeHoBo**	60 kPa	90 kPa	0.52	5 N/m	Exponential	100 GPa/m	60 GPa	100 GPa/m	5 MPa
NeHoBo	**NeHoBo**	100 kPa	200 kPa	0.6	5 N/m	Exponential	100 GPa/m	60 GPa	∞	N.A.

The model was run in two stages. First, a gravity stage where self-weight was applied. Then, a second stage where the lateral loading was considered. The lateral loading consisted, separately, of the following:

- A quasi-static, **cyclic pushover** with twenty cycles in the push and pull directions. Controlled by displacement at the top and middle floors. The displacement increased linearly in between cycles up to **100mm**. This was the validation with the laboratory test, see Esposito (2016a).
  - Idem, but the displacement maximum was set at **250mm**.
- A quasi-static, monotonic pushover in the **pull** direction up to 100mm.
- A quasi-static, monotonic pushover in the **push** direction up to 100mm.
- A base excitation in the form of an **accelerogram** for the synthetic MPE signal (Tomassetti, 2017) applied in the horizontal and the vertical directions. Scaled up to:
  - 0.25g (0.35g total magnitude)
  - 0.35g (0.50g total magnitude)
  - 0.70g (1.0g total magnitude, for verification purposes)

These cases are illustrated in figure 4.33: at the top for the original case with concrete floors, and at the bottom for the comparison case with the NeHoBo floor modelled with strips. In both graphs the backbone of cyclic pushover of the experimental results is included for comparison. In these curves, the cyclic pushover of the concrete floors case was calibrated to the experimental results (top graph, blue curve).
Many observations can be read from these figures:

- The house with concrete floors (case 1) is stiffer than the house with the NeHoBo floors (case 2). This can be seen by comparing the maximum top displacements during the small earthquake.
- Case 2 is 25% lighter than case 1. This leads to reduced capacity as the weight helps balance the lateral force. However, the reduction is greater than what would correspond to the reduced mass only.
- Case 1 is able to dissipate more energy than case 2; this is likely due to the diminished participation of the side piers in case 2.
- The maximum displacements during the earthquake signals are noticeably higher for case 2.
- The behaviour during a monotonic pushover shows less damage and reaches higher forces than during a cyclic pushover. This is expected and further validates the results.
- For the strongest earthquake (with an unrealistic PGA of 1.0g), both cases reach the collapse state. However, case 2 occurs earlier than case 1, likely because the maximum top lateral displacement that triggers collapse via the second order effect of the weight of the structure, is reached earlier.
  This high PGA was run so as to verify the ability of the model to produce a collapse situation.
  For a PGA of 0.35g in the weak direction of the structure, both cases mostly returned to the centre.
- It can be seen that for the medium earthquake, but also for the cyclic pushover which is only in the longitudinal direction, the NeHoBo strips separate from each other. This allows (or was caused by) vertical cracking in the masonry wall. During the cyclic pushover, this occurs over many cycles as the walls become damaged, while during the induced earthquake, this occurs rapidly over the few intense cycles.
- Case 1 seems to benefit significantly by the contact of the top of the piers with the rigid concrete floors, in comparison with case 2 where the single NeHoBo strip cannot impose strong forces on the piers. This was done to better replicate the laboratory test but, in the Zijlvest house, this connection doesn't exist.

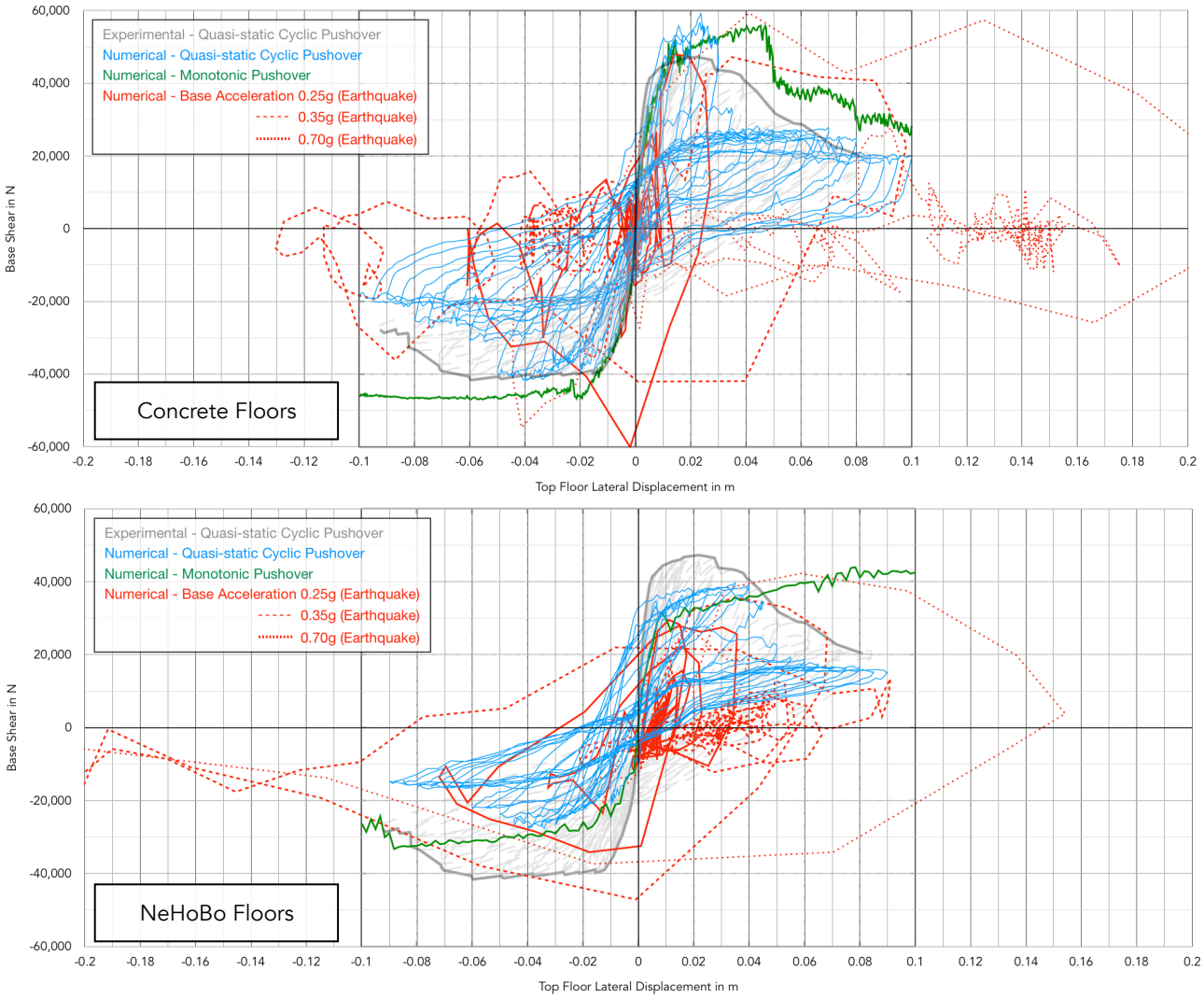

Figure 4.33. Force-displacement curves for the comparison of a terraced house with concrete floors or NeHoBo floors. The displacement is measured on the centroid of the floor.

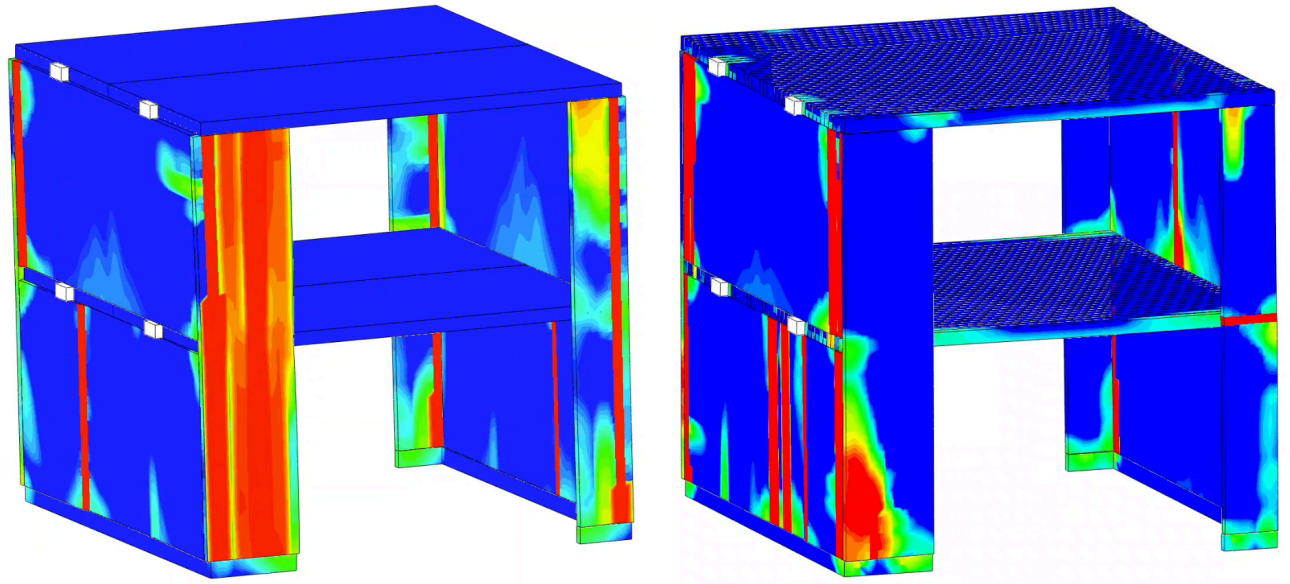

Figure 4.34. Model impressions showing crack areas (in red) for the concrete floor case (left) and the NeHoBo floor case (right) for the cyclic pushover to 100mm.

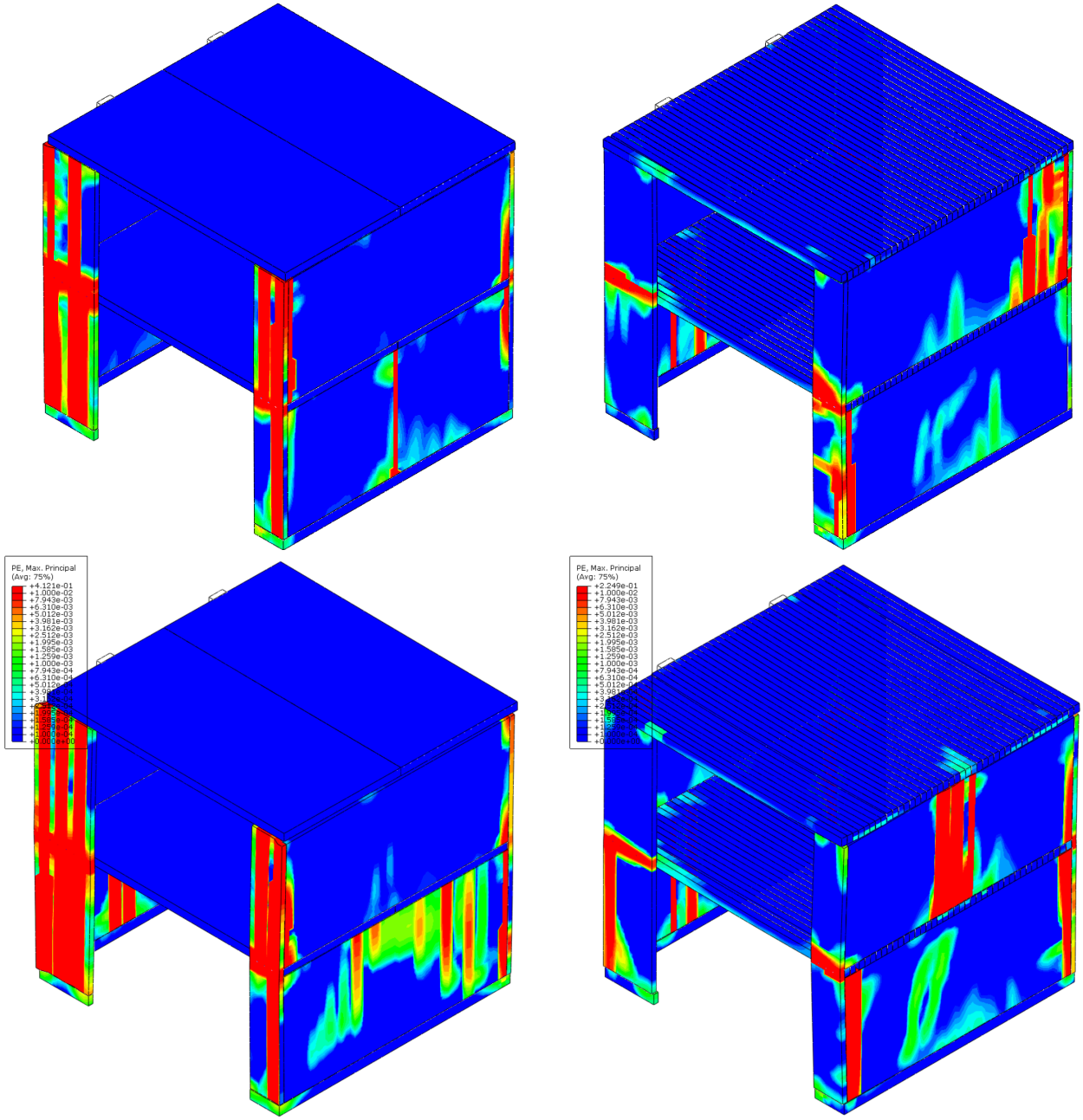

Figure 4.35. Top, earthquake at 0.25g (Resultant 0.35g); bottom, earthquake at 0.35g (Resultant 0.50g).

Important Limitations of These Preliminary Models

The models have been run with a 45° angle for the incoming earthquake. This was done because the separation of the floors was deemed to be more likely at a combination of earthquake directions. However, the two horizontal directions also need to be evaluated independently.

Moreover, vertical cracking seems to be related to the separation of the NeHoBo strips. It is possible that this is influenced by the direction of the mesh. Additional models with tetrahedral elements need to be run to evaluate this effect.

Further, during the cyclic pushover analysis, loads are applied via the jacks at the centre of the concrete floor plates. The concrete floors are designed to distribute these loads to the other elements of the structure. For the NeHoBo strips, the application of the lateral loads during the pushover analyses is trickier, because it is precisely the behaviour of the floor that is being analysed. In figure 4.34, some damage can be seen around the strips that receive the outside lateral force. The inclusion of additional elements would further modify the behaviour of the floor. Therefore, the best comparison is done via the excitation at the base of the model, since here no interactions with the floor are needed.

4.3. Computational Models With DIANA

This section reports the results coming from the finite element modelling and analysis of the Nehobo floor described in Section 4.2.2 with the software Diana 10. The software involves the use of an implicit solver, therefore is able to provide more reliable results with respect to an explicit one, although while coping with development of large nonlinear phenomena, convergence troubles can be encountered and the solution may not always be provided.
Therefore, the performance of numerical analyses with both softwares aims at the cross-validation of the results and at the synergic use of the advantages of both softwares.

Following the results obtained with Abaqus on Model 1, some comments can be done on which boundary constrains could be more realistic to be analyses (consider comparison between basic model and model with additional floor boundaries). If the floor is not supported on the lateral walls (Figure 4.36 on the left) and the floor is pushed with a uniform load, not much shear would develop between the plates and the interface between floor and wall will fail more easily. Supporting with friction the floor also on the lateral edges would lead to results more similar to a "beam-type" behaviour (Figure 4.36 on the right). The most common situation in Dutch building practice of terraced houses is that the floors are supported on the longitudinal walls only, whereas the façades run continuously from an inter-storey to another. Therefore, the situation of Figure 4.36 b is most likely to occur and will be assumed in the following analyses.

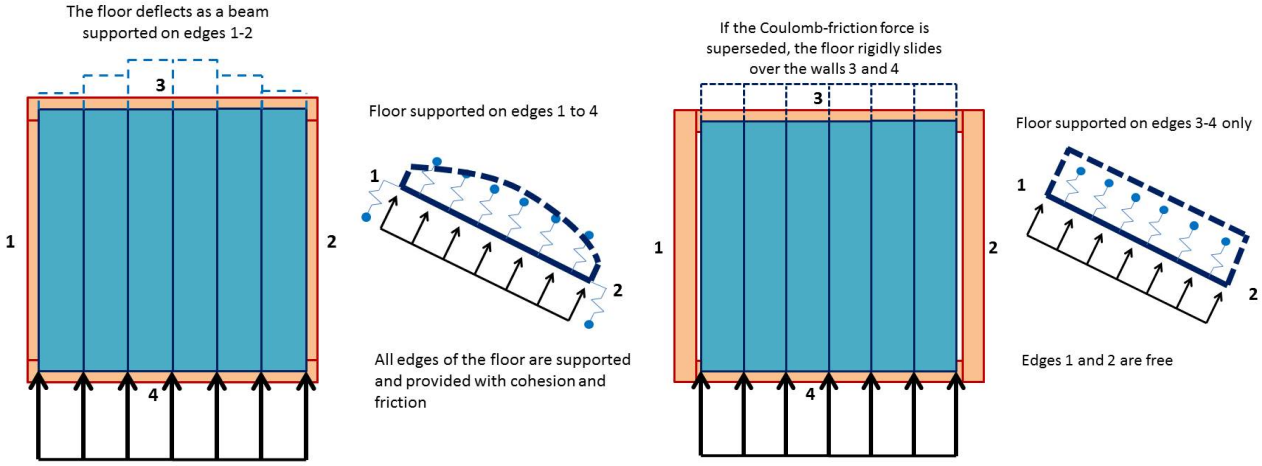

Figure 4.36. Qualitative deformation of the Nehobo floor subjected to lateral force: Left, floor supported on all the 4 lateral walls; and right, floor supported on two walls only.

The geometry of the floor is the same of the one referred as “Model 2” in Section 4.2.2, with a span of 7.7m and a width of 5.4m (Figure 4.37). Supporting masonry stubs have been modelled below the floor. The boundary constraints have been applied according to Figure 4.37. The floor is build up as a 2.5D model, using quadratic shell elements for both the Nehobo plates and the masonry portions. In particular, layered shell elements (CQ40L) have been used for the Nehobo plates, to account for the different properties of the plates and the upper concrete layer. The masonry walls have been instead modelled with regular flat shell elements (CQ40S). 3D line interface elements (CL24I) have been used to model the plate-to-plate and plate-to wall connections (Figure 4.38). These interface are provided with a Coulomb- friction behaviour in-plane (local x and z directions) and a Gap-brittle behaviour in tension (opening) direction (local y direction). Nehobo plates, concrete top layer and masonry walls have been also provided with nonlinear properties in tension modelled with Total Strain Rotating Crack Model. Linear elastic behaviour is assumed in compression.

Some simplifications have been reasonably adopted:

- upper masonry walls stubs have been modelled;
- side piers have been modelled, but perfect restrains are assumed on those vertical edges;

- embedded reinforcements are excluded from modelling since only in-plane behaviour has been investigated in this stage and moreover, to avoid deflection of the floor with unrealistic deformations, the overburden has been applied directly at the floor supports;
- the concrete top layer is modelled within the layered shell element approach and therefore is perfectly bonded to the lower section of the floor. The sliding at the plate-concrete layer interface is assumed to be hardly occurring.

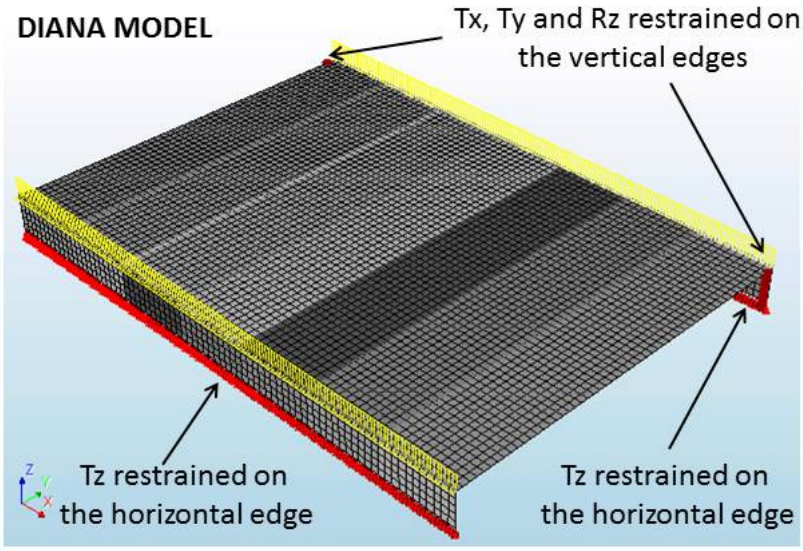

Figure 4.37. Diana finite element model with identification of the assigned boundary constraints.

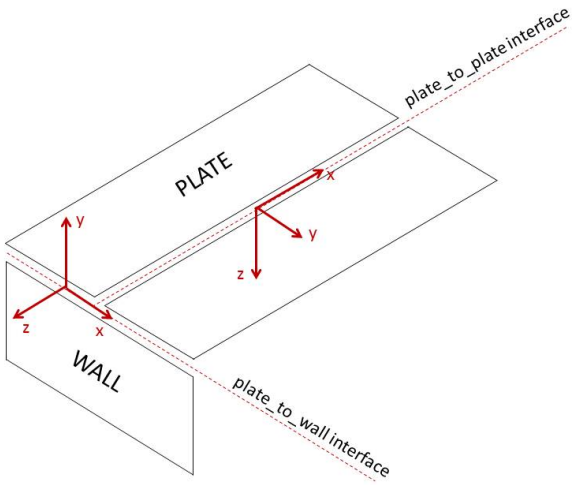

Figure 4.38. Interface elements and pertinent local axes definition.

The model of the floor has been subjected to some of the variation analyses reported in Section 4.2.2. The selected cases were among the ones showing the larger effect on the capacity. The following issues have been analysed:

- Influence of overburden: S1, S2, S3;
- Influence of the plate-to-wall interface properties: S1, S6;
- Influence of the plate stiffness: S1, S13;
- Influence of the linear/nonlinear behaviour of the walls: S1, S14, S17.

The capacity curves obtained in the different cases are reported in Figure 4.39. Considering the various cases, the capacity ranges between 15 and 35 kN. The obtained values are lower than those obtained through the Abaqus model 2.

All the analyses suddenly diverged with sharp sliding of the plates (Figure 4.40), therefore the failure is quite brittle and cannot be followed through very large displacements, as done with the Abaqus model. Nevertheless, the curves present a very good convergence before the sudden divergence, hence results can be assumed as numerically reliable and even if some curves still present an ascending trend, they seem to almost approach a plateau. It is reasonable to assume that the numerical capacity could not be much higher, even by overcoming the convergence troubles.
Part of the difference between Abaqus and Diana results could be related to the modelling assumptions and this should be further explored. The results are preliminary and could be further developed.

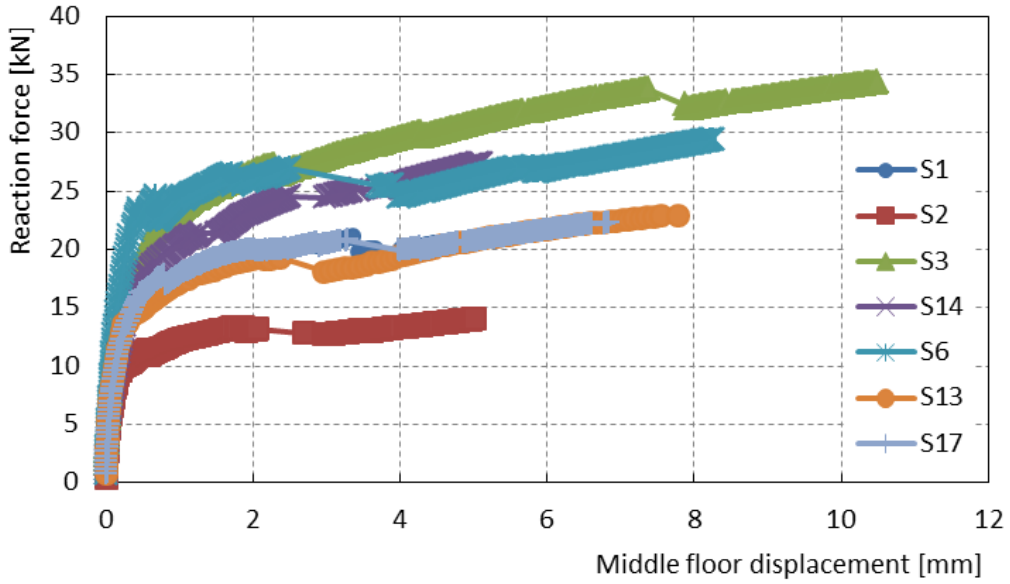

Figure 4.39. Envelope of the capacity curves obtained in the different sensitivity analyses.

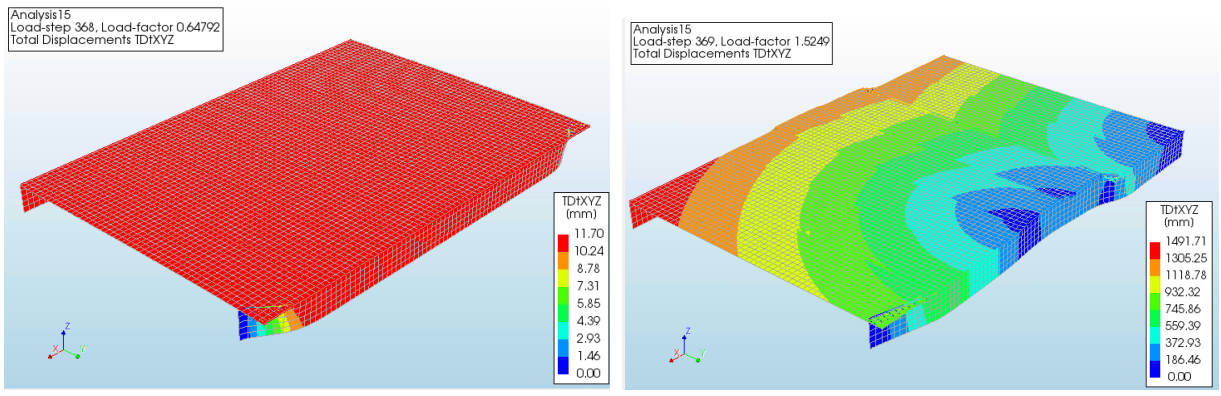

Figure 4.40. Total displacement contour for the analysis S3 at the end of the capacity curve (left) and at the subsequent unconverged step (right).

In terms of the effect of the single analysed parameters, the Diana analyses confirmed the results obtained with the Abaqus model:

- the level of the overburden plays the largest role in the results and this can be easily assessed (Figure 4.41a);
- the variation of material properties of the floor in a reasonably large range does not involve a dramatic change in the capacity. This is a positive outcome, due to the uncertainties often affecting the material properties of structural components and connections on site (Figure 4.41b-c);
- the assumption of linear elastic behaviour of the masonry wall parts causes an overestimation of the capacity, even if the Diana model showed a lower effect with respect to the Abaqus one (Figure 4.41d).

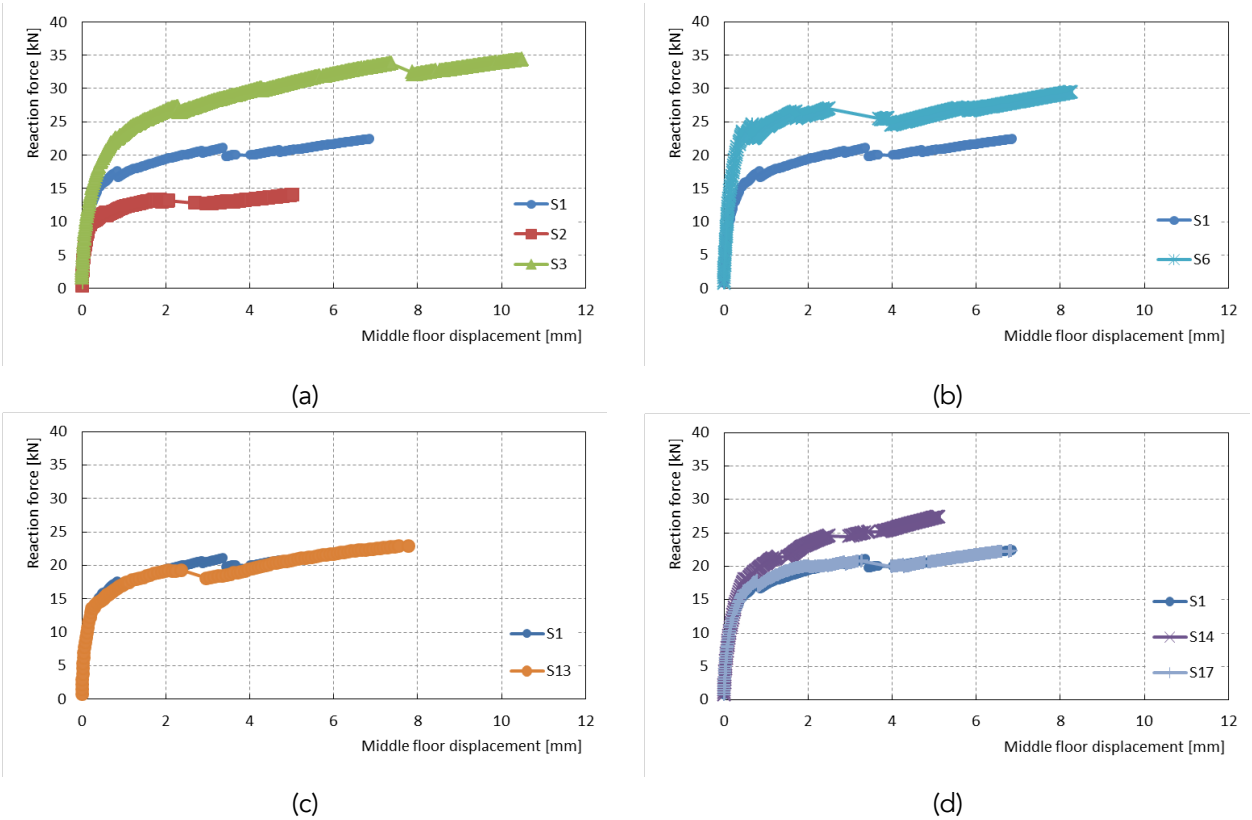

Figure 4.41. Effect of several parameters on the capacity curve: (a) overburden; (b) plate-to-wall interface properties; (c) plate stiffness; (d) walls material properties and linear/nonlinear behaviour.

While the dimensions and parameters used in these models are related to floor models 2 in Abaqus, the boundary conditions are more alike floor models 1. In the former case, the upper stubs provide additional friction and cohesion which increase the capacity; moreover, the rigid restraint at the side of the bearing wall, also fosters more local failure, reducing the capacity. In this light, the results provided in this section nicely fall in between models 1 and 2.

4.4. Verification With Analytical Models

To better understand and validate the computational models, analytical models or "hand calculations" have been performed. Four sets of calculations are presented here: a verification of the slide-over capacity of the floors, a computation of the tensile stresses in the weak direction of the floors, a calculation of the in-plane shear capacity of the floors , and a static determination of the forces in the floor during earthquake motions.

4.4.1. Slide-Over Capacity of the Floors

The capacity at the interface between the floors and their supporting walls is governed by cohesion and friction. The thickness of the wall is 0.1m.

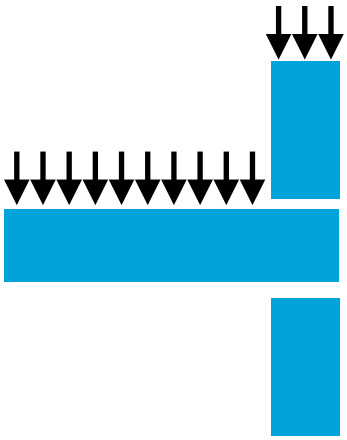

Figure 4.42. Sketch of s the connection of the floor and its supporting walls.

The normal force acting on a stretch meter of this connection is 28.5kN. It is composed from 13.5kN resulting from the floor loads (3kN/m^2 from the self-weight of the floor and 2kN/m^2 from the live loads) and 15kN from the wall overburden.
F_N=5.40m/2·(3kN/m^2+2kN/m^2)+0.15MPa·0.1m=28.5kN/m.

The friction coefficient is μ=0.6 and the cohesion is 0.15MPa. This results in a maximum friction force of 32kN/m:
f=28.5kN/m · 0.6 + 0.15MPa· 0.1m = 32 kN/m.

If the floor were to slide over the entire wall, the capacity would be 32kN/m·7.70m=246kN. However, since the supporting wall has little stiffness in its out-of-plane direction, if offers no resistance to the floor. Hence, the wall moves with the floor, and no sliding occurs.
Only the edges of the wall, which are restrained by the side piers, are stiff enough in the out-of-plane direction to develop a force against the sliding of the floors.
With an analytical model, it is difficult to estimate how much of the wall contributes to the capacity. From the computational models, between a quarter and one plate (that is between 0.3m and 1.1m) of bearing wall slides in respect to the floors. For floor model 1, where the side of the wall is restrained, failure of more local; for floor model 2, where the side of the wall is connected to the side pier, the failure surface extends.

This is in agreement with the results from floor model 1, where a capacity of around 25 kN was found. This would correspond to sliding at only 0.40m at each side.

For floor model 2, where the wall at the top also provides friction and cohesion, the capacity is larger (in the order of 130kN).
F_N=5.40m/2·(3kN/m^2+2kN/m^2)+2·0.15MPa·0.1m=43.5kN/m.
f=43.5kN/m · 0.6 + 2·0.15MPa· 0.1m = 56 kN/m.
This corresponds to one plate sliding at each side.

4.4.2. In-Plane Bending Capacity of the Floors

The floors behave as a deep beam in-between the side piers (see sketch in figure 4.43). Because the floors are not connected to the side piers, the restraint occurs through the bearing walls, this reduces slightly the distance between the (imaginary) supports (see previous subsection).

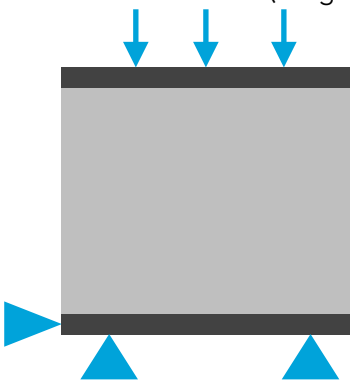

Figure 4.43. Analytical model of the floor as a deep beam.

The floors have dimensions of 5.40mx7.70m. The distance between the imaginary supports (the centroid of the reaction forces) will be assumed to be 6.50m.
The normal force to be transmitted through the floor will be assumed to be the maximum of 130kN (else the floor would slide-over). This corresponds to a distributed load of approximately 15 kN/m.

For the calculation of the stresses in the deep beam, the internal arm is assumed to be 0.6 of the height of the beam (the floor span), so 0.6· 5.4m. The tension zone is assumed to be 0.2 of the floor span (0.2· 5.4m). Based on the tested properties of the floor, a better estimation of the non-linear stress distribution still needs to be performed.

The bending moment can be computed with:
$M=q\cdot(L_{free})^2/8$
$M=15\cdot (6.50m)^2/8=80kNm$

Tension in the beam follows from internal equilibrium:
$T=M/(arm)$
$T=80kNm/(0.6\cdot5.4)=25kN$

The maximum tensile stress can be computed by assuming a triangular distribution of tension stresses:
$\sigma=2\cdot T/(t\cdot d_t)$
$\sigma=2\cdot 25kN/(0.2\cdot 5.4m\cdot 0.2m)=0.23$ MPa

This tensile stress needs to be resisted by the floor and the part of the bearing walls close to the floor (these act as flanges to the floor).
From this, it is clear that a strong floor will load the walls less than a weaker floor. Nonetheless, the force transmitted through the floor may never reach the value of 130kN; this will be evaluated in section 4.4.4.

4.4.3. In-Plane Shear Capacity of the Floors

(in progress)

4.4.4. Earthquake Forces on the Floor

A simple spectral analysis can be performed to estimate the forces that the houses are subjected to during an earthquake. Due to the lateral seismic acceleration, the mass of the house becomes a lateral force. If only one side of the structure is rigid, the forces developed from the tributary zone around the floors (see figure 4.44) will need to travel through the connection between the floor and its supporting wall.

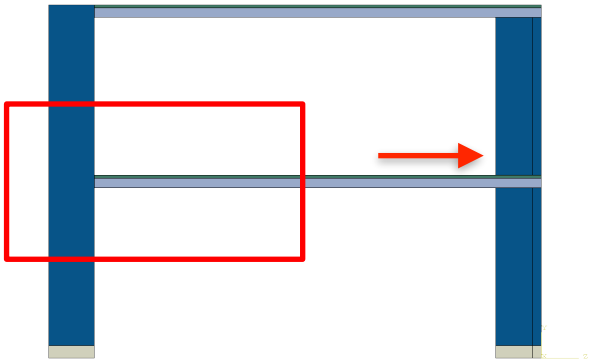

Figure 4.44. Sketch of the house and the tributary zone for earthquake forces running through the floor.

The total weight of the structure is approximately 650kN. The mass of walls, floors, live loads and attached masses (outer leaves) in the tributary zone of the floors is around 150kN/g.

For a return period of 2475 years, the maximum peak ground acceleration (PGA) in the area of Groningen is expected to be 0.35g (NEN, 2017). However, the spectral pseudo-acceleration depends on the period of the structure. A model of the Zijlvest house (see section 4.2.3) was used to estimate the period. The natural vibration period was pegged at 2 seconds (see next page).
For a period of 2s, NEN (2017) specifies a pseudo acceleration of 0.075g (see figure 4.45); this is larger than what the MPE signal produces (0.043g).

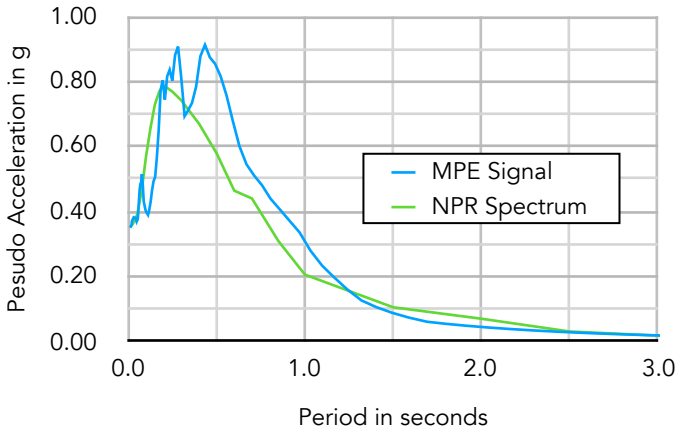

Figure 4.45. Spectra of the MPE signal compared to that obtained at NEN (2017).

At an acceleration of 0.075g, the normal force through the floor is 0.075·150kN=11kN. At 0.043g, it is 6.5kN.
For a PGA of 0.35g, the models of the house showed forces between 2kN and 4kN; this is comparable to the static analysis. The difference in this force is probably due to: the incurrence into the non-linear zone by the side piers since as they become damaged the force they can transmit to the upper structure reduces (the period increases); and/or, due to the fact that the normal force is not transmitted entirely to one side of the structure, perhaps due to the contribution of the bearing walls in their out-of-plane direction.

Analytical Estimation of the Natural Period

The predominant natural period of the structure can also be estimated analytically using the following relationship for a system with a single degree of freedom:

$$T=2\pi\cdot\sqrt{\frac{m}{K_L}}$$

Where:
m is the mass of the structure that is expected to participate
K_L is the lateral stiffness of the structure.

Since the total weight of the building is 650kN, the participating mass will be assumed to be 60'000kg. To estimate the lateral stiffness two simple models will be used: to compute the contribution of the two lateral piers (figure 4.46, left), and to add the contribution of the bearing walls (figure 4.46, right).

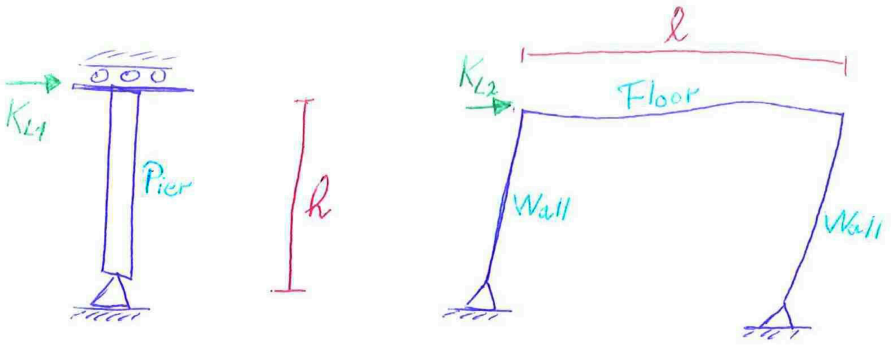

Figure 4.46. Models for estimating the lateral stiffness of the structure.

The first model assumes that the continuation of the lateral pier provides sufficient constraint such that it can be modelled as fixed. In the second model, this constraint is provided by the floors resting on the bearing walls. From the models, the lateral stiffness can be computed:

$$K_{L1}=2\cdot\frac{3\cdot EI_{pier}}{h^3} \qquad K_{L2}=\frac{12\cdot EI_{wall}\cdot EI_{floor}}{h^2\cdot(L\cdot EI_{wall}+2h\cdot EI_{floor})}$$

Element	Young's Modulus	Thickness	Length	Inertia	Section Stiffness
	E (GPa)	t (m)	ℓ (m)	I (m^4)	EI (Nm^2)
Pier	2.0	0.5	0.1	1.042E-03	2.083E+06
Wall	2.0	0.1	7.7	6.417E-04	1.283E+06
Floor	2.0	0.2	7.7	5.133E-03	1.027E+07
h (m)	2.7	**K_{L1}**	6.351E+05	K_L	9.828E+05
L (m)	5.4	**K_{L2}**	3.477E+05		N/m

The total lateral stiffness of the structure is then approximately 1 MN/m. This results in a period of 1.6s.

It is important to note that for high values of drift, the pier is expected to crack precisely at the level of the floors which would then reduce its lateral stiffness. Moreover, lumping the entire mass of the building at the level of the first floor and using a single degree of freedom model reduces the period.

The estimation can be improved by using a model with two degrees of freedom: one for each floor and assuming the mass of the roof to be at the level of the second floor.
In this case, the two degrees of freedom formulate a stiffness and a mass matrix as shown next:

$$K=\begin{bmatrix} 2K_L & -K_L \\ -K_L & K_L \end{bmatrix} \qquad M=\begin{bmatrix} m_1 & 0 \\ 0 & m_2 \end{bmatrix}$$

For this case, the storey lateral stiffness is assumed to be 1 MN/m as obtained from the previous analysis. The mass is subdivided in 35ton for the first storey and 25ton for the second storey.

$$\lambda := \begin{bmatrix} \frac{1}{2}\,\frac{\left(m_1 + 2\,m_2 + \sqrt{m_1^2 + 4\,m_2^2}\right) K_L}{m_1\,m_2} \\ -\frac{1}{2}\,\frac{\left(-m_1 - 2\,m_2 + \sqrt{m_1^2 + 4\,m_2^2}\right) K_L}{m_1\,m_2} \end{bmatrix}$$

Eigenvalue vector for a structure with two degrees of freedom.

The eigenvalues for this matrix system are computed; then, the natural period for each vibration mode is derived. The first vibration mode has a period of 1.7s, while the second mode has a period of 0.7s. The relative importance of the modes will depend on the type of excitation.

The goal of this subsection is to increase the confidence in the value for the natural period computed with the numerical model. The value of 2 seconds obtained with the numerical tool, considering that it is better suited at expressing the complexity of the materials, elements, and connections, seems reasonable when compared with the value of 1.7 seconds achieved with the analytical approximation.

Another uncertainty are the Young's moduli of the materials. The stiffness of the floors has not yet been assayed. The stiffness of the masonry walls has been assumed to be on the low side considering that they possess some pre-damage. The periods computed here will vary with the square root of the difference between the real and the assumed Young's moduli.
In this light, if the Young's moduli are twice as high and the connections, both at the base of the structure and at the floors, can be considered to be perfectly rigid, the natural period will decrease. In this worse-case scenario, the computed period can be as low as 1s. This would increase the forces computed with the spectrum by 300%.
However, the forces to which the floors are subjected too are unlikely to increase since the piers are unable to transmit these high forces to the rest of the structure. If each pier of 0.5m in length takes 33% of the earthquake shear, that is ⅓·(0.2g·600kN/g)=40kN, the tension stress at the base of the pier would be in the order of 20MPa. It should be clear that this is not realistic; instead, the piers will crack at both upper and lower sections, possibly incurring into rocking. This will significantly reduce the lateral stiffness of the structure and produce a higher natural period.

4.4.5. Additional Resistance due to the Walls

In section 4.4.1 the slide-over friction capacity of the floor-wall connection was analysed, and in section 4.4.2 the deep-beam behaviour leading to in-plane tensile stresses was observed. These tensile stresses, however, can also be resisted by the frictional behaviour between the floor and the walls.
In the CUR (1988) report about the joints in prefabricated floor panels, if the joints are incapable of coping with these tensile stresses, they are assumed to be taken by the walls.
However, especially in older structures, these walls may already be partially cracked. Hence, it can be assumed that friction can only be developed at the side of the walls (see figure 4.47).

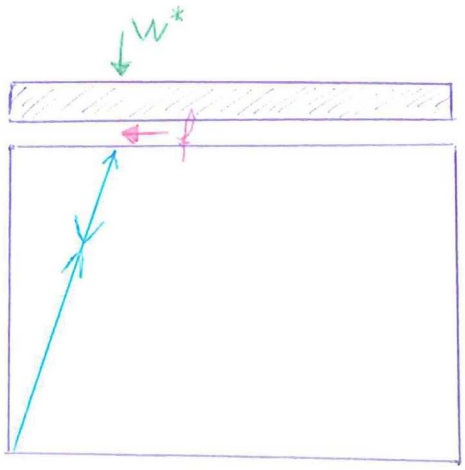

Figure 4.47. Sketch of strut model for maximum friction force between floors and walls.

Depending on the length of the wall that is assumed to be uncracked, the inclination of the compressive strut in the wall will vary. Conservatively, the width of one panel can be used. In this case, for panels of 1m in width and walls of 2.50m in height, the maximum friction force that can be developed is 25% of the weight over the friction zone. The overburden on the wall is 28.5kN/m, meaning that the friction force, with a friction coefficient of 0.66 can rise to 4kN.

From section 4.4.4, the normal force on the floor is around 15kN, which leads to a resultant tension in the floors of 3kN (section 4.4.2). This means that the weight of the structure is capable of producing sufficient friction between the wall and the floor to fully withstand the tension stresses developed by the in-plane, deep-beam behaviour of the wall, assuming that the floor cannot withstand tensile stresses.

4.5. Recommendations for the Design and Modelling of Structures With NeHoBo Floors

Based on the numerical and analytical models presented here, some preliminary suggestions can be made regarding the approach towards the modelling of NeHoBo floors in structures.

4.5.1. Strut -And-Tie Analytical Models

For analytical models, the direct tensile strength, friction angle and shear cohesion are relevant. These are listed in table 4.7. A sketch of a suggested analytical model is also presented in figure 4.48. Here, the contribution of friction with the supporting walls can also be included, approximately one meter (the width of one panel can be considered when evaluating this effect (see section 4.4.5).

Table 4.7. Summary of properties required for analytical models

Direct Tensile Strength	Internal Friction Angle	Internal Shear Cohesion	Self-Mass	External Friction Angle
f_t	φ, μ	c	ρ	φ, μ
55 kPa	33°, 0.65	250 kPa	1700 kg/m^3	26°, 0.5

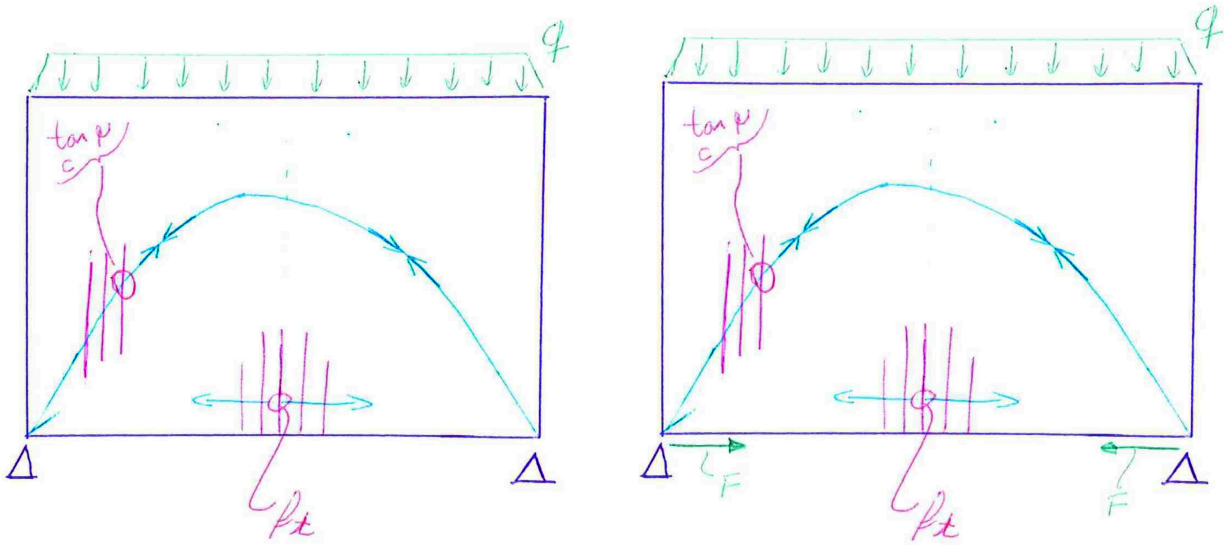

Figure 4.48. Proposed analytical model. Left, without contribution of the supporting walls; right, with their contribution.

4.5.2. Finite Element Models

In FEMs, a plate with orthotropic material properties can be used to model NeHoBo floors. The plate can be linear-elastic (in which case the stress field should be verified) or can be modelled non-linearly; the suggested material properties are listed in table 4.8. A more complex modelling approach is also possible; in this case, the reader is referred to section 4.2.

Table 4.8. Suggested mean material properties for FEMs with NeHoBo Floors.

Material Properties	Unit	Top Concrete Layer		
		Not present	Damaged	In Good Condition
Modulus of Elasticity in the direction Parallel to the Rebar	**GPa**			*4.0*
Modulus of Elasticity in the direction Transversal to the Rebar	**GPa**			*3.5*
Flexural strength in the direction Parallel to the Rebar (OOP)	**MPa**	*2.8*	*4.0*	*4.2*
Tensile strength in the direction Parallel to the Rebar	**MPa**	*0.25*	*0.30*	*0.50*
Tensile strength in the direction Transversal to the Rebar	**MPa**	**0.09**	**0.11**	**0.22**
Fracture Energy in the direction Parallel to the Rebar (Flexural, OOP)	**N/m**			
Fracture Energy in the direction Transversal to the Rebar (Flexural, IP)	**N/m**			

Values in cursive are estimated (preliminary). Empty cells will be filled.

4.6. Comparisons and Conclusions From the Computational Models

Micro models were run to estimate the behaviour of laboratory tests. Some of these tests have been run and particular observations have been made. These need to be replicated with the micro models to verify that the parameters used lead to the experimental observations. For example, during in-plane bending tests, pre-existing cracks in the concrete layer lead to initial cracking through the brick (instead of debonding of the brick-mortar interface). This crack then diverged towards the brick-mortar zone, leading to sliding inside the sample. Specific cases of pre-damage need still to be modelled at the micro-scale to understand the relationship between the overall capacity and the material and interface parameters of the concrete, brick and mortar.
Nonetheless, from the failure mechanisms, material properties have been deduced for use in composite constitutive material models.

Many floor models with varying boundary conditions and material parameters have been run. The capacity of the connection between the floor and its supporting walls has been pegged between 20kN and 150kN, the high difference can be traced to the boundary conditions set to the floor. The lower capacity corresponds to the case of floors on the upper levels of a structure, where the benefitting gravity loads are lower and no restricting upper wall is present. For the upper floors, however, the expected loads are also lower.
In any case, it would seem that the floor itself is capable of transmitting the maximum loads achievable by the floor-wall connections.

For the specific case of the Zijlvest houses, the forces to be transmitted in-plane by the floors during an earthquake of 0.35g (fully in the weak direction) can be conservatively set at 15kN. The capacity of the connection between the floors and their supporting walls is decisively greater than 15kN as shown by multiple models and analytical calculations. The tensile stresses developed by the deep-beam action of the floor for an in-plane-distributed force of 15kN over 7.70m, are estimated to be lower than 50 kPa (linear-elastically from section 4.4.2). From the experimental tests, it would seem that the floors (without the contribution of their concrete layer) have a flexural capacity of 110kPa and a direct tensile strength upwards of 60 kPa. This means that they don't rely on the walls to withstand the tensile stresses.

The maximum forces acting on the floors are directly attributable to the strength of the lateral-bearing elements (side piers) and the mass on the structure. Estimations have been done based on configuration of the Zijlvest donor houses. However, the case of stronger piers (after strengthening measures, for instance) and the resulting higher forces still needs to be analysed.

The analysis of the influence of the NeHoBo floor-system on a structure has yielded expected results: the more flexible floors reduce the participation of the lateral-bearing elements leading to a more flexible structure and associated higher lateral displacements. Whether this affects the near-collapse capacity of the structure in a detrimental manner cannot yet be judged. The comparison with unrealistically stiff and strong laboratory floors has not yielded differences sufficiently important to draw a solid conclusion.
At least the following models are still required to obtain a more confident picture of the influence of the floors on the behaviour of the structure:

- Models with the earthquake signal fully in the independent directions,
- Model with variations in the mesh direction or element geometry,
- Models with other types of floors, in particular, more realistic precast concrete plates.

Chapter 5

Preliminary Conclusions

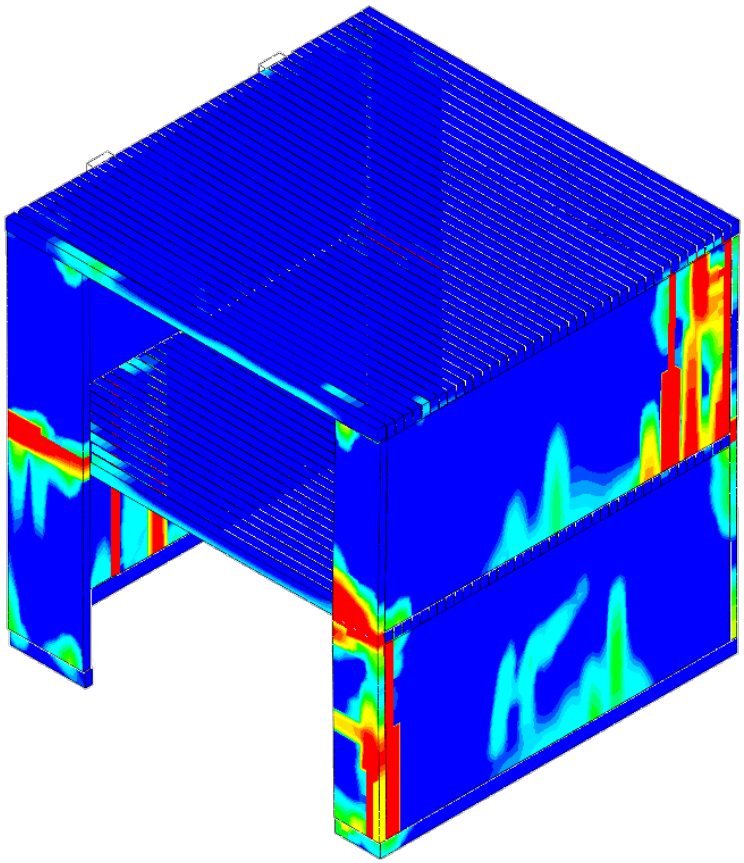

TU Delft

5. Preliminary Conclusions

Most of the extracted NeHoBo floor panels received at the laboratory of the TU Delft contain cracks in the concrete layer. PVC tubes for electrical wiring are embedded in the concrete layer and cracks can be found precisely at the location of these tubes. Cracks where also found at locations where it appears no electrical tubes are found. The cracks are likely due to shrinkage effects. Observations from the in-plane bending test in the weak direction of the material, indicate that a pre-crack in the concrete is a weak location in the sample resulting in sample failure through the entire thickness following the pre-crack in the concrete layer. One sample was tested without a severe pre-crack in the concrete layer which resulted in a significantly higher capacity for flexural strength, at 0.22MPa versus 0.11MPa for the pre-cracked samples (the latter is an average of four samples). Since only one undamaged sample has been tested so-far, additional tests are need to draw conclusions regarding the contribution of the concrete in case it is undamaged.

Shear tests for the brick-mortar interface were performed by eliminating the contribution of the concrete layer. It is not certain if a concrete layer is always present or whether the concrete layer is damaged. By testing only the brick-mortar interface, a lower boundary for the shear properties can be found. It follows that adding a concrete layer will only increase the shear capacity of the NeHoBo floor.
Six samples are tested with two different pre-compression levels (0.1MPa and 0.6MPa). Based on the regression line plotted for the test results, a cohesion value of 0.27MPa and a friction coefficient of 0.66 is found. The observed failure mechanism was similar for all samples: sliding between the brick and mortar interface. Details of the bricks (small sawtooth at the surface) were clearly visible in the detached mortar interface indicating a clean debonding of the brick-mortar interface. Possibly showing that the mortar is stronger than the interface itself.

Table 5.1 shows a comparison between the values found so far with the experimental test and those used in the initial numerical models.

Table 5.1. Comparison of average materials properties.

Material property		Experimental Tests			Range used in Numerical models
		Average values	Standard deviation	5% Characteristic	
Density	**kg/m³**	1666	16	N.A.	1700
Flexural strength*	**MPa**	0.11	0.03	0.0605	0 - 0.2
Direct tensile strength*	**MPa**	0.075†	0.011	0.055	0 - 0.1
Mortar-Brick Cohesion	**MPa**	0.27	0.078	0.15	0 - 0.2
Mortar-Brick Coefficient of friction	**[-]**	0.66	0.162	0.4	0.5 - 0.6

† Derived from in-plane bending test flexural strength results.
* between brackets considering only samples with a damaged concrete layer.

Based on educated guesses for the material properties of the components of the NeHoBo floor-system, numerical models of the floor and the floor-wall environment were run. From these preliminary models, it would seem that opening of the joints inside and between the plates is unlikely. The limits of the in-plane behaviour of the floor system are governed by its boundary conditions and its connections to the rest of the structure. Apparently, if extreme compressive or shearing in-plane loads are acting on the floor, failure occurs at the supports with the walls with a sliding-over mechanism.

However, these extreme forces may never be achieved due to the low intensity of the earthquake and the capacity of the lateral-bearing elements of the structure. For the case of the Zijlvest donor houses, the lateral piers become damaged and are incapable of transmitting higher lateral forces to the rest of the structure. A static analysis using the spectrum provided by NEN (2017) shows that (for a PGA of 0.35g) the forces on the floor would be limited to 15kN. A non-linear computational models shows damage of the piers already at lower forces, indicating that a force of 15kN would not be reached.
Nonetheless, the direct tensile strength of the floors, disregarding the contribution of the potentially cracked concrete top layer, seems to be sufficient to withstand the force of 15kN. With a deep-beam calculation, it results that this force leads to tensile stresses of 50kPa in the floor. The conservative direct tensile strength of the floor, measured with the in-plane bending test, appears to be around 55kPa.

Moreover, a validated model of a house with solid concrete floors tested at the TU Delft (Esposito, 2016a) was used for comparison by replacing the floors in the model with a representation of the NeHoBo floors. These two models were compared in terms of their behaviour during a quasi-static cyclic pushover and multiple base excitations with an earthquake accelerogram. No significant reduction in strength capacity was observed; however, the stiffness of the structure appears to reduce when employing the NeHoBo floors. At this point, the results show that no detrimental influence on the near collapse state is directly recognisable but this still requires investigation.

Additional models and tests are still required to better understand the global and local failure mechanisms that govern the capacity of the floors. The final version of this report needs and will evaluate the following:

- additional laboratory tests to better represent the parameters measured and their distributions, in particular:
  - more in-plane bending tests,
  - bond tests,
  - out-of-plane bending tests,
- additional variations of computational models with a more in-depth understanding of the influence of NeHoBo floors.

IV. References

Esposito. 2016a. & Terwel, Ravenshorst, Schipper, Messali, Rots | Cyclic pushover test on an unreinforced masonry structure reseambling a typical Dutch terraced house. – TU Delft

de Roo. 1991. & Straman | Numerieke Analyse van de Schijfwerking in Geprefabriceerde Vloeren. – Cement nr 11, p76-80

Tena-Colunga. 2015. & Chinchilla-Portillo, Juárez-Luna | Assessment of the diaphragm condition for floor systems used in urban buildings. – Engineering Structures, 93,

Rots. 2017 | Proposal: Testing and modelling of NeHoBo floors for Groningen seismic assessments. Delft University of Technology

Jafari. 2017, Esposito, R. | Material tests for the characterisation of replicated solid clay brick masonry. Delft University of Technology. Report number C31B67WP1-12, version 01, 16 August 2017.

Esposito. 2016b. & Messali, Rots | Tests for the characterisation of replicated masonry and wall ties. - Delft University of Technology. version 08, 18 April 2016.

NEN. (2017) | Online Tool to Determine Seismic Response Spectra. http://seismischekrachten.nen.nl/webtool.php. Retrieved on December 19th, 2017.

Tomassetti. 2017. & Kallioras, Graziotti, Correia | Preliminary report on the construction of the building prototype at the LNEC laboratory. – Lisbon, March 2017

CUR. 1988 | Voegen in geprefabriceerde vloeren – civieltechnisch centrum uitvoering research en regelgeving (CUR).

Appendix

Testing and Modelling of NeHoBo Floors

TU Delft

V. Appendix

V.1 Masonry Material Properties

Table A.1. Overview of average material properties from NAM-2 (2016) and NAM-3 (2017) companion test results for clay-brick "weak masonry".

			NAM-2 2016			NAM-3 2017		
			Average	St. dev.	C.o.V.	Average	St. dev.	C.o.V.
Compressive strength of mortar	f_m	MPa	3.81	0.34	0.09	3.84	0.43	0.11
Flexural strength of mortar	f_{mt}	MPa	1.40	0.17	0.12	1.57	0.11	0.07
Normalized compressive strength of element prescribed by producer	f_b	MPa	28.31	2.92	0.10			
Flexural strength of brick	f_{bt}	MPa	6.31	0.72	0.11			
Elastic modulus of brick from bending test	E_b	MPa	8049	423	0.05			
Compressive strength of masonry in the direction perpendicular to bed joints	f'_m	MPa	14.02	0.56	0.04	11.35	0.83	0.07
Elastic modulus of masonry in the direction perpendicular to bed joints	E_1	MPa	4380	605	0.14	2919	442.00	0.15
	E_2	MPa	4068	783	0.19	2731	732.00	0.27
	E_3	MPa	4590	603	0.13	3087	315.00	0.10
Poisson ratio of masonry in the direction perpendicular to bed joints	ν	-	0.14	0.02	0.11	0.14	0.004	0.03
Fracture energy in compression for loading perpendicular to bed joints	$G_{f\text{-}c}$	N/mm	28.52	3.4	0.12	26.05	3.15	0.12
Compressive strength of masonry in the direction parallel to bed joints	$f_{m,h}$	MPa	13.11	2.41	0.18			
Elastic modulus of masonry in the direction parallel to bed joints	$E_{1,h}$	MPa	3332	565.00	0.17			
	$E_{2,h}$	MPa	3664	689.00	0.19			
	$E_{3,h}$	MPa	3207	592.00	0.18			
Fracture energy in compression for loading parallel to bed joints	$G_{f\text{-}c,h}$	N/mm	35.1	6.63	0.19			
Masonry bending strength with the moment vector parallel to the bed joints and in the plane of the wall	f_{x1}	MPa	0.16	0.03	0.18			
Youngs modulus from OOP1	E_{fx1}	MPa	3756	1789	0.21			
Masonry bending strength with the moment vector orthogonal to the bed joint and in the plane of the wall	f_{x2}	MPa	0.65	0.17	0.25			
Youngs modulus from OOP2	Efx2	MPa	7080	593	0.08			
Masonry bending strength with the moment vector orthogonal to the plane of the wall	f_{x3}	MPa	0.46	0.09	0.20	0.35	0.14	0.40
Youngs modulus from IP bending	E_{fx3}	MPa	2924	480	0.16	2084	526	0.25
Flexural bond strength	f_w	MPa	0.15	0.05	0.32	0.09	0.03	0.35
Masonry (bed joint) initial shear strength	f_{v0}	MPa	0.20			0.14		
Masonry (bed joint) shear friction coefficient	μ		0.69			0.79		
Residual masonry (bed joint) initial shear strength	$f_{v0,res}$	MPa	0.05			0.03		
Residual masonry (bed joint) shear friction coefficient	$\mu_{\rho\varepsilon\sigma}$		0.60			0.71		